SYNTHESIS OF PORPHYRIN-BASED POLYHEDRAL OLIGOMERIC SILSESQUIOXANE MOLECULES FOR IMPROVED PHOTODYNAMIC THERAPY OF CANCER CELLS

by

Paolo Siano

A thesis submitted to the faculty of
The University of North Carolina at Charlotte
in partial fulfillment of the requirements
for the degree of Master of Science in
Chemistry

Charlotte

2020

Approved by:

DocuSigned by:
Dr. Juan Vivero-Escoto
86E53750BE664DE...
Dr. Juan L. Vivero-Escoto

DocuSigned by:
24D80E2A1AB642D...
Dr. Swarnapali De Silva Indrasekara

DocuSigned by:
Dr. Michael G. Walter
D058924A09FC419...
Dr. Michael G. Walter

DocuSigned by:
Mariya Munir
644D77B9E95442C...
Dr. Mariya Munir

ABSTRACT

PAOLO SIANO. Synthesis of porphyrin-based polyhedral oligomeric silsesquioxanes molecules for improved photodynamic therapy of cancer cells. (Under the direction of Dr. JUAN L. VIVERO-ESCOTO)

Polyhedral Oligomeric Silsesquioxane (POSS) materials are a class of nanostructured compounds based on Si-O linkages forming a cage with a silicon atom at each vertex, where substituents are bound tetrahedrally determining the physical and chemical properties of the cage. The vast variety of functional groups that can be added to the cage allows for this class of nanocomposites to be used in a variety of applications such as design of novel materials, bioimaging and drug delivery to name a few. Photosensitizers like porphyrins used in light-activated therapies are hydrophobic molecules leading to self-aggregation in aqueous media, causing decreased bioavailability for biomedical applications. We hypothesize that by using the multifunctionality of POSS platform, we can selectively introduce photosensitizer(s), with targeting and hydrophilic groups for tuning the final properties of the POSS derivatives. The aims for my project are: **1)** synthesize porphyrin-based octaaminopropyl-POSS and the trimethylammonium version, and **2)** fabricate porphyrin-based bifunctional POSS system containing a targeting group. These novel molecules will be used for the selective elimination of cancer cells.

DEDICATION

I would like to dedicate this to my family and friends for their support and love.

"Consider your origin. You were not born to live like brutes but to follow virtue and knowledge." *Dante Alighieri, The Divine Comedy.*

ACKNOWLEDGEMENTS

First and foremost, I would like to express my sincere gratitude to my advisor Dr. Juan L. Vivero-Escoto for his support during my Masters' research, for his patience, motivation, enthusiasm, and mentorship. His guidance helped me in the research and writing of this thesis. Besides my advisor, I would like to thank the rest of my thesis committee: Dr. Swarnapali De Silva Indrasekara, Dr. Mariya Munir, and Dr. Michael G. Walter, for their encouragement, insightful comments, and questions.

My sincere thanks also go to Dr. Markus Etzkorn, whose ability to explain and share his passion for organic chemistry made me feel really passionate about the subject; Dr. Craig Ogle, who has been a great advisor to me and a friend; Dr. Jordan Poler, who has given me great suggestions and help during my studies of physical chemistry; Dr. Daniel Rabinovich, who has supported me and helped me throughout my doubts and thoughts about which PhD school to choose (and what TV series to watch), and finally Dr. Richard Jew for being a great advisor, professor and friend who has motivated me throughout my academic career at UNCC.

I would like to thank my fellow lab colleagues in the V-Lab for the sleepless nights we were working together, and for all the fun we have had in the last years. I have learned so much about the skills necessary in a chemistry lab from Dr. Zachary Lyles, Dr. Mubin Tarannum and Hemapriyadarshini Vadarevu. They have been a great help to me and have become dear friends.

I would like to thank my family who were the ones that noticed my passion for life sciences and encouraged me to pursue a career in chemistry. I could never thank them enough for their support and most importantly their never-ending love. Particularly, I am

most thankful and grateful to my brother, who has been my best friend and guide since I was born.

Finally, I would like to thank my partner, Delfina Erochenko Gentile, for being by my side all these years and never for a second letting me get upset about my mistakes.

TABLE OF CONTENTS

LIST OF TABLES

LIST OF FIGURES

LIST OF ABBREVIATIONS

AP-IB-MP	Aminopropyl-hexaisobutyl-mercaptopropyl-POSS
APTES	(3-aminopropyl) triethoxysilane
DCC	N,N'-dicyclohexylcarbodiimide
DMA	9,10-dimethylanthracence
DMAP	4-dimethylaminopyridine
DMF	Dimethyl Formamide
DMSO	Dimethyl Sulfoxide
ISC	Intersystem Crossing
MOA-POSS	Octa-methylpropylammonium-POSS
MPTES	(3-aminopropyl) trimethoxysilane
NHS	N-hydroxysuccinimide
NP	Nanoparticle
OA-POSS	Octa-aminopropyl-POSS
OLED	Organic Light-Emitting Diode
PDI	Photodynamic Inactivation
PDT	Photodyamic Therapy
POSS	Polyhedral Oligomeric Silsesquioxanes
PS	Photosensitizer
QA	Quartenary Ammonium
ROS	Reactive Oxygen Species
TGA	Thermo Gravimetric Analysis

THPP	5,10,15,20-tetra(m-hydroxyphenyl)-porphyrin
TMAOH	Pentahydrate tetramethyl ammonium hydroxide in methanol

CHAPTER 1: INTRODUCTION

1.1 Polyhedral oligomeric silsesquioxanes (POSS)

In the past decades there have been several efforts in developing controlled release drug delivery systems to deliver a precise amount of a drug, increase the effect of the drug on the body, and protect it from physiological degradation.[1] Along that idea, versatile families of sophisticated three-dimensional nanoblocks have been designed, such as polyoxometalates, fullerenes, and mesoporous silica (MSNs), which bear multiple reactive functionalities on their surfaces.[2] These systems have emerged as promising nanocarriers in drug delivery because of their outstanding properties in promoting therapeutic efficacy; such as good water solubility, long *in vivo* circulation times, efficient bioavailability, high preferential accumulation at the tumor sites and minimized side effects against normal tissues. However, the therapeutic efficacy of nanocarriers isn't optimal, since they lack sufficient drug loading efficiency and do not release drugs in a controlled manner.[3-5] Hence, it is desirable to develop a family of drug delivery systems who also exhibit a controlled drug loading capacity, specifically intracellular drug release in tumor environments.

Recently, nanohybrids comprised of both inorganic and organic moieties, have emerged as promising materials. Polyhedral oligomeric silsesquioxane (POSS) has attracted considerable interest for several biomedical applications, such as drug delivery, cellular imaging, biosensors, and tissue engineering systems because of its organic−inorganic structure, biocompatibility, and nontoxicity.[6-8] These types of compounds allow for precise control of functionalization of targeting agents on their surfaces.

Polyhedral oligomeric silsesquioxane (POSS) is a class of three-dimensional cage-like nanostructures applied in many fields.[9-13] The term silsesquioxane indicates a $RSiO_{3/2}$ unit, which exhibits the chemically inert and thermally stable properties of Si-based materials. Furthermore, in silsesquioxane the fragment *sil-* denotes silicon, *sesqui-* indicates that each silicon is bound to 1.5 oxygens and, *ane-* points at the bond between a Si atom and a R group, where R could be a potentially reactive moiety. POSS has a cage-like structure, where each Si atom placed at a vertex is tetrahedrally bound to three O atoms and one R substituent. The latter determines the chemical and physical properties of the cage (**Figure 1**).[14]

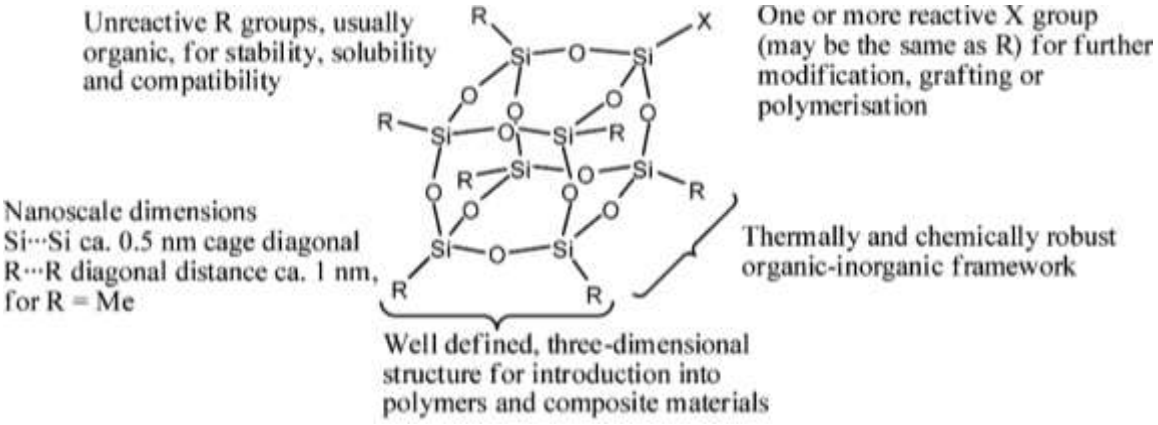

Figure 1. The physical and chemical properties of POSS are characterized by the bound groups. Because of its 3D network, POSS compounds are used in polymeric and nanocomposite materials, in which they could be inserted with reactive groups present on the cage.[14]

The nomenclature used for siloxane polymers is also applied to POSS compounds, where a silicon atom bearing three oxygen atoms, a SiO_3 unit, is denoted by the letter "T".[14] The most common POSS compounds are the ones having formula T_8R_8, indicating an octameric cage. Whereas other siloxane cages, such as T_4, T_6, T_{10}, T_{12}, have also been reported,[15, 16] the octameric cage, T_8, is the most common POSS isomer observed, because the Si atoms exhibit an optimal tetrahedral configuration, which results in minimum ring

strain. In comparison, the T_4 and T_6 need bulky substituents to make up for the ring strain, while the T_{10} and T_{12} are formed by the cage rearrangement of T_8 POSS and are difficult to separate due to the formation of different isomers.[14, 17, 18] POSS's three-dimensional structure makes this compound very valuable for polymeric and nanocomposite materials. The addition of this thermally and chemically robust compound enhances polymers' mechanical and thermal properties (**Figure 1**).[14]

1.2 Synthesis of polyhedral oligomeric silsesquioxanes

There are two main strategies to synthesize POSS compounds: 1) using a precursor containing less than eight silicon atoms under catalytic amounts of an acid (hydrolytic condensation approach) and 2) starting from a partially condensed POSS under catalytic amount of a base (corner capping approach). As mentioned, T_8 POSSs are the most common and hence we will focus our discussion on the synthesis of the cubic octameric cages.

1.2.1 Hydrolytic condensation approach

The formation of a T_8 cage through a hydrolytic condensation involves chloro- or alkoxy- silanes, ($RSiX_3$), as precursors, and catalytic amounts of an acid, such as HCl, to increase yields (**Figure 2**).[19] A large number of POSS compounds can be prepared using this methodology with different functional groups such as alkyl, alkylene, aryl, and arylene moieties. These groups can be used as reactive groups for further modification to fabricate polymeric or delivery materials.[20, 21]

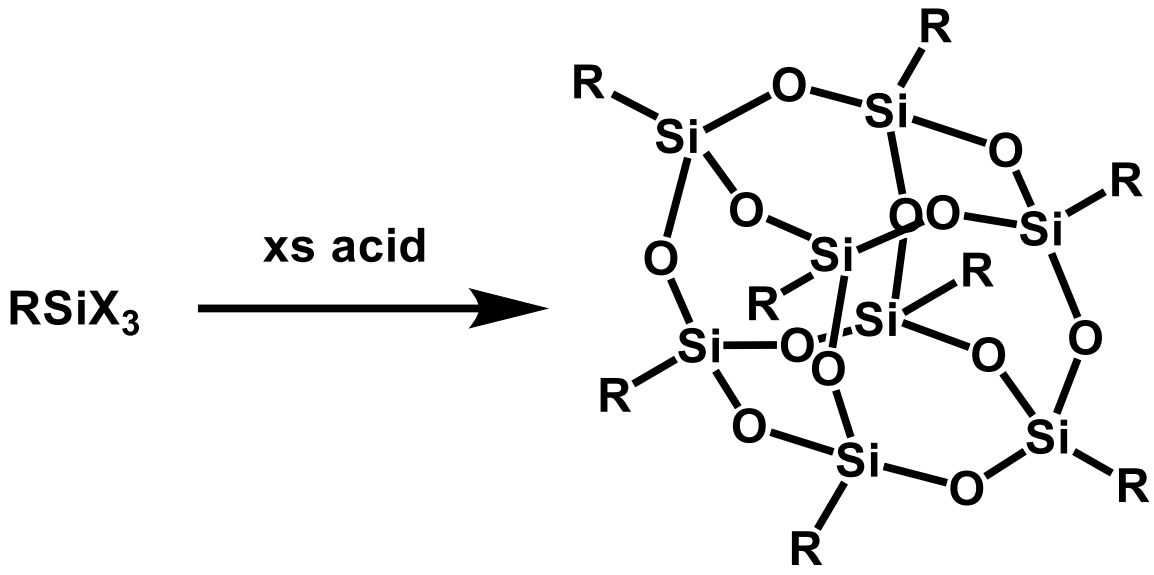

Figure 2. Hydrolytic condensation of an organosilane monomer to afford a fully symmetrical POSS.[18] This reaction proceeds through the addition of excess acid in the solution.

The hydrolytic condensation approach offers the possibility of generating a fully symmetrical cage. Nevertheless, it has a few disadvantages such as the long reaction times that can vary from one week to as long as three months. Moreover, the yields are often poor, typically between 20% and 30%. Most likely due to the formation of isomers in the mixture (i.e. non-polyhedral silsesquioxanes and the formation of other lower or higher oligomers of POSS).[14, 18, 20, 22] To obtain higher yields with less amounts of byproducts, catalysts such as trifluoromethanesulfonate, are often employed.[19]

1.2.2 Corner Capping Approach

The corner capping approach of a partially condensed POSS affords unsymmetrical POSS cages, with molecular formula T_8R_7R', in high yields (>70%). The general reaction pathway involves a partially condensed silsesquioxane trisilanol, $R_7Si_7O_9(OH)_3$,

(commercially available) in the presence of a base such as trimethylamine or tetraalkylammonium hydroxide (**Figure 3**).[18]

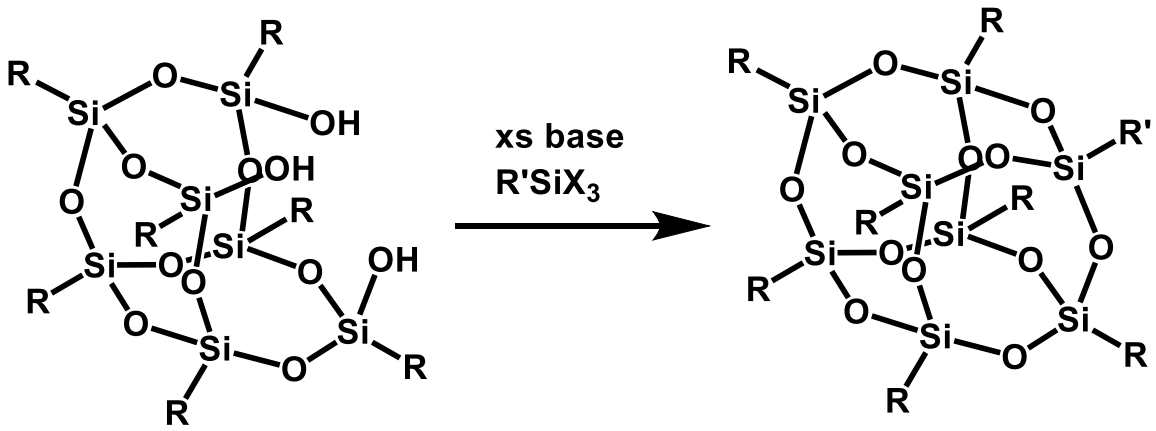

Figure 3. Corner capping of a partially condensed trisilanol POSS with an organosilane to afford an unsymmetrical POSS. The organosilane added bears a reactive functionality. This reaction proceeds through the addition of excess base in the mixture.

1.3 Stability of polyhedral oligomeric silsesquioxanes

The stability of POSS compounds is determined by the groups bound to the cage, Generally, these compounds are air-stable and thermo gravimetric analysis (TGA) measurements show degrading temperatures up to 500 ºC.[14]

1.3.1 Stability of Octa-aminopropyl-POSS (OA-POSS)

OA-POSS is one of the most versatile POSS precursors for many organic/inorganic hybrid materials, due to the reactivity of its primary amines. The most common synthesis for OA-POSS affords the hydrochloride salt, stored in a methanoic solution below 0 ºC. This can be converted to the free amine version by eluting methanoic or ethanoic solutions across an exchange resin, or treating the solution with a base, such as triethylamine or potassium bicarbonate.[23] The neutralization to the free amine is difficult to control and

obtain without damaging the Si/O framework, and degrading the overall cage. The Si/O framework of OA-POSS degrades in two ways. In the first, as shown in **Figure 4**, the aminopropyl moieties on OA-POSS promote an intramolecular nucleophilic attack to the silicon atom bonded on the same group. This mechanism leads to the formation of silanols disrupting the cage. POSS compounds with unreactive R substituents do not show this type of mechanisms.

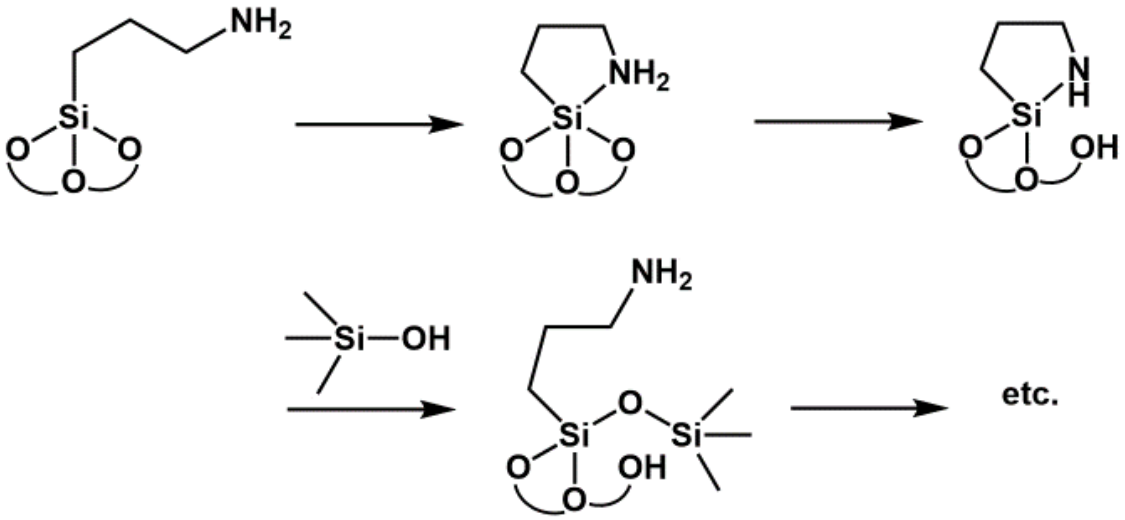

Figure 4. Degradation mechanism of OA-POSS. The aminopropyl moieties on OA-POSS promote an intramolecular nucleophilic attack to the silicon atom bonded on the same group. This mechanism leads to the formation of silanols disrupting the cage.[20]

Furthermore, when OA-POSS is found in an aqueous solution, the presence of water encourages the hydrolysis of the cage and consequential degradation of the Si-O-Si framework. This type of degradation is not seen for bulkier R substituents, which can shield the cage.[24] The hydrochloride salt of OA-POSS is stable for several months in a methanoic solution, in DMSO or DMF, at temperatures below 0℃.[9] Ongoing tests are being carried out to determine the exact shelf life of the hydrochloride salt OA-POSS in methanol, DMSO and DMF. On the contrary, OA-POSS is stable in methanol for a few weeks at temperatures below 0℃, but its shelf-life decreases to a few hours in bulk.[14, 20, 24]

1.4 Multifunctional polyhedral oligomeric silsesquioxane

One of the advantages that can be foreseen for POSS is the ability to precisely control the functionalization of this material with more than one functional group. Several strategies have been explored to pursue this goal. Recently, a luminescent POSS has been synthesized from aminopropyl-heptaisobutyl-POSS. This molecule was synthesized through two subsequent corner capping reactions to afford a reactive carboxylic functionality and a fluorescein derivative to yield a molecule of interest in the biomedical field.[25] Moreover, Carniato et al. developed a bifunctional POSS where one Si corner has been substituted by a titanium-isopropyl moiety. This was achieved through a multistep process involving two corner capping reactions.[26] Also, Froelich et al. have synthesized a bifunctional POSS, containing different emitting dyes. These showed an increase in thermal stability of the free emitter and were used as fabrications for organic light-emitting diode (OLED) devices.[27]

Although reactions on POSS cages are well known,[28, 29] controlling subsequent steps such as corner opening and corner capping on a siloxane cage is troublesome,[29] but important as the final product is a compound with different functionalities that can be exploited in several fields.[26] Adding functionalities to the cage have initially proven to be difficult, reporting poor yields and complex procedures;[30, 31] still, these modifications are very interesting in the design of novel materials with well-defined properties.[32, 33] The issues that arise with adding functionalities to a cage are experimental and sterical.

Adding more than one different functionality to the cage involves a multistep process. Starting from a completely condensed POSS, the cage will be cleaved to one of its corners via “corner opening” under the addition of a base, such as tetraethylammonium hydroxide.

Subsequently, the open corner comprised of silanol groups, will be capped with an alkoxy- or chloro- silane, such aminopropyltriethoxysilane. Next, the corner opening step is repeated, where the Si opposite to the one bearing the most reactive groups is cleaved. Finally, the last corner is capped with another silane. The corner opening steps are quite complex as they involve opening one SiO_3 unit through harsh conditions that require a long reflux, and rough basic conditions that could compromise the Si/O framework. This could significantly inhibit the success of the addition of an extra functionality. Lastly, subsequent corner capping yields the final product with a supplemental functionality (**Figure 5**).[14, 34]

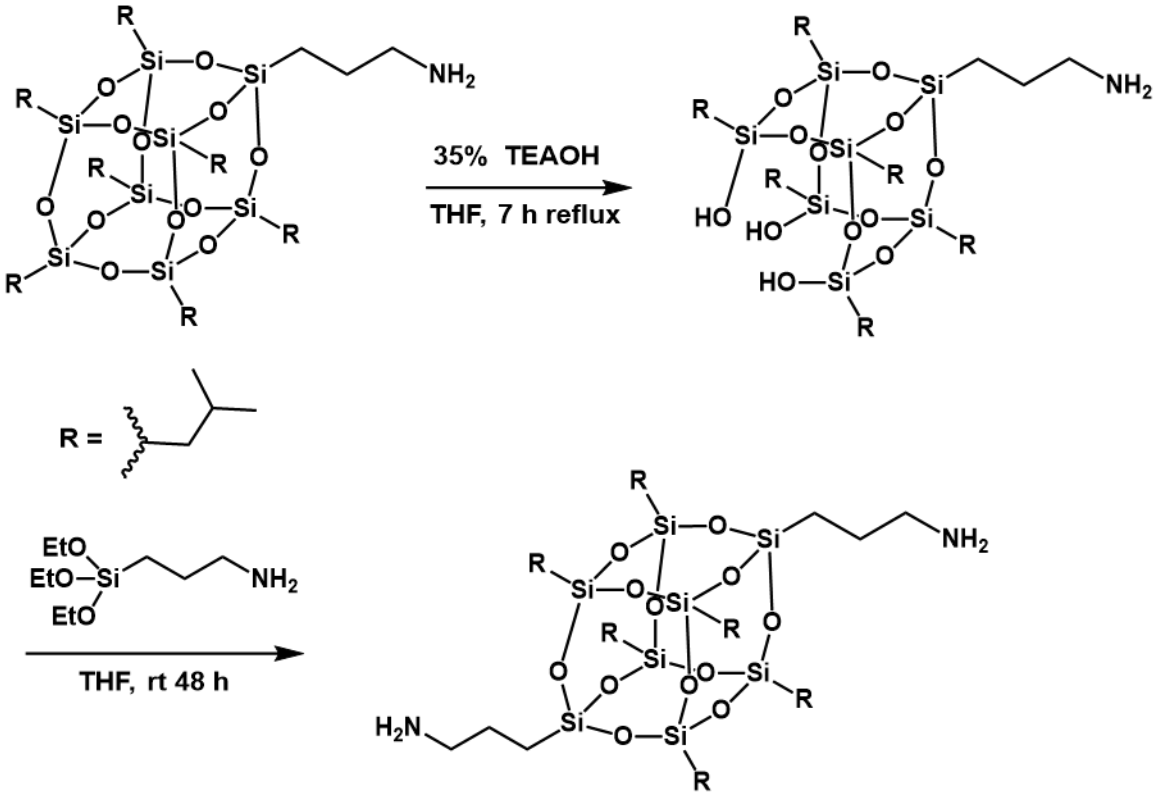

Figure 5. Reaction pathway of a multifunctional POSS. Starting from a completely condensed POSS, the cage is cleaved via "corner opening" under the addition of a base. Subsequently, the open corner is capped with an alkoxy- or chloro- silane. Next, the corner opening step is repeated, where the Si opposite to the one bearing the most reactive groups is cleaved. Finally, the last corner is capped with another silane. [34]

1.5 Structural Characterization of Polyhedral Oligomeric Silsesquioxanes

Several POSS compounds (T_8R_8 and T_8R_7R') are air stable, soluble in common organic solvents used in laboratories and are bright white in color, or pale yellow if a protonated substituent is present, such as an ammonium salt.

a. NMR Characterization of Polyhedral Oligomeric Silsesquioxane. The electronic effect of the T_8 cage in T_8R_8 and T_8R_7R' compounds have been shown by ^{13}C NMR chemical shift studies to be electron-withdrawing, similar to that of the CF_3 group, which has an effect on reactions taking place on the cage.[35, 36] The shifts of the organic moieties present on the POSS are not affected by the cage and their overall chemical and magnetic environment is equivalent to their siloxanes counterpart; for this reason, in ^{1}H NMR and ^{13}C NMR the shifts for the organic substituents are comparable to the non-POSS analogs. The sensitivity for ^{29}Si NMR greatly changes with a siloxane cage compared to non-caged siloxane. Typically, T_8R_8 POSS compounds show a single shift in ^{29}Si NMR with chemical shifts ranging from -65 to -70 ppm.[14] There are specific cases such as aryl-T_8 with a shift between -77 to -83 ppm,[37, 38] POSS cages containing fluoride ions around -83 ppm.[39] In addition, POSS cages with siloxy substituents give ^{29}Si NMR chemical shifts around -110 ppm.[40, 41] Therefore, the sensitivity of ^{29}Si NMR makes this technique an important tool for identification of different substituents on the POSS cage. The signal in ^{29}Si NMR for T_8R_7R' differ from the T_8R_8; that instead of only one peak, three peaks are observed, which correspond to four chemically inequivalent Si atoms, in the unsymmetrical POSS compound (**Figure 6**). The intensities of the peaks correspond 1:3:4, according to the distance from the Si bearing the different substituent. However, the four signals are often close together and difficult to resolve.[18]

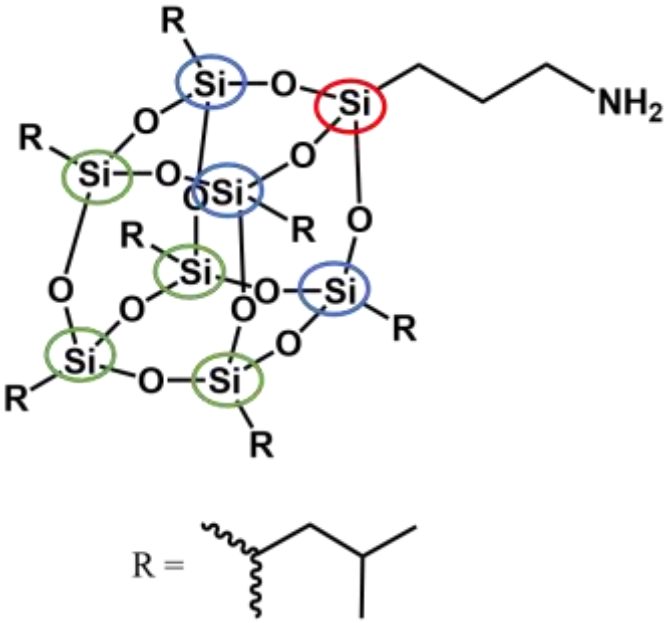

Figure 6. Chemical inequivalence of the Si atoms of a multifunctional POSS. In ^{29}Si NMR for T_8R_7R' three peaks are observed, which correspond to four chemically inequivalent Si atoms (shown in red, blue and green according to their distance from the aminopropyl group). The intensities of the peaks correspond 1:3:4, according to the distance from the Si bearing the different substituent.

b. <u>Infrared Spectroscopic Characterization of Polyhedral Oligomeric Silsesquioxanes.</u>

Infrared (IR) spectroscopy is a technique used for solid POSS and for hybrid materials containing POSS. The IR vibrational spectrum for POSS is peculiar, in that the fingerprint region shows a few stretching vibrations that denote the formation and integrity of the cage. For example, the Si-O-Si linkages of the cage give rise to a sharp but broad stretching vibration around 1100 cm^{-1} (**Figure 7**). This vibration is very characteristic of POSS cages as compared to the stretching vibrations of a ladder siloxanes, which show between 1030 and 1055 cm^{-1}.[14, 42-46]

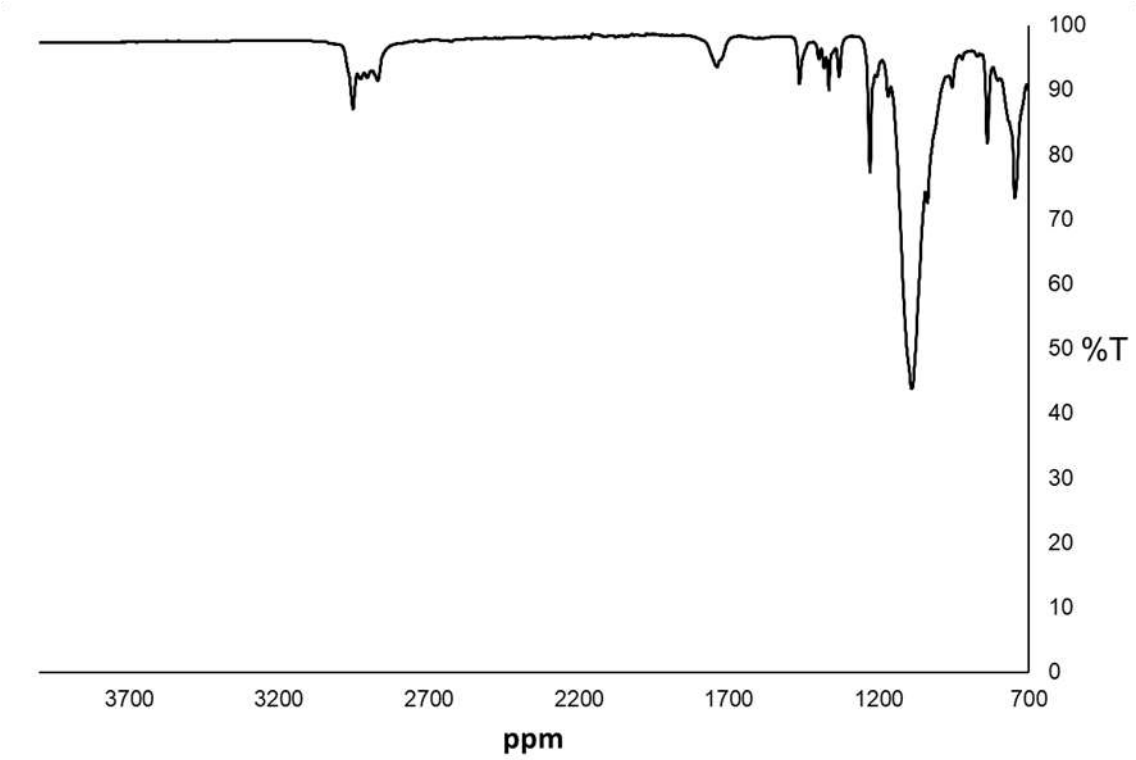

Figure 7. FTIR of a POSS cage. The Si-O-Si stretching vibration is evident at 1100 cm^{-1}, which indicates the formation of a condensed cage.

c. Mass Spectroscopy Oligomeric of Polyhedral Oligomeric Silsesquioxanes.

Mass spectrometry techniques have been used to analyze the molar mass of POSS compounds. MALDI and ESI-MS are helpful tools when determining the masses of "low" molecular weight POSS compounds; however, the intensity of the laser may pose a problem in the fragmentation of the larger ions.[47] Furthermore, effectively analyzing the mass of POSS compounds will confirm the formation of the desired cage. MALDI-TOF mass spectrometry has be used to characterize high molecular weight POSS derivatives such as glycoclusters prepared using $T_8(CH{=}CH_2)_8$ (up to ca. m/z = 5000),[48] a bis-POSS derivative of a phthalocyanine (m/z = 3656),[49] octakis-POSS substituted metallophthalocyanines (m/z = 7676-7681),[50] and poly-pyrene substituted POSS species (m/z = 3436).

d. Crystal X-Ray Diffraction Studies of Polyhedral Oligomeric Silsesquioxanes. X-Ray diffraction is a useful tool to corroborate the structure of an inorganic compound. In fact, many T_6, T_8 and T_{10} POSS cages have had their structures determined by single crystal X-ray diffraction.[14, 46] It was found that the Si-O bond lengths mostly fall in the range between 1.60-1.63 Å, in accordance to values from other siloxanes.[51] Moreover, there are specific cases in which Si-O-Si angles, of a T_8 or T_{10} POSS cage shift significantly: for example, the Si-O-Si angles of T_8 $(OSnMe3)_8 \cdot 4H_2O$ fall within 136.35-172.13° [52, 53] and 140.76-160.68° in T_8Cy_8.[54] However, on average the individual Si-O-Si angles for POSS compounds range between 147.5–150.8°. These variations in angles arise from the flexibility of the Si/O framework along with more flexible substituents.[54]

1.6 Photodynamic Therapy/Inactivation (PDT/PDI)

In photodynamic therapy and photodynamic inactivation (PDT and PDI), light, oxygen and a photosensitizer (PS), such as porphyrin, are used to generate reactive oxygen species (ROS), such as singlet oxygen ($^1O_2$), to cause cellular death. Once irradiated the PS undergoes a transition to a higher energy level. At this point the PS can either relax back, causing fluorescence, or "jump" to a forbidden energy state through intersystem crossing (ISC). Here, the molecule is found at the triplet state and can generate $^1O_2$ via two mechanisms. Type I mechanism occurs when the PS shares electrons with the surrounding molecules, such as molecular oxygen. On the other hand, a Type II mechanism occurs when the PS relaxes back to the singlet state, releasing energy to the environment causing the formation of ROS (**Figure 8**).

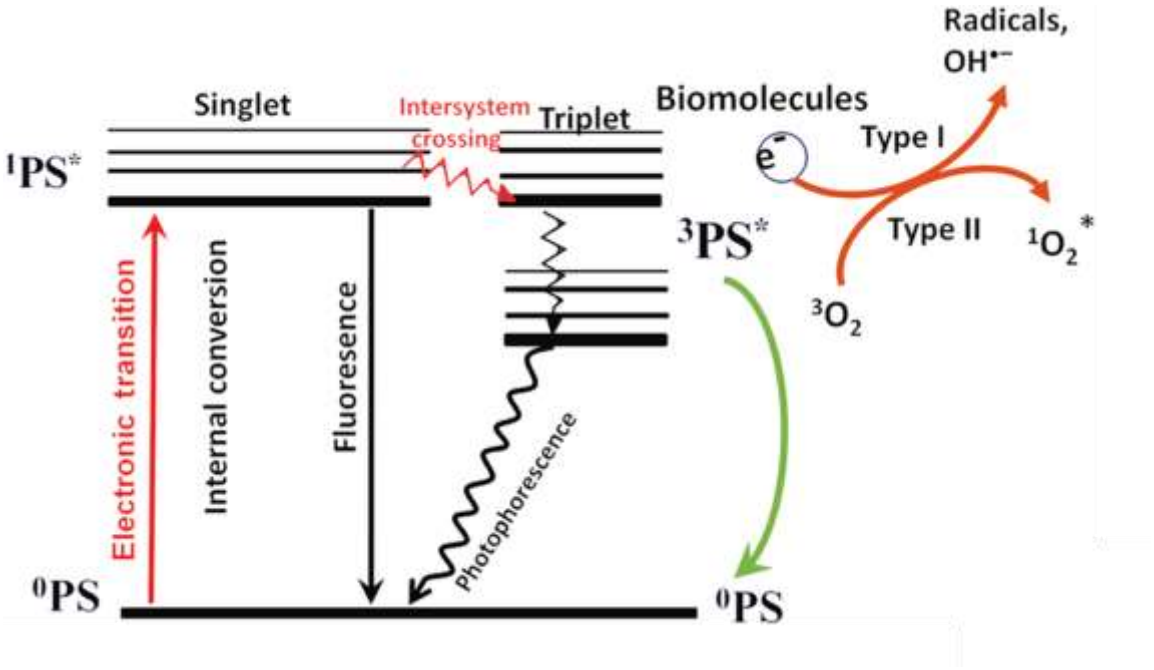

Figure 8. The PS undergoes a transition to a higher energy level, where it can relax back (fluorescence) or "jump" to a forbidden energy state through intersystem crossing (ISC). The molecule here can generate ROS via two mechanisms. Type I mechanism occurs when the PS shares electrons with the surrounding molecules, whereas a Type II mechanism occurs when the PS relaxes back to the singlet state, releasing energy to the environment.

Conventional PS have poor water solubility and aggregate through π-π stacking and hydrophobic interactions, causing the PS to prematurely quench before reaching their targeted goal.[55] To overcome these issues PS are usually incorporated into liposomes,[56-59] micelles,[60-62] metal nanoparticles (NPs),[63-66] polymeric NPs,[67, 68] protein-based NPs,[69, 70] mesoporous silica NPs,[71, 72] graphene oxide[73, 74] and quantum dots.[75, 76] These methods provide physical encapsulation of the PS, and although it is often effective it doesn't afford high loading capacity.

1.7 Applications

POSS compounds have been studied in detail to investigate their structure, optimize their synthesis and discover the scope of chemical transformations that could be implemented without damaging the siloxane cage. Due to their physicochemical structure

and properties, this class of materials has found a wide array of applications in elastomers,[77, 78] thermosets,[79] thermoplastics,[79] liquid crystalline polymers,[23, 80] dendrimers,[81] low dielectric materials,[82] electrolytes,[81, 83] holographic gratings,[84] laser materials,[85] cosmetics,[14] dental and medical applications,[9, 12, 23, 25, 44, 78, 81, 83, 86, 87] space applications,[11, 88-91] biology,[44, 86, 92-94] resists,[18] bioimaging,[6, 81, 95-97] tissue engineering,[98] biodetection,[6, 99, 100] and antimicrobial treatment.[101-103]

1.7.1 Biomedical applications of polyhedral oligomeric silsesquioxanes

POSS compounds show an inert nature, low inflammatory responses, and biocompatibility. POSS nanostructures have been evaluated for various fields in diverse areas of biomedical fields such as drug delivery, dental applications, biomedical devices, implants and tissue engineering.

POSS compounds have found important applications in photodynamic therapy and photodynamic inactivation. Both PDT and PDI rely on the presence of a photosensitizer, oxygen and light to kill cancer cells or pathogens, respectively. PS are usually hydrophobic compounds that aggregate in aqueous media resulting in self-quenching and reduced phototoxic effect.

a. <u>Incorporations of POSS compounds into electrolytes-photosensitizers for multi-amplified antimicrobial activity</u>:

PDI inactivates pathogen bacteria via the generation of ROS, such as singlet oxygen $^1O_2$, and lately it has been shown to be extremely useful in the field as no bacterial resistance has been found.[104-107] Recently, quaternary ammonium (QA)-POSS has been conjugated to electrolytes to probe the interactions towards bacteria. It was shown that because of its light harvesting properties, broad UV-vis absorption spectrum,[108] cationic

pendant groups, and binding ability towards bacteria,[109, 110] QA-POSS conjugated to electrolytes and PS, such as porphyrin, report effective bacterial toxicity. Moreover, oligoelectrolytes containing pendant terminal QA-POSS groups showed great affinity for Gram-negative cellular membrane and were able penetrate it (**Figure 9**).[111] Specifically the PS, oligo-(p-phenylenevinylene) electrolytes (OPVEs) have been grafted onto a QA-POSS for antimicrobial activity to enhance cationic charges, increase the solubility of the PS, and cellular membrane penetration,[112] facilitating $^1O_2$ diffusion. This system showed multiamplified antibacterial efficacy under white light doses (400-700 nm, 6 mWcm^{-2}, 5 min, 1.8 Jcm^{-2}) to *Escherichia coli* (8 μM) and *Staphylococcus aureus* (500 nM).[94]

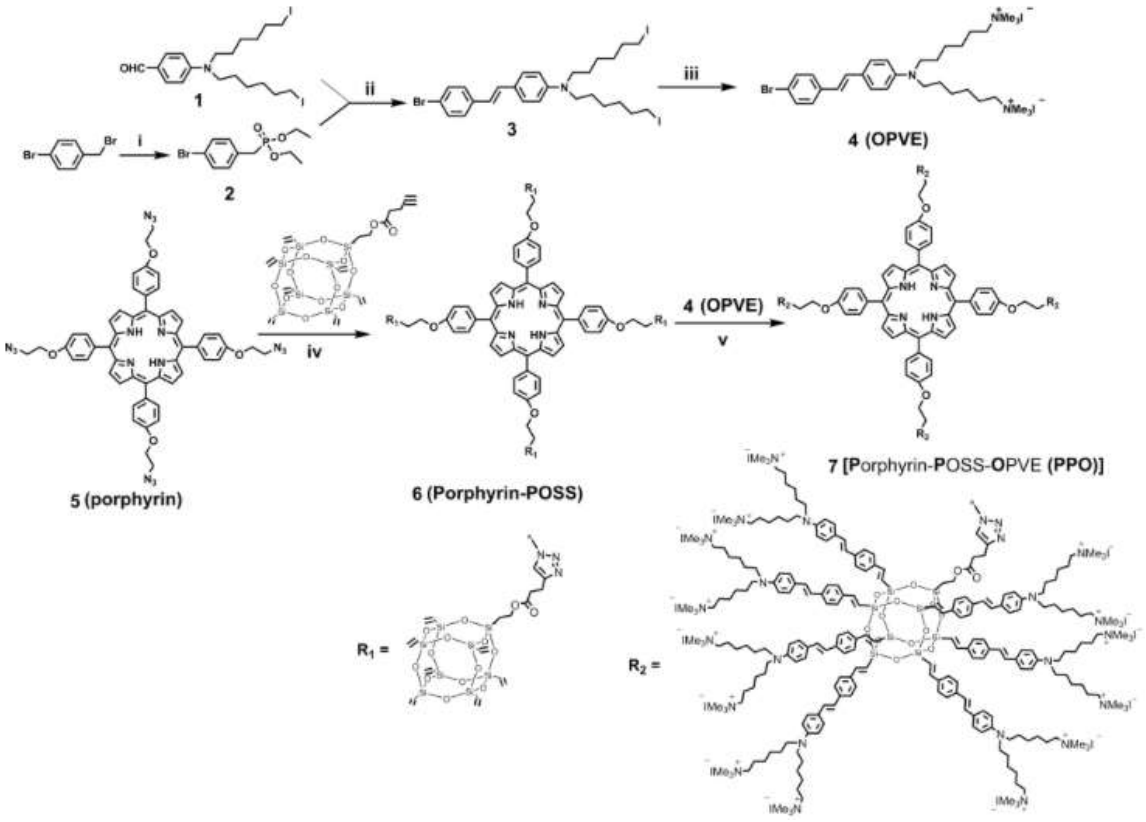

Figure 9. Synthetic Route to Porphyrin–POSS–OPVE (PPO)[94]. The POSS-Porphyrin system shown exhibits multiamplified antimicrobial activity where the QA groups have light-harvesting properties capable of increasing ROS production. Furthermore, the presence of QA-POSS enhanced cellular uptake and solubility of the PS, facilitating $^1O_2$ diffusion.

b. A crosslinked 3-D network structure involving POSS, chlorin e6 (Ce6) and a PEG coating.[10]

The nanohybrid showed excellent aqueous stability, low toxicity and high drug loading capacity (19.8 wt%). Moreover, due to the conjugation with POSS, this system exhibited enhanced cellular uptake, specifically intracellular accumulation within the mitochondria and endoplasmic reticulum was observed, leading to high anticancer efficiency under light exposure, and negligible dark toxicity and side effects. Because of the aforementioned reason this system showed improved PDT efficacy (**Figure 10**).

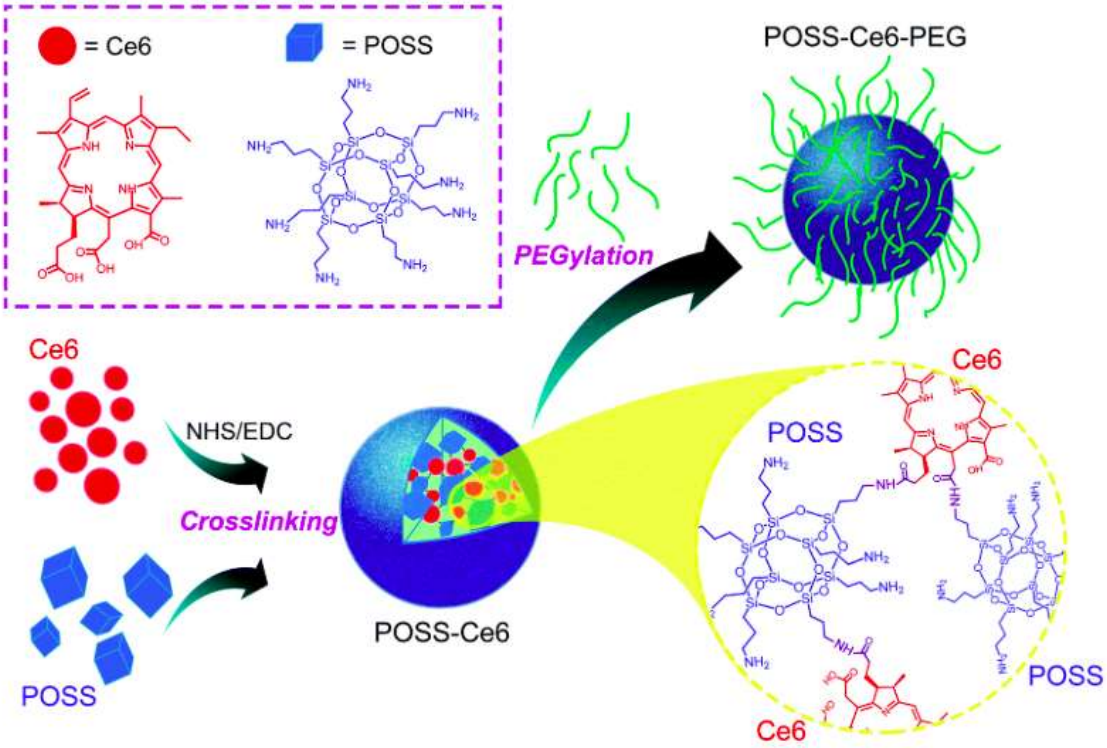

Figure 10. Schematic illustration showing the synthetic method of POSS-Ce6-PEG NPs.[10] This nanohybrid encapsulates the POSS-Porphyrins network, increasing aqueous stability and drug loading capacity.

c. Alternating copolymer involving maleimide isobutyl polyhedral oligomeric silsesquioxane (MIPOSS) for enhanced phototoxicity.

An amphiphilic block copolymer has been synthesized, where porphyrin and POSS were installed on the backbone in an alternating fashion. The self-aggregation of the porphyrins was effectively reduced by the steric cage structure of POSS units and alternating structure as the system self-assembles into nanoparticles in water. This allowed for enhanced singlet oxygen production, improving PDT efficacy against human lung cancer (**Figure 11**).[86]

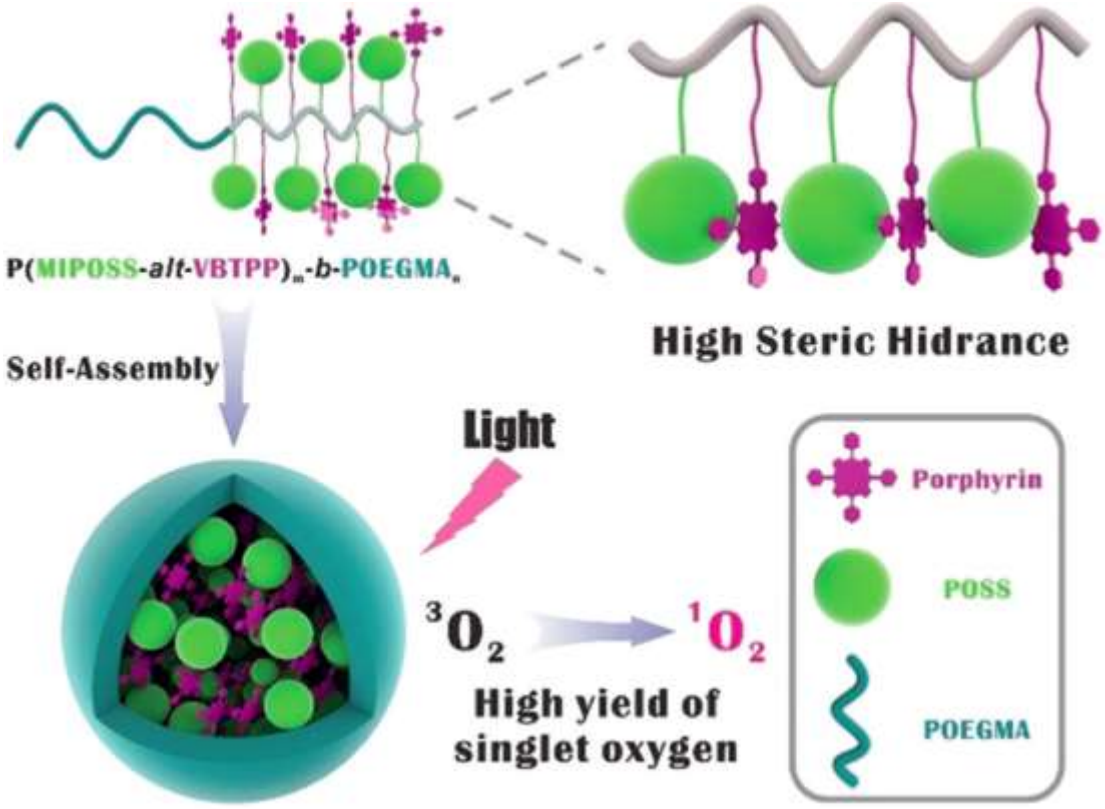

Figure 11. Schematic illustration showing the approach to the formation of the alternating copolymer synthesized. This system decreases interactions among porphyrins, through steric hindrance, and allows enhanced production of singlet oxygen due to the presence of POSS units.[86]

d. Organic−inorganic hybrid photosensitizers for highly effective photodynamic cancer therapy.

Recently and organic-inorganic hybrid photosensitizer was synthesized based on biodegradable POSS scaffolds and 5,10,15,20-tetra(*m*-hydroxyphenyl)-porphyrin (THPP).

This incorporation of a photosensitizers into the robust POSS 3D framework makes the THPP molecules isolated, avoiding self-quenching of the excited states. The hybrid possesses high water solubility, excellent stability, good biocompatibility, and high singlet oxygen production efficiency. In vivo studies indicate that the photosensitizer excellent PDT performance with a low dose (0.4 mg/kg) and light density (72 J/cm2) (**Figure 12**).[87]

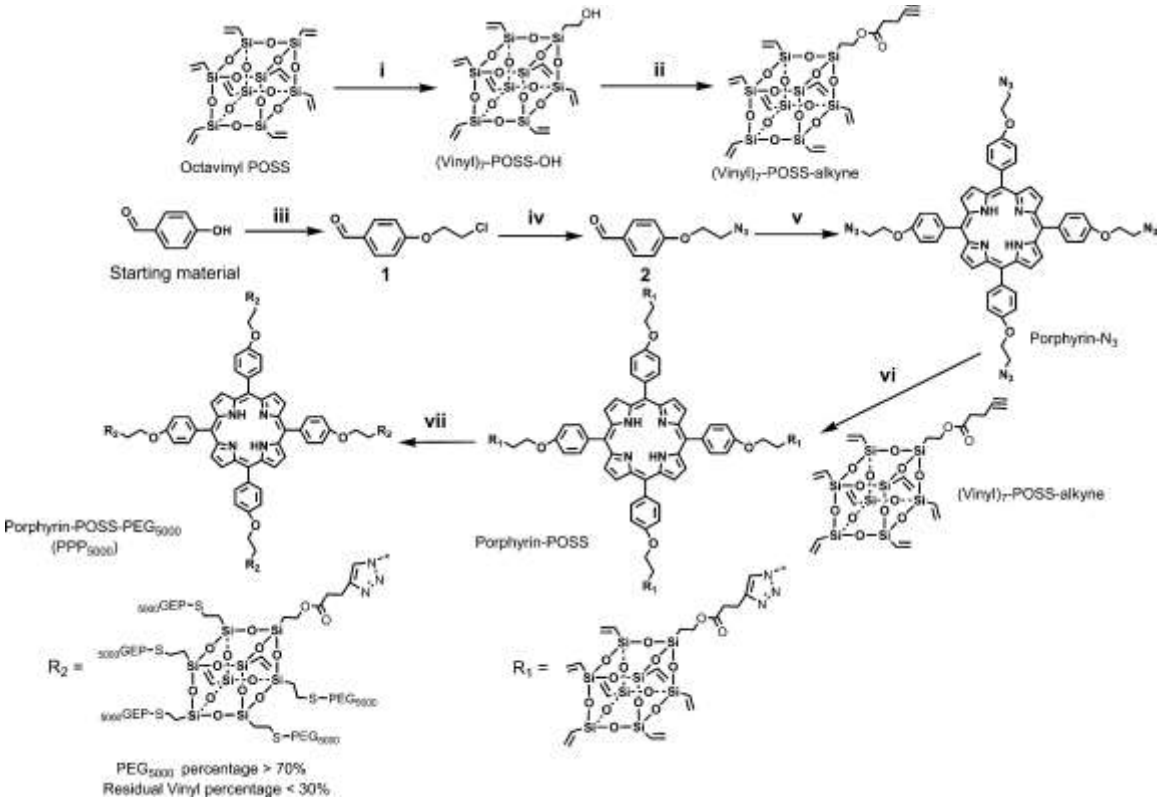

Figure 12. Schematic illustration showing the synthetic approach to the formation of the organic-inorganic hybrid involving octavynil-POSS and THPP. This isolates THPP avoiding self-quenching of the excited states. The hybrid possesses high water solubility, excellent stability, good biocompatibility, and high singlet oxygen production efficiency.[87]

1.8 POSS compounds in this Thesis

1.8.1 Octa-aminopropyl-POSS (OA-POSS)

OA-POSS is a three-dimensional organosilicon oligomer synthesized through the hydrolytic condensation of a trifunctional organosilicon monomer, aminopropyltriethoxysilane, in methanol under catalytic amounts of hydrochloric acid. The

functional moiety on OA-POSS are aminopropyl groups, which make it an interesting precursor for further functionalization on the cage (**Figure 13**). Several syntheses have been carried out that highlighted the difficulty in obtaining good yields, typically between 20% and 30%,[20, 22] so, to overcome this issue, several catalysts have been employed.[19, 113]

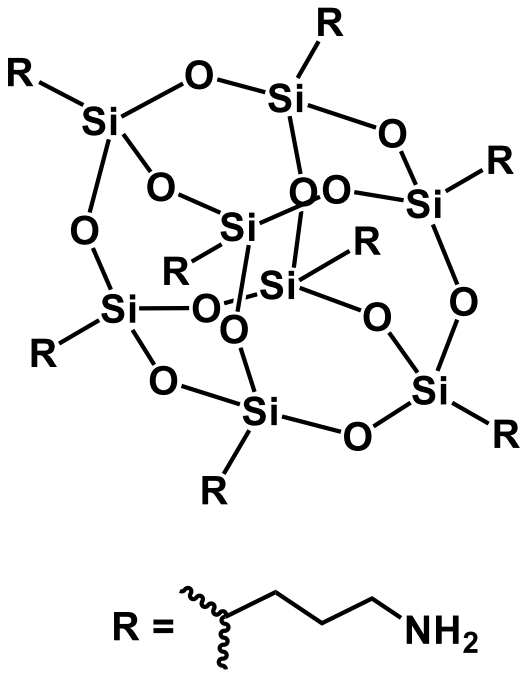

Figure 13. Molecular structure of octa-aminopropyl-POSS.

1.8.2 Octa-methylpropylammonium-POSS (MOA-POSS)

MOA-POSS is a three-dimensional organosilicon oligomer synthesized through consecutive alkylation of the free amine present on the aminopropyl moieties of OA-POSS (**Figure 14**). This compound is of particular interest to study its interactions with cells and bacteria and understand how the permanent charge surrounding the cage affects its properties.[23]

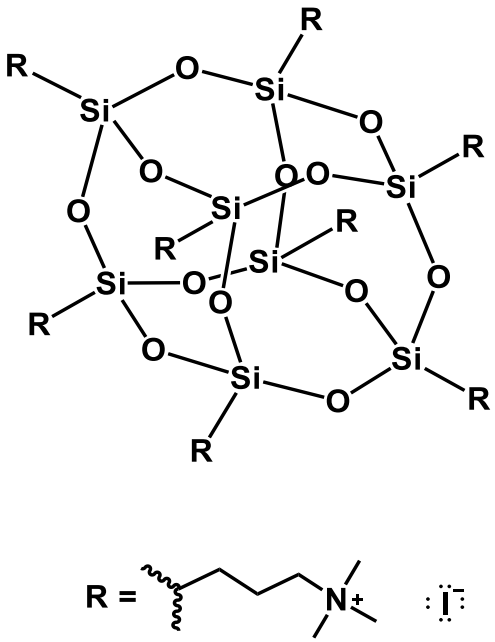

Figure 14. Molecular structure of octa-methylpropylammonium-POSS.

1.8.3 Multifunctional aminopropyl-hexaisobutyl-mercaptopropyl-POSS (AP-IB-MP)

As mentioned previously, POSS compounds bearing multiple functionalities are important to develop for various applications. Although functionalization of an unsymmetrical POSS has been shown to be straightforward, further modifying the cage with another functionality hasn't been achieved successfully.[14] This is because the methodology employed to add a third functionality can damage the Si/O framework. Looking at these challenges, I have synthesized a multifunctional POSS with two different reactive functionalities, an aminopropyl and a mercaptopropyl moiety, and an unreactive functionality, such as an isobutyl group (**Figure 15**). A multifunctional POSS allows us to probe its reactivity for further conjugation reactions.

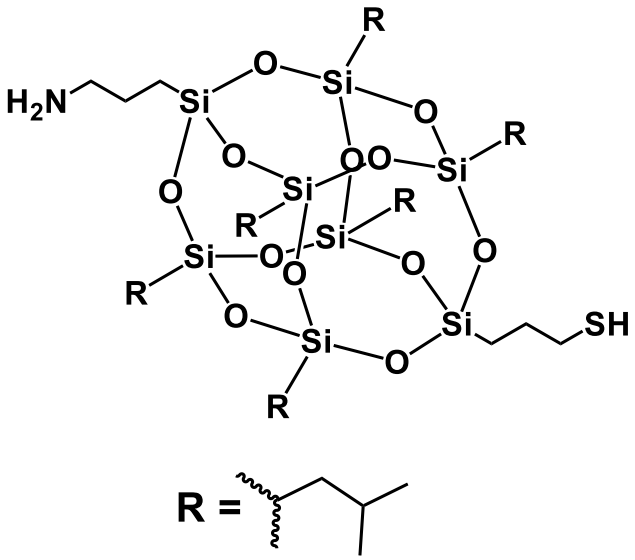

Figure 15. Molecular structure of aminopropyl-hexaisobutyl-mercaptopropyl-POSS.

1.9 Research objective

The main goal of this Thesis is to exploit the chemical properties of POSS to develop new delivery systems. In particular, two novel POSS-Porphyrin molecules containing propylammonium or *N, N', N''*-trimethyl-propylammonium groups are synthesized and characterized. The PDT properties of these POSS-Porphyrin compounds were evaluated. We hypothesize that the positively charged groups on the ammonium moieties will interact electrostatically with the membrane of cancer cell to enhance the PDT efficacy. Moreover, a multifunctional POSS molecule is also synthesized and characterized as part of this Thesis.

Conjugation of POSS to a photosensitizer, such as porphyrin, allows for the synthesis of compounds that play an important for biochemical applications, while avoiding those issues associated with the synthesis and purification of porphyrin-like compounds. POSS is considered a useful tool kit to overcome these difficulties, such as purification through column chromatography, which are troublesome to manage effectively for these compounds, poor yields associated to the struggle in thorough

purification, and ease of functionalization.[114] POSS compounds represent an interesting material not only for their properties but also for their multifunctionality, to which several functional groups can be added, developing useful hybrid platforms that can bear different targeting agents.

1.9.1 Specific Aims

To achieve the goals proposed in this Thesis the following specific aims were pursued:

1. Synthesis and physicochemical characterization of POSS-Porphyrins molecules.
2. Photophysical characterization of POSS-Porphyrins.
3. Synthesis and physicochemical characterization of multifunctional POSS.
4. PDT and PDI evaluation of POSS-porphyrin molecules.

1.9.2 Innovation

This proposal is innovative because: 1) Two novel POSS-Porphyrin molecules are synthesized and characterized in this project. 2) The PDT properties of these POSS-Porphyrin molecules are evaluated for the first time.

CHAPTER 2: EXPERIMENTAL SECTION

2.1 Materials and Methods.

All commercial solvents were of reagent grade or higher and were used as received. All experiments with moisture/air-sensitivity were performed in anhydrous solvents under a nitrogen atmosphere. Column chromatography was performed using silica G60 (70-230 mesh). Trisilanol hepta(isobutyl) POSS was purchased from Hybrid Plastics. (3-aminopropyl) triethoxysilane (APTES) was purchased from Alfa Aesar. Pentahydrate tetramethyl ammonium hydroxide in methanol (TMAOH), *N,N'*-diisopropylethylamine, pyrrole, benzaldehyde, 4-formylbenzoic acid, boron trifluoride etherate ($BF_3 \cdot Et_2O$), p-chloranil, *N*-hydroxysuccinimide (NHS), *N,N'*-dicyclohexylcarbodiimide (DCC), 4-dimethylaminopyridine (DMAP), iodomethane and dimethylanthracence (DMA) were purchased from Sigma-Aldrich. Potassium carbonate was purchased from EMD. Roswell Park Memorial Institute (RPMI 1640), fetal bovine serum (FBS), penicillin-streptomycin (pen-strep), phosphate buffer saline (PBS, 1X), trypsin were purchased from Corning.

NMR spectra were recorded at room temperature in $CDCl_3$ and DMSO-D_6 solvents using a 300 MHz or 500 MHz JEOL NMR spectrometer. Mass spectra were collected by a Voyager Biospectrometry Laser MALDI-TOF, and a spectrometer thermal Scientific MSQ Plus ESI spectrometer. Infrared spectra of liquid and solid sampled were collected in KBr pellets on a Perkin-Elmer 100 IR spectrophotometer, from 4000 to 700 cm^{-1}. UV-vis spectra were recorded on a Cary 300 UV-visible spectrophotometer in a range between 300 and 800 nm. Fluorescence were collected using a Delta Vision Elite Workstation based on an inverted microscope (1X-70; Olympus) equipped with a 100x, 1.4 NA oil immersion lens. Photophysical properties were measured using a RF-5301 PC

spectrofluorophotometer Shimadzu.

2.2 Synthesis and physical characterization of porphyrin derivatives.

2.2.1 Synthesis and Characterization of 5-[4-carboxyphenyl]-10,15,20-triphenylporphyrin (Porphyrin-COOH).

In a 1000-mL round bottom flask CH_2Cl_2 (700 mL) was degassed using nitrogen gas for 30 min. Pyrrole was purified by using a Pasteur pipet with silica gel. This process yields a transparent solution as indication that the polypyrrole has been removed. Purified pyrrole (3.5 mL, 50 mmol), benzaldehyde (3.8 mL, 37.5 mmol), and 4-formylbenzoic acid (1.8768 g, 12.5 mmol), were sequentially added to the flask. Then, boron trifluoride etherate ($BF_3{\cdot}Et_2O$, (0.2 mL, 1.6 mmol) was immediately added to the reaction flask, which was covered with aluminum foil. The solution was stirred at room temperature for 24 h under nitrogen atmosphere. After the completion of the first step, p-chloranil (9.229 g, 37.5 mmol) was added to the flask and the reaction stirred for 19 h at room temperature, in dark conditions. After the reaction completed, the tetrachloro-hydroquinone byproduct was filtered through gravimetric filtration. The solvent was removed with rotary evaporation. The remaining solid was purified using a column chromatography on silica gel (DCM:Ethanol ; 97:3).[115] On the TLC three spots were observed associated to the targeted compound and impurities. The first and second bands eluted first and were orange and yellow, respectively. These corresponded to tetraphenylporphyrin (TPP) impurities. The last band was dark red and corresponded to the targeted compound. After purification, the compound was dried and obtained as a dark purple powder (Yield= 25.3% wt).

^{1}H NMR (500 MHZ, $CDCl_3$, ppm) δ = 8.89 (d, 2H), 8.77 (d, 2H), 8.85 (s, 4H), 8.45 (d, 2H), 8.32 (d, 2H), 8.22 (m, 6H), 7.76 (m, 9H), −2.77 (s, 2H).

FTIR (KBr pellets, cm^{-1}) = 3700-2400 (b, ν_{COOH}), 1692.4 ($s, \nu_{C=O}$), 1600 (s, $\nu_{C=C}$). MALDI: m/z 659.02 $[M-H]^+$ observed; 658.88 calculated.

2.2.2 Synthesis and Characterization of 5-[4-(succinimidyloxycarbonyl)phenyl]-10,15,20-triphenylporphyrin (Porphyrin-NHS)

In a 25-mL round bottom flask, compound 10 (40.0 mg, 0.06 mmol) was reacted with NHS (8.3 mg, 0.07 mmol) in CH_2Cl_2 (10 ml) in the presence of DCC (18.6 mg, 0.09 mmol) and DMAP (7.3 mg, 0.06 mmol). The reaction was stirred at room temperature for 72 h, under nitrogen atmosphere. Once the reaction was completed, the dicyclohexylurea byproduct was filtrated by gravimetric filtration and the CH_2Cl_2 was dried using a rotary evaporation. Finally, the crude product was purified using column chromatography on silica gel (DCM:Methanol ; 9:1).[115] On the TLC two spots were observed associated to the targeted compound and the parent porphyrin. The first band eluting was red and corresponded to Por-COOH. The last band was orange and corresponded to the targeted compound. A dark brown solid was obtained after evaporation of the solvent (Yield= 22.6% wt).

^1H NMR (500 MHZ, $CDCl_3$, ppm) δ = 8.77 (m, 8H), 8.52 (d, 2H), 8.37 (d, 2H), 8.24 (m, 6H), 7.76 (m, 9H), 2.94 (brs, 4H), –2.77 (s, 2H).

FTIR (KBr pellets, cm^{-1}) = 3319 (s, ν_{N-H}), 2916 (m, ν_{C-H}), 2848 (m, ν_{C-H}), 1738 ($s, \nu_{C=O}$), 1603 (s, $\nu_{C=C}$).

MALDI: m/z 755.29 $[M-H]^+$ observed; 755.23 calculated.

2.2.3 Synthesis and Characterization of Octaaminopropyl-POSS (OA-POSS)

To a 50-mL round bottom flask containing methanol (24 mL), APTES (3 mL, 12.82 mmol) was added and the mixture stirred at room temperature for 5 min. After the time has elapsed, HCl (4.05 mL, 37% m/v) was added dropwise in the solution (addition time: 5 min). The reaction stirred at room temperature for 7 days. The product was purified via centrifugation, washing twice with methanol. Compound 8 was stored in the freezer at -4 ºC [113] (Yield = 45.5% wt).

^{1}H NMR (300 MHz, DMSO-D_6, ppm) δ: 8.2 (s, 3H; -NH_3^+), 2.79 (t, 2H; -C$H_2$$NH_3^+$), 1.74 (m, 2H; -$CH_2CH_2CH_2NH_3^+$), 0.74 (t, 2H; Si-C$H_2$).

^{13}C NMR (300 MHz, DMSO, ppm) δ: 40.7 (-C$H_2$$NH_3^+$), 21.3 (-$CH_2CH_2NH_3^+$), 9.2 (Si-C$H_2$); ^{29}Si NMR (500 MHz, DMSO with 0.1% TMS, ppm) δ: -69.2.

FTIR (KBr pellets, cm^{-1}): = 3134 (s, ν_{N-H}), 2944 (s, ν_{C-H}), 2876 (s, ν_{C-H}), 1489 (m, ν_{C-N}), 1098 (s, $\nu_{cage-Si-O-Si}$).

MS (ESI): m/z (%): 441.19 $[M-2H]^{2+}$ observed; 440.75 calculated.

2.2.4 Synthesis and Characterization of Octaaminopropyl-POSS-5-[4-(succinimidyloxycarbonyl) phenyl]-10,15,20-triphenylporphyrin (OA-POSS-Porphyrin)

In a 20-mL round bottom flask compound 8 (9.2 mg, 0.0078 mmol) was mixed in DMSO (10 mL) with DIPEA (7.1 mg, 9.6 μL, 0.0546 mmol). The solution was stirred at room temperature for 30 min. Next, compound 10 (11.8 mg, 0.0156 mmol) was added to the reaction mixture and the reaction stirred at room temperature for 24 h. Once the reaction was completed, the resulting mixture was filtrated with THF and stored in DMSO at -4 ºC. The final product was purified by using column chromatography on silica gel

(DCM:MeOH ; 15:1). On the TLC three spots were observed associated to the targeted compound, the parent porphyrin and impurities. The first band to elute was dark red and corresponded to the targeted compound. The second band was orange and corresponded to Por-NHS. And the last band was black and corresponded to impurities. After purification, compound 11 was dried and obtained as a dark red powder. (Yield = 53.2% wt)

^{1}H NMR (500 MHZ, DMSO-D_6, ppm) δ = 8.77 (m, 8H), 8.22 (m, 10H), 7.76 (m, 9H), 3.24 (t, 2H), 2.75 (t, 14H), 1.65 (m,16H), 0.65 (t, 16H).

^{29}Si NMR (500 MHz, DMSO-D_6, with 0.1% TMS, ppm) δ = -61.2 (one Si-$CH_2CH_2CH_2NH_2$), -69.6 (three Si close to Si-$CH_2CH_2CH_2NH_2$), -70.9 (remaining four Si on the cage).

FTIR (KBr pellets, cm^{-1}): = 3385 (s, ν_{N-H}), 2992.8 (m, ν_{C-H}), 1658.6 (m, $\nu_{C=O}$), 1425 (m, ν_{C-N}), 1279 (m, ν_{Si-C}), 1113 (s, $\nu_{cage-asym-Si-O-Si}$), 899 (m, $\nu_{cage-sym-Si-O-Si}$), 708 (s, ν_{Si-C}). MS (ESI): m/z (%): 217.21 $[M-8H]^{8+}$ observed; 214.09 calculated.

2.2.5 Synthesis and Characterization of Methyl-Octapropylammonium-POSS (MOA-POSS)

The reaction was performed using a previous protocol with slight modifications.[6] In a 50-mL round bottom flask, potassium carbonate (1.4 g, 10 mmol) was dispersed in acetonitrile (25 mL) and compound 8 (500 mg, 0.43 mmol) was added. The solution was sonicated for 30 min at 40 ℃. After then, iodomethane (0.55 mL, 13.5 mmol) was added dropwise to the mixture. The temperature was increased 82 °C to using an oil bath. The solution was stirred for 48 h and was kept under reflux. The final product was obtained after extraction from methanol and washing with acetone (three times). The solvent was removed with a rotary evaporator to afford a white solid (Yield = 63.4 % wt).

^{1}H NMR (500 MHz, D_2O, ppm) δ: 3.19 (m, 2H; -C*H*$_2$N$^+$(CH$_3$)$_3$), 2.97 (s, 9H; -N$^+$(C*H*$_3$)$_3$), 1.74 (m, 2H; -CH$_2$*C*H$_2$CH$_2$N$^+$(CH$_3$)$_3$), 0.45 (t, 2H; Si-C*H*$_2$).

^{13}C NMR (300 MHz, DMSO, ppm) δ: 68.89 (s, -*C*H$_2$N$^+$(CH$_3$)$_3$), 52.97 (s, -CH$_2$N$^+$(*C*H$_3$)$_3$), 16.71 (s, -*C*H$_2$CH$_2$N$^+$(CH$_3$)$_3$), 8.61 (s, Si-*C*H$_2$).

^{29}Si NMR (500 MHz, D_2O, ppm) δ: -67.2 (s, T^3).

FTIR (KBr pellets, cm^{-1}): = 3532 (s, ν_{N-H}), 2926 (m, ν_{C-H}), 1445 (m, ν_{C-N}), 1379 (m, ν_{Si-C}), 1032 (s, $\nu_{cage-asym-Si-O-Si}$), 919 (m, $\nu_{cage-sym-Si-O-Si}$).

MS (ESI): m/z (%): 153.89 [M-2H]$^{2+}$ observed; 155.00 calculated.

2.2.6 Synthesis and Characterization of Methyl-Octapropylammonium-POSS-5-[4-(succinimidyloxycarbonyl)phenyl]-10,15,20-triphenylporphyrin (MOA-POSS-Porphyrin)

The reaction was carried out following the previously described procedure with slight modifications.[6] In a 10-mL round bottom flask, potassium carbonate (0.1 g, 0.724 mmol) was dispersed in acetonitrile (5 mL) and compound 11 (30 mM, 6 mL mg, 0.18 mmol) was added. The solution was sonicated for 30 min at 40 ℃. After then, iodomethane (1.1 mL, 27 mmol) was added dropwise to the mixture. The temperature was increased 82 °C to using an oil bath. The solution was stirred for 48 h and was kept under reflux. The final product was obtained after extraction from methanol and washing with acetone (three times). The solvent was removed with a rotary evaporator to afford a white solid (Yield = 81.4 % wt).

^{1}H NMR (500 MHZ, DMSO-D_6, ppm) δ = 8.67 (m, 8H), 8.48 (d, 2H), 8.32 (d, 2H), 8.25 (m, 6H), 7.65 (m, 9H), 3.24 (m, 16H), 2.94 (s, 63H), 1.93 (m, 16H), 0.39 (t, 16H).

^{29}Si NMR (500 MHz, DMSO-D_6, with 0.1% TMS, ppm) δ = -61.2 (one Si-$CH_2CH_2CH_2NH_2$), -69.6 (three Si close to Si-$CH_2CH_2CH_2NH_2$), -70.9 (remaining four Si on the cage).

FTIR (KBr pellets): = 3323 (s, ν_{N-H}); 2872 (m, ν_{C-H}); 1660 (s, ν_{C-O}); 1428 (m, ν_{C-N}); 1372 (m, ν_{Si-C}); 1017 (s, $\nu_{cage-asym-Si-O-Si}$); 931 (m, $\nu_{cage-sym-Si-O-Si}$).

2.2.7 Synthesis and Characterization of Aminopropyl-Heptaisobutyl-POSS (AP-IB-POSS)

Heptaisobutyltrisilanol (2.00 g, 2.5 mmol) was mixed in a 25-mL round bottom flask with ethanol (12 mL) and tetraethylammonium hydroxide (40.0 μL, 35% in H_2O). APTES (1.14 mL, 5.0 mmol) was added to the reaction vessel and the solution magnetically stirred at 40.0 ℃ for 60h. Upon completion, the final product was purified via centrifugation and washed twice with ethanol, twice with acetonitrile and then twice with methanol. AP-IB-POSS dried overnight under high-vacuum and was stored in the freezer at -4 ℃. (Yield = 89%)

^{1}H NMR (300 MHz, $CDCl_3$, ppm) δ: 0.85 (m, 16H; CH_2-Si), 0.99 (d, 42H; -CH_3), 1.53 (m, 4H; -CH_2C$H_2$$CH_2NH_2$), 1.85 (m, 7H; -$CH_2CH$($CH_3$)$_2$), 2.69 (t, 2H, -C$H_2$$NH_2$).

^{13}C NMR (300 MHz, $CDCl_3$, ppm) δ: 44.82 (s, -C$H_2$$NH_2$), 25.84 (s, -C$H_3$), 23.95 (s, -$CH_2CH_2$$CH_2$$NH_2$), 22.57 (s, -$CH_2CH$($CH_3$)$_2$) 9.30 (s, -C$H_2$-Si).

^{29}Si NMR (500 MHz, $CDCl_3$ with 0.1% TMS, ppm) δ: -66.7 (one Si-$CH_2CH_2CH_2NH_2$), -67.5 (three Si close to Si-$CH_2CH_2CH_2NH_2$) and -67.3 (remaining four Si on the cage).

FTIR (KBr pellets): = 3659 (s, ν_{N-H}), 2967 (s, ν_{C-H}), 1398.8 (m, ν_{C-N}), 1233 (m, ν_{Si-C}), 1071 (s, $\nu_{cage-asym-Si-O-Si}$), 908 (m, $\nu_{cage-sym-Si-O-Si}$).

MALDI (m/z): 874.58 [calculated for $[M-H]^+$] 875.12.

2.2.8 Synthesis and Characterization of Partially Condensed Trisilanol Aminopropyl-hexaIsobutyl-POSS (AP-hexaIB-POSS).

AP-IB-POSS (1.00 g, 1.65 mmol), along with 35%TEAOH (0.5 ml, 1.69 mmol) and THF (25 ml) were charged into a 50-mL round-bottomed flask. The reaction was magnetically stirred for 7h under air atmosphere and the temperature was slowly increased to reflux at 80 ℃. Upon completion, the reaction was stopped, and it was cooled off. Once the flask was at T_{room}, the solution was neutralized with few ml of 2M HCl, and then filtered by suction filtration to remove the salts formed. The solution was dried under high vacuum overnight and the final product was purified by methanol extraction to provide a yellowish gel (Yield = 67.6%).[34]

^{1}H NMR (500 MHz, $CDCl_3$, ppm) δ: 0.54 (m, 14H; CH_2-Si), 0.90 (d, 36H; -CH_3), 1.30 (m, 4H; -$CH_2CH_2CH_2NH_2$), 1.80 (m, 6H; -$CH_2CH(CH_3)_2$), 3.32 (t, 2H, -CH_2NH_2).

^{13}C NMR (300 MHz, $CDCl_3$, ppm) δ: 52.93 (s, -CH_2NH_2), 30.40 (s, -$CH_2CH_2CH_2NH_2$), 25.86 (s, -CH_3), 23.89 (s, -$CH_2CH(CH_3)_2$), 22.48 (s, -$CH_2CH(CH_3)_2$) 7.58 (s, CH_2-Si).

^{29}Si NMR (500 MHz, $CDCl_3$ with 0.1% TMS, ppm) δ: -58.9 (three Si-OH), -67.5 (one Si-$CH_2CH_2CH_2NH_2$) and -68.3 (remaining three Si on the cage).

FTIR (KBr pellets): = 3363 (s, ν_{O-H}), 2956 (m, ν_{C-H}), 1383 (m, ν_{C-N}), 1231 (m, ν_{Si-C}), 1095, 1030 (s, $\nu_{cage-asym-Si-O-Si}$).

MALDI (m/z): 792.29 [calculated for $[M-H]^+$] 792.43.

2.2.9 Synthesis and Characterization of Aminopropyl-hexaIsobutyl-Mercaptopropyl-POSS (AP-hexaIB-MP-POSS)

Briefly, AP-hexaIB-MP-POSS (214.0 mg, 0.270 mmol) was mixed in a 10-mL round bottom flask with THF (5 mL) and MPTES (262 mg, 1.1 mmol). The reaction was magnetically stirred at T_{room} for 48h. Once the reaction was stopped, the mixture was dried under vacuum overnight and the final product was purified by methanol extraction, to afford a white solid. (Yield = 75.2%)

^{1}H NMR (500 MHz, $CDCl_3$, ppm) δ: 0.54 (m, 16H; C*H*$_2$-Si), 0.82 (d, 36H; -CH_3), 1.25 (m, 3H; -SH,-NH_2), 1.50-1.72 (m, 10H; -$CH_2CH(CH_3)_2$, -$CH_2CH_2CH_2SH$, $CH_2CH_2CH_2NH_2$), 2.52 (t, $CH_2CH_2CH_2$SH), 3.32 (t, 2H, -C*H*$_2$$NH_2$).

^{13}C NMR (300 MHz, $CDCl_3$, ppm) δ: 52.93 (s, -*C*H_2NH_2), 30.31 (s, -CH_2CH_2*C*H_2SH, -CH_2CH_2*C*H_2NH_2), 25.92 (s, -*C*H_3), 23.88 (s, -CH_2*C*H(CH_3)$_2$), 22.48 (s, -CH_2*C*H_2CH_2SH) 9.58 (s, *C*H_2-Si).

^{29}Si NMR (500 MHz, $CDCl_3$ with 0.1% TMS, ppm) δ: -66.8 (one Si-$CH_2CH_2CH_2$SH), -67.1 (one Si-$CH_2CH_2CH_2NH_2$), -67.5 (three Si on the cage closer to the Si bearing the mercaptopropyl group), 67.9 (three Si on the cage closer to the Si bearing the aminopropyl group).

FTIR (KBr pellets): = 2975 (m, $\nu_{C\text{-}H}$), 1390 (m, $\nu_{C\text{-}N}$), 1231 (m, $\nu_{Si\text{-}C}$), 1075 (s, $\nu_{cage\text{-}asym\text{-}Si\text{-}O\text{-}Si}$), 950 (m, $\nu_{cage\text{-}sym\text{-}Si\text{-}O\text{-}Si}$).

MALDI (m/z): 891.27 [calculated for $[M\text{-}H]^+$] 892.12.

2.3 Photophysical Characterization of Porphyrins and Porphyrin based materials

2.3.1 UV-vis and Fluorescence

The spectra were recorded from 300 nm to 800 nm, and the absorbance relative to the porphyrin derivatives was measured at 515 nm. Spectra were recorded against solvent blanks (DMSO) at concentrations of 10^{-4} M, in quartz cuvettes (1 cm path length). These were acid washed and rinsed with deionized water.

2.3.2 Singlet Oxygen Quantum Yields

Stock solutions in DMF (10^{-4} M) of porphyrin or porphyrin based compounds were prepared in volumetric flasks and diluted to achieve sample concentrations of 10^{-6}. The singlet oxygen quantum yields were determined through an indirect method using dimethylanthracence (DMA) as the singlet oxygen probe. Several solutions containing DMF were air saturated and prepared with DMA (50 μM) and the PS ($\sim$ 5 μM), and then were covered with aluminum foil to avoid any premature quenching. Quartz cuvettes (1 cm x 1 cm) were filled with 1 mL of the solution and placed in a Spectrofluorophotometer (xenon lamp, Shimadzu RF-5301 PC) and irradiated at 515 nm, for 600s. The absorbance decay of DMA was monitored at 380 nm. (Equation 1).

$$\Phi\Delta,S = \Phi\Delta,R \cdot \frac{mS}{mR} \cdot \frac{1-10^{-absReference}}{1-10^{-absSample}} \qquad \text{Equation (1)}$$

where $\Phi\Delta$,S is the singlet oxygen quantum yield of the sample, and m is the slope of the plotted data relative to the area of the emission peak against the absorption of the reference.[116]

2.3.4 Fluorescence Quantum Yield

The fluorescence quantum yields were measured according to the comparative method described by the following equation.

$$\Phi F,\text{Sample} = \Phi F,\text{Reference} \cdot \frac{mSample}{mReference} \cdot \frac{n^2 sample}{n^2 reference} \qquad \text{Equation (2)}$$

where ΦF,Reference represents the fluorescence quantum yield of a fluorophore reference, m is the slope of the plotted data relative to the area of the emission peak against the absorption of the fluorophore, whereas n is the refractive index.[117] The fluorescence quantum yields ΦF,Sample of the porphyrin derivatives where taken in DMSO solution of concentrations ranging from 3 μM to 15 μM, at an excitation wavelength of 520 nm, with the excitation and emission slits of 2 nm. Tetraphenylporphyrin was used as a reference with a fluorescence quantum yield of 0.12 in benzene.[116]

2.4 Partition coefficients

The partition coefficient of porphyrin derivatives was measured in an *n*-butanol/water mixture, and then correlated with corresponding values in *n*-octanol/water using a reported calibration curve.[118] Distilled water and butanol were thoroughly mixed for 24 h at 25 ℃ to achieve solvent saturation in both phases. Then, the porphyrin derivatives in bulk were added to the mixture and the phases separated through a separatory funnel. The UV-vis absorbance of the compounds in water and *n*-butanol was recorded at 515 nm.

$$\log P_{BW} = \log \left(\frac{Ab}{Aw} \cdot \frac{Vw}{Vb}\right) \qquad \text{Equation (3)}$$

Where A_b is the absorbance of *n*-butanol, A_W, the absorbance of water, V_W the volume of water and V_b the volume of *n*-butanol. The partition coefficient of porphyrin

derivatives in *n*-octanol/water was obtained with equation 4, according to the calibration curve previously mentioned for *n*-octanol/water.[118]

$$\log P_{OW} = -0.54 + 1.55 \cdot \log P_{BW} \qquad \text{Equation (4)}$$

2.5 Cell culture

MDA-MB-231, a human invasive TNBC cell line, was purchased from American Type Culture Collection (ATCC). Breast cancer cells were cultured in RPMI 1640 medium (supplemented with 10% FBS, 1% pen-step) at 37 °C with 5% CO_2 atmosphere. The culture media was changed every other day. All cell cultures were maintained in 25 cm^2 or 75 cm^2 cell culture flasks and the cells were passaged at 70-80% confluency every 2-4 days. The cell survival was tested by the CellTiter 96® AQueous Assay (MTS assay). The absorbance was measured at a wavelength of 490 nm in a plate reader Multiskan FC.

2.6 *In vitro* cyto- and phototoxicity

The phototoxicities of 5-(4-carboxyphenyl)-10,15,20-triphenylporphine, OA-POSS-Porphyrin and MOA-POSS-Porphyrin were tested by using the MTS assay. For this study, MDA-MB-231 cells were seeded in a 96-well plate at a density of 5 x 10^3 cells per well in 100 µL of complete media and incubated at 37 °C in 5% CO_2 atmosphere for 24 h. After removing the cell culture medium, OA-POSS-Porphyrin and MOA-POSS-Porphyrin, at different concentrations (0.01 - 0.5 µM), were prepared in cell media from a stock solution in DMSO with a final volume of the organic solvent not larger than 1 % vol. After 48 h of incubation in the presence of OA-POSS-Porphyrin and MOA-POSS-Porphyrin, the culture media was removed, and the cells were washed twice with phosphate buffer solution. MDA-MB-231 cells were illuminated with the red light (630 nm) at a fluence rate

of 24.5 mW/cm^2 for 20 min. Control experiments were maintained in the same conditions, but in the dark for the same interval of time. After irradiation, the media was replaced, and the cells were allowed to grow for an additional 24 h. To measure the phototoxic and cytotoxic (dark toxicity) effects of the experiments above described, the treated MDA-MB-231 cells were subjected to cell viability assay using the Cell Titer 96 Aqueous solution assay. To perform the assay, the cell media was removed, and the cells were washed twice with phosphate buffer solution (PBS). Fresh media (100 µL) together with 20 µL of CellTiter was added into each well and incubated for 2-3 h at 37 °C in 5% CO_2 atmosphere. Cell viability (%) was calculated as follows: viability = $(A_{sample}/A_{control}) \times 100\%$, where A_{sample} and $A_{control}$ denote absorbance values of the sample and control wells measured at 490 nm, respectively. The results are reported as the average ± SD of three experiments. The EC_{50} values are determined using GraphPad Prism (v8.1.2, La Jolla California, CA, USA) fitting the viability data to a sigmoidal curve mathematical model.

2.7 Statistical Analysis

All the data in this Thesis are represented as mean ± SD unless mentioned otherwise. To compare Φ_Δ values, the statistical analysis was performed with one-way ANOVA using Tukey's multiple comparison test. For the singlet oxygen quantum yields measurements GraphPad prism was used (n = 3). For the cell viability studies, GraphPad prism was used to calculate the EC_{50} values (n = 6). All the statistical analyses were performed using GraphPad Prism (v8.2.0 for Windows) with $\alpha = 0.05$ and reported as stars assigned to the p-values; ****$p \leq 0.0001$, ***$p \leq 0.001$, **$p \leq 0.01$, *$p \leq 0.05$, and ns $p > 0.05$.

CHAPTER 3: RESULTS AND DISCUSSIONS

Two novel POSS-Porphyrin systems, OA-POSS-Porphyrin and MOA-POSS-Porphyrin have been synthesized to probe their efficacy in PDT. The functional groups bound to the POSS cage are aminopropyl moieties, and methylated propylammonium groups. Our hypothesis is that by tuning the substituents on the cage their physical and chemical properties, and finally their cellular interaction will change accordingly. Furthermore, singlet oxygen and fluorescence quantum yields have been determined to understand the energy pathways the molecules undertake, once irradiated. To grasp the whole picture, partition coefficients have been measured to see whether the addition of a POSS cage, bearing hydrophilic groups, changes the hydrophilicity in porphyrin for *in vitro* studies.

Finally, A pH-dependent molecule such as OA-POSS-Porphyrin should undergo less cellular uptake compared to MOA-POSS-Porphyrin, which has a permanent positive charge on its periphery, and can interact strongly with the negatively charged bilayer phospholipid membrane.

3.1 Synthesis and Characterization of OA-POSS-Porphyrin

3.1.1 Synthesis and Characterization of 5-[4-carboxyphenyl]-10,15,20-triphenylporphyrin (Porphyrin-COOH).

The synthesis of hybrid POSS-Porphyrin system was obtained by chemical conjugation of OA-POSS and Porphyrin-NHS. Firstly, 5-[4-carboxyphenyl]-10,15,20-triphenylporphyrin (Porphyrin-COOH) was synthesized through a cyclization reaction involving pyrrole, benzaldehyde and 4-formylbenzoic acid under catalytic amounts of

borontrifluoride etherate. The compound obtained was subsequently reduced using p-Chloranil. The reaction pathway follows the mechanism shown (**Figure A1**).

The formation of the porphyrin system follows a series of electron transfers between pyrrole, benzaldehyde and 4-formylbenzoic acid, where borontrifluoride etherate acts as a Lewis acid to catalyze the reaction. In the first step of the mechanism, the carbonyl group-bearing the oxygen shares a pair of electrons with borontrifluoride, increasing its electrophilicity. Pyrrole then acts as a nucleophile and attacks the electrophilic carbonyl group through a series of electron transfers. In the following step, the boron oxide derivative accepts a proton to generate a good leaving group and re-establishing aromaticity in the system. This facilitates the attack of another pyrrole to the electrophilic center. These steps are repeated to eventually form a non-aromatic macrocycle. The oxidation of said macrocycle generates the fully conjugated porphyrin ring.

The successful synthesis of Porphyrin-COOH was confirmed with ^{1}H NMR, FTIR and MALDI-TOF. ^{1}H NMR depicted the characteristic coupling pattern associated to the hydrogens on the β-pyrrole at 8.89-8.77 ppm (doublet and singlet, respectively); the chemical shifts corresponding to the hydrogens on the phenyl substituent at 7.76–7.70 and 822–8.18 ppm, and finally hydrogens on the carboxy phenyl groups showing up at 8.45 and 8.32 ppm (**Figure 16**). Additionally, the FT-IR spectra showed the stretching vibrations corresponding to the hydroxyl stretch of a carboxylic acid between 3700-2400 cm^{-1}, the carbonyl stretching vibration at 1692.4 cm^{-1}, and the carbon-carbon stretching vibration associated to sp^2 carbons at 1600 cm^{-1}. Finally, MALDI-TOF was used to determine the molecular ion for the compounds identified at 658.88 m/z.

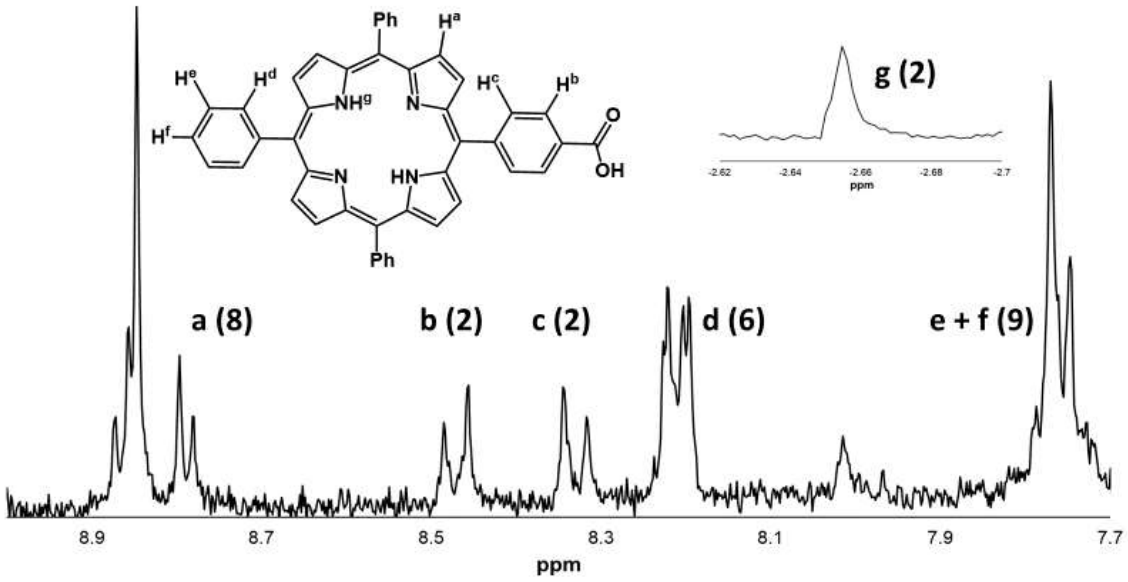

Figure 16. ^{1}H NMR of Por-COOH shows the eight pyrrole hydrogens appear between 8.89 and 8.77 ppm, the hydrogens on the carboxyphenyl substituent appearing at 8.45 and 8.32 ppm, according to their distance from the carboxy group, the protons on the phenyl groups closest to the porphyrin ring appear between 8.22 and 8.18 ppm, and finally the last protons on the phenyl groups showing up between 7.76 and 7.70 ppm.

3.1.2 Synthesis and Characterization of 5-[4-(succinimidyloxycarbonyl)phenyl]-10,15,20-triphenylporphyrin (Porphyrin-NHS)

The synthesis of Porphyrin-NHS was carried out through NHS chemistry with 4-dimethylaminopyridine (DMAP) and *N-N'*-dicyclohexylcarbodiimide (DCC) as catalysts, according to the following mechanism (**Figure A4**). Initially, DMAP deprotonates Porphyrin-COOH to generate a reactive nucleophile, which attacks the carbon on the DCC allene analog. The negatively charged nitrogen on DCC will abstract a proton from the protonated base. The hydroxyl group on NHS will then nucleophilicly attack the carbonyl unit on Porphyrin-COOH to form a tetrahedral transition state, encouraging DCC to leave

as the best leaving group, forming dicyclohexylurea and the desired Porphyrin-NHS.

The successful synthesis of Porphyrin-NHS was confirmed with ^{1}H NMR, FTIR and MALDI-TOF. ^{1}H NMR depicted the characteristic coupling pattern associated to the hydrogens on the β-pyrrole rings as one doublet and one singlet at 8.90-8.77 ppm (doublet and singlet respectively); the chemical shifts corresponding to the hydrogens on the phenyl substituent at 7.76–7.72 and 8.24–8.20 ppm, the hydrogens on the ester phenyl group appearing at 8.37 and 8.52 ppm. Finally, the signal corresponding to the NHS aliphatic region appear at 2.94 ppm. The FT-IR spectra showed the stretching vibrations corresponding to the carbonyl at 1737 cm^{-1}, and the carbon-carbon stretching vibration associated to sp^2 carbons at 1603 cm^{-1}. Additionally, MALDI-TOF was used to determine the molecular ion for the compounds identified at 755.29 m/z (**Figure 17**).

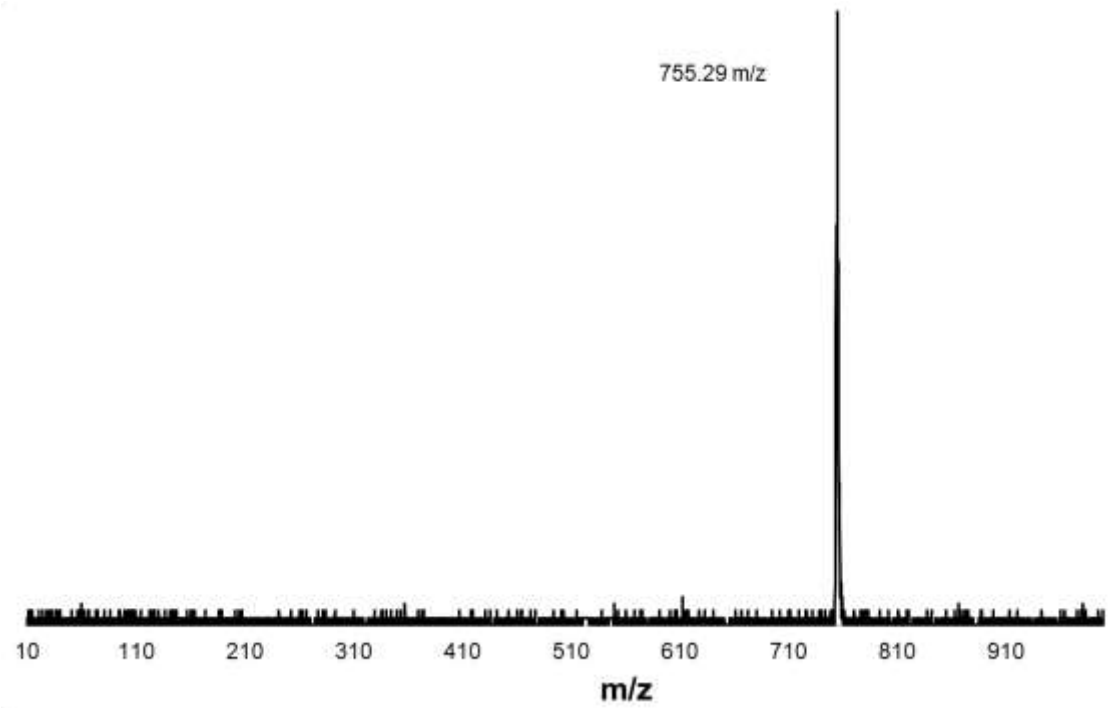

Figure 17. MALDI-TOF of Porphyrin-NHS. The mass calculated for the molecule is 755.23 m/z and the molar mass obtained is 755.29 m/z.

3.1.3 Synthesis and characterization of octaaminopropyl-POSS (OA-POSS).

OA-POSS was synthesized through a hydrolytic condensation of aminopropyltriethoxy silane (APTES), in the presence of hydrochloric acid, as shown from the following reaction mechanism (**Figure A7**). In acidic conditions the free amine is protonated readily followed by the ethoxy groups on the organo silane moiety. The water present in solution nucleophilicly attacks the Si center, encouraging the protonated ethoxy group to leave. The presence of a hydroxyl group on the molecule allows the formation of hydroxyl bridges among other organosilanes, which eventually forms the final cage.

The successful synthesis of OA-POSS was confirmed with ^{1}H, ^{13}C, ^{29}Si NMR, FTIR and MS-ESI. ^{1}H NMR showed the shifts attributed to the aminopropyl moiety, where the methylene unit closest to the Si atom appears at 0.74 ppm, the next unit at 1.74 ppm and the last

unit at 2.79 ppm. In ^{13}C NMR the aminopropyl group appeared at 9.2 ppm, 21.3 ppm and 40.7 ppm for the corresponding carbons in increasing distance from the Si atom. ^{29}Si NMR was used to confirm the integrity and symmetry of the cage. As depicted in the spectrum, only one signal appears at -69.2 ppm indicating symmetry in the compound (**Figure 18**). This is characteristic of POSS cages synthesized through a hydrolytic condensation from an organo silane precursor. Furthermore, this value agrees with the literature to that of an octameric cage.[14, 17-20, 44, 81, 113, 119] Vibrational frequencies are an important tool to analyze the integrity and effective synthesis of POSS compounds. In FT-IR the characteristic stretching vibration of the Si-O-Si framework was seen at 1098 cm^{-1} (s, $\nu_{cage\text{-}asym\text{-}Si\text{-}O\text{-}Si}$), further confirming the formation of a siloxane cage. Finally, ESI was employed where a signal at 441.19 m/z was seen corresponding to two positive charges present on the cage.

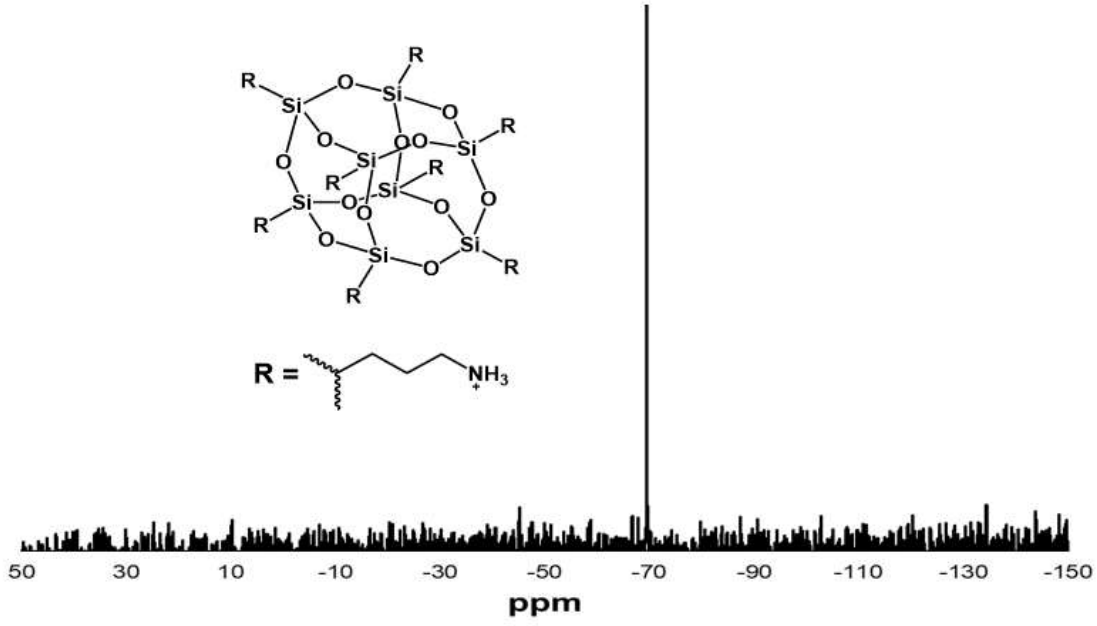

Figure 18. ^{29}Si NMR of OA-POSS shows one signal corresponding to one magnetically and chemically equivalent Si atom. This is a significant confirmation as it corroborates the integrity of the cage.

3.1.4 Synthesis and Characterization of Octaaminopropyl-POSS-5-[4-(succinimidyloxycarbonyl)phenyl]-10,15,20-triphenylporphyrin (OA-POSS-Porphyrin)

The synthesis of octaaminopropyl-POSS-5-[4-(succinimidyloxycarbonyl)phenyl]-10,15,20-triphenylporphyrin (OA-POSS-Porphyrin) was performed through the esterification reaction of previously synthesized OA-POSS and Porphyrin-NHS in the presence of *N-N'*-diisopropylethylamine (DIPEA), according to the following mechanism (**Figure A12**). The free amine on the POSS cage attacks the carbonyl unit on Porphyrin-NHS to form a tetrahedral intermediate where NHS acts as the best leaving group. Once deprotonated, NHS leaves and abstracts a proton from the protonated amide on the POSS-Porphyrin system to yield the desired product.

The successful synthesis of OA-POSS-Porphyrin was confirmed with ^{1}H, ^{29}Si NMR, FTIR and MS-ESI. ^{1}H NMR showed the characteristic shifts attributed to the aminopropyl moiety, where the methylene unit closest to the Si atom appears at 0.65 ppm, the next unit at 1.65 ppm and the last unit at 2.75 ppm. Additionally, the methylene unit next to the amide bond is shifted to 3.24 ppm. The aromatic region, corresponding to the porphyrin, reported the same pattern previously described. Furthermore, ^{29}Si NMR was used to confirm the integrity and symmetry of the cage. Three signals appear at -61.2, -69.6 and -70.9 ppm, in accordance to the distance from the silicon atom bearing the porphyrin derivative (**Figure 19**). In FTIR the characteristic stretching vibration of the Si-O-Si framework was seen at 1113 cm^{-1} (s, $\nu_{\text{cage-asym-Si-O-Si}}$), further confirming the integrity of the siloxane cage. Finally, ESI was employed to characterize OA-POSS-Porphyrin. A peak at 214.09 m/z was seen corresponding to seven positive charges present on the cage.

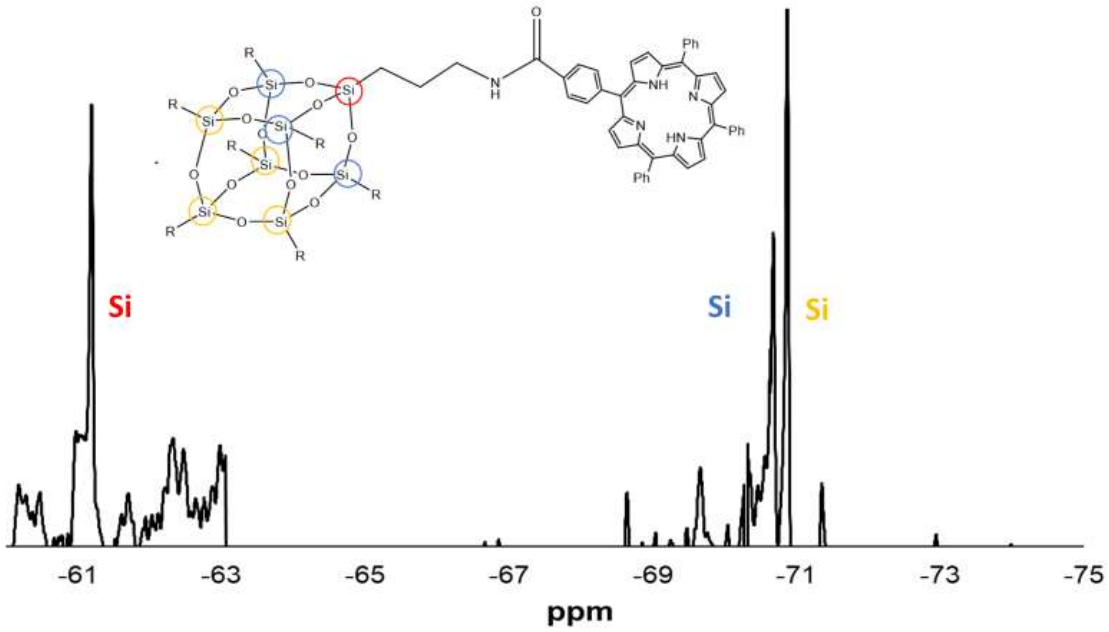

Figure 19. ^{29}Si NMR of OA-POSS-Porphyrin shows three signals corresponding to three inequivalent silicon atoms. This corroborates the effective conjugation of Por-NHS with OA-POSS.

3.2 Synthesis and Characterization of MOA-POSS-Porphyrin

3.2.1 Synthesis and Characterization of Methyl-Octapropylammonium-POSS (MOA-POSS).

The synthesis of Methyl-Octapropylammonium-POSS (MOA-POSS) was afforded via a methylation reaction of previously synthesized OA-POSS using excess methyl iodide and potassium bicarbonate as a catalyst (**Figure A16**). Briefly, potassium bicarbonate acts as a base and catalyst to deprotonated the ammonium sites on the octa-ammoniumpropyl-POSS cage that would inhibit further reactions. After deprotonation, the free amine undergoes successive alkylation from the excess methyl iodide present in solution.

The successful synthesis of MOA-POSS was confirmed with ^{1}H, ^{13}C, ^{29}Si NMR, FT-IR and MS-ESI. ^{1}H NMR showed the shifts attributed to the methylated aminopropyl moiety, where the methylene unit closest to the Si atom appears at 0.45 ppm (shifted from the methylene

unit of an aminopropyl moiety with a free amine), the next unit at 1.74 ppm and the last methylene shifts significantly compared to OA-POSS to 3.19 ppm. Furthermore, the methyl groups show up at 2.97 ppm (**Figure 20**). Based on the ^{13}C NMR, the methylene units appear at 8.61 ppm, 16.71 ppm and 68.89 ppm, whereas the methyl units exhibit a strong signal at 52.97 ppm. Using ^{29}Si NMR only one signal was observed at -67.2 ppm indicating symmetry in the compound, in accordance with the literature.[23] FTIR depicted the characteristic stretching vibration of the Si-O-Si framework was seen at 1032 cm^{-1} (s, $\nu_{\text{cage-asym-Si-O-Si}}$), further confirming the formation of a siloxane cage. Finally, ESI-MS shows a peak at 155.00 m/z corresponding to eight 8 positive charges.

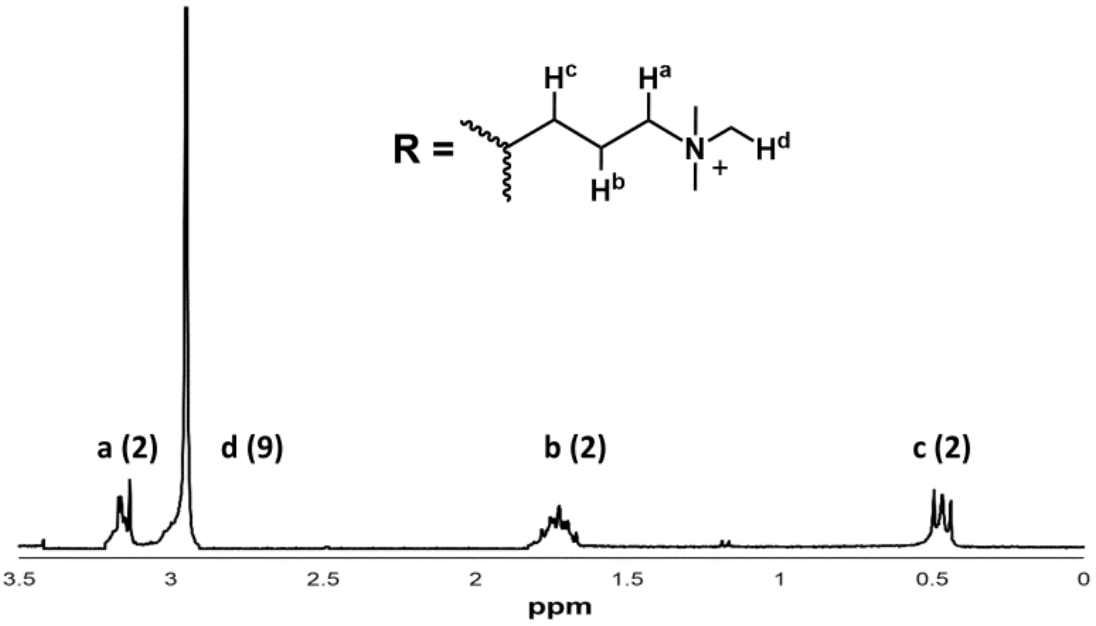

Figure 20. ^{1}H NMR of MOA-POSS shows the methylene unit closest to the Si atom appears at 0.45 ppm the next unit at 1.74 ppm and the last methylene at 3.19 ppm. Furthermore, the methyl groups show up at 2.97 ppm.

3.2.2 Synthesis and Characterization of Methyl-Octapropylammonium-POSS-5-[4-(succinimidyloxycarbonyl)phenyl]-10,15,20-triphenylporphyrin (MOA-POSS-Porphyrin)

The synthesis of MOA-POSS-Porphyrin was afforded via a methylation reaction of previously synthesized OA-POSS-Porphyrin using methyl iodide and potassium carbonate as a catalyst (**Figure A21**).

The successful synthesis of MOA-POSS-Porphyrin was confirmed with ^{1}H and ^{29}Si NMR, FTIR. The ^{1}H showed the shifts attributed to the propyl ammonium moiety, where the methylene unit closest to the Si atom appears at 0.39 ppm, the next unit at 1.93 ppm and the last unit at 3.24 ppm. The methyl substituents, as seen earlier, appear at 2.94 ppm. The aromatic region, corresponding to the porphyrin, reported the same pattern previously described. ^{29}Si NMR was used to confirm the integrity and symmetry of the cage. Three signals appear at -61.2, -69.6 and -70.9 ppm, in accordance to the distance from the silicon atom bearing the porphyrin derivative. Using FTIR the characteristic stretching vibration of the Si-O-Si framework was observed at 1017 cm^{-1} (s, $\nu_{\text{cage-asym-Si-O-Si}}$), further confirming the integrity of the siloxane cage. (**Figure 21**). ESI was not obtained due to possible fragmentation of the molecule during the measurement.

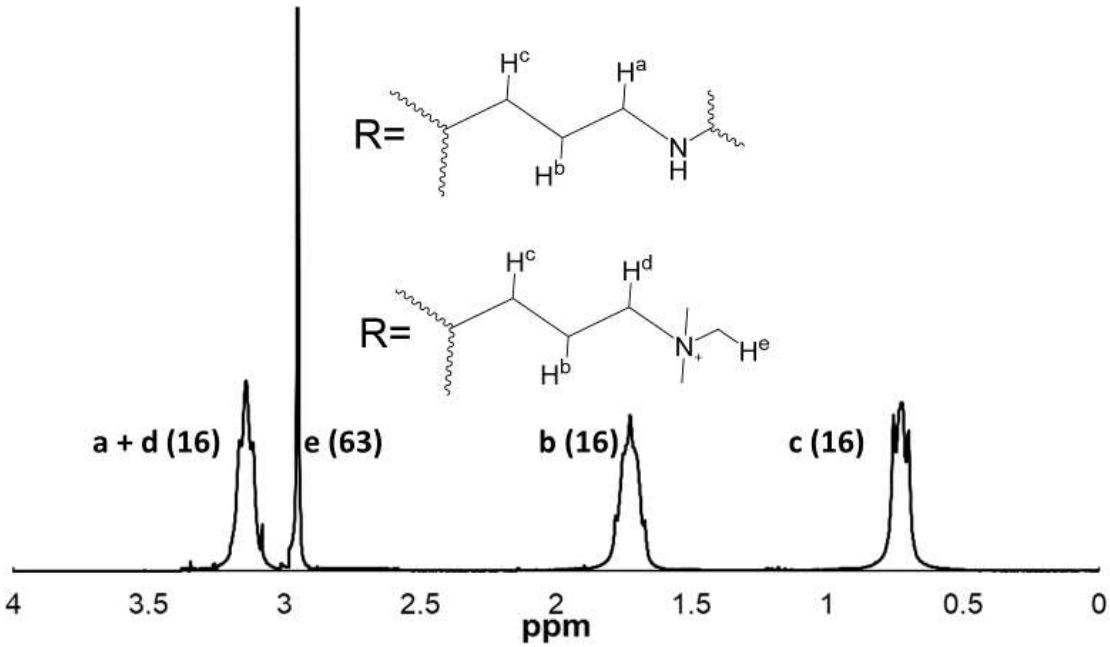

Figure 21. Aliphatic region of the ^{1}H NMR of MOA-POSS-Porphyrin. This shows the shifts attributed to the propyl ammonium moiety, where the methylene unit closest to the Si atom appears at 0.39 ppm, the next unit at 1.93 ppm and the last unit at 3.24 ppm. The methyl substituents, as seen earlier, appear at 2.94 ppm.

3.3 Synthesis and characterization of trifunctional-POSS.

3.3.1 Synthesis and characterization of aminopropyl-heptaisobutyl-POSS (AP-IB-POSS)

The synthesis of aminopropyl-heptaisobutyl-POSS (AP-IB-POSS) was carried out through a corner capping reaction, with aminopropyltrimethoxy silane (APTMS) of previously purchased trisilanol-isobutyl-POSS, under catalytic amounts of tetraethylammonium hydroxide (TEAOH) (**Figure A24**). The hydroxyl sites on the cage are deprotonated by TEAOH to activate an oxygen anion, which nucleophilicly attacks APTMS leaving behind a methoxide ion to afford the final product.

The successful synthesis of AP-IB-POSS was confirmed using ^{1}H, ^{13}C and ^{29}Si NMR, FTIR and MALDI. The ^{1}H NMR exhibited the peaks corresponding to the isobutyl moiety and the amino propyl group; specifically, the methyne unit appears at 1.85 ppm and the methyl groups at 0.99 ppm. Furthermore, the methylene units adjacent to the cage appear for both functional groups at 0.85 ppm. The next two methylene units on the aminopropyl substituent

appear at 1.53 and 2.69 ppm, in order of distance from the cage. The ^{13}C NMR shows the methylene units next to the free amine at 44.82 ppm, the next methylene unit in the aminopropyl substituent at 23.95 ppm, the methyl groups at 25.84 ppm, the methyne unit at 22.57 ppm and finally the methylene units closer to the cage at 9.30 ppm. ^{29}Si NMR showed three distinct peaks at -66.7 ppm, related to the silicon bearing the aminopropyl moiety, -67.5 ppm related to the silicon atoms one bond away from the previous silicon, and -67.3 ppm related to the silicon atoms two or more bonds away from the silicon bearing the different substituent. In FT-IR the characteristic stretching vibration of the Si-O-Si framework was seen at 1071 cm^{-1} (s, $\nu_{cage\text{-}asym\text{-}Si\text{-}O\text{-}Si}$), further confirming the formation of a siloxane cage (**Figure 22**). Finally, MALDI was employed and a peak at 874.58 m/z was observed.

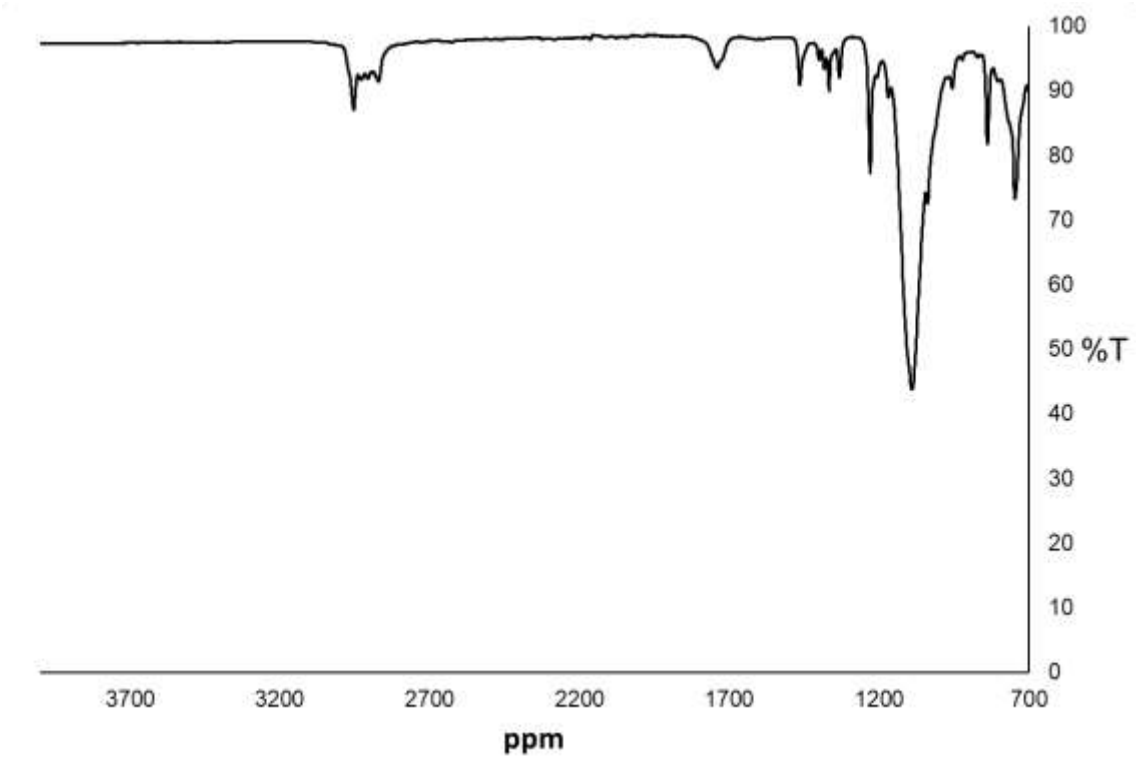

Figure 22. FTIR of AP-IB-POSS. The Si-O-Si stretching vibration is evident at 1071 cm^{-1}, which indicates the formation of a condensed cage.

3.3.2 Synthesis and Characterization of Partially Condensed Trisilanol Aminopropyl-hexaIsobutyl-POSS (AP-hexaIB-POSS).

The synthesis of aminopropyl-hexaisobutyl-POSS (AP-hexaIB-POSS) was carried out through a corner opening reaction of previously synthesized AP-IB-POSS under reflux, using catalytic amounts of TEAOH (**Figure A29**). Previously synthesized AP-IB-POSS was reacted under reflux at 85 ℃ with TEAOH. These conditions allowed the hydroxide ions to damage the Si/O framework by attacking the cage at the silicon atom. It is still unclear why the corner that is being opened is the one opposite to the most reactive functional group on the cage.[14]

The successful synthesis of AP-hexaIB-POSS was confirmed using ^{1}H, ^{13}C and ^{29}Si NMR, FT-IR and MALDI. The ^{1}H NMR exhibited the peaks corresponding to the isobutyl moiety and the amino propyl group; specifically, the methyne units appear at 1.80 ppm with six hydrogens (compared to the seven from the AP-IB-POSS), and the methyl groups at 0.90 ppm, with 36 hydrogens. Furthermore, the methylene units adjacent to the cage appear for both functional groups at 0.54 ppm. The next two methylene units of the aminopropyl substituent appear at 1.30 and 3.32 ppm, in order of distance from the cage. The ^{13}C NMR shows the methylene units next to the free amine at 52.93 ppm, the next methylene unit in the aminopropyl substituent at 30.40 ppm, the methyl units at 25.86 ppm, the methyne unit at 22.48 ppm and finally the methylene units closer to the cage at 7.58 ppm. ^{29}Si NMR showed three distinct peaks at -58.9 ppm, corresponding to the silicon atoms bearing the hydroxyl groups, -67.5 ppm, related to the silicon bearing the aminopropyl moiety and -68.3 ppm corresponding to the remaining three silicon atoms. In FT-IR the characteristic stretching vibration of the Si-O-Si framework was seen at 1095 and 1030 cm^{-1} (s, $\nu_{\text{cage-asym-Si-O-Si}}$), indicating asymmetry in the cage

(**Figure 23**). Also, a stretching vibration at 3363 (s, $\nu_{O\text{-}H}$) was observed relative to the silanols stretching vibrations.

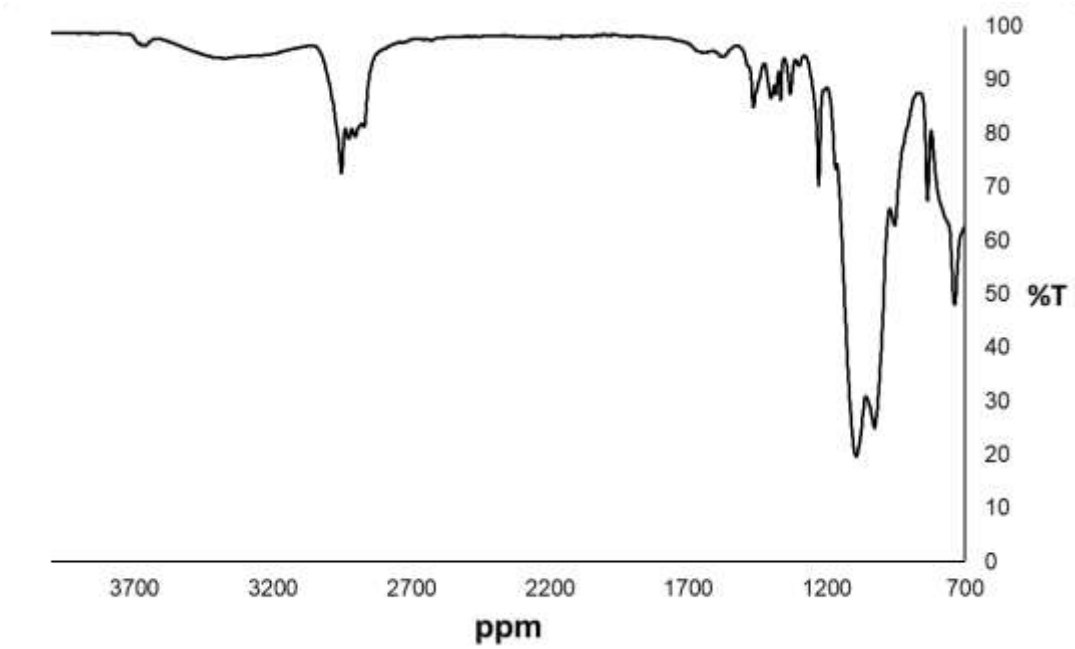

Figure 23. FTIR of AP-hexaIB-POSS. The Si-O-Si stretching vibration has clearly split and widened, indicating symmetry I the cage. The stretching vibration at 3363 cm^{-1} corresponds to the hydroxyl stretch of a silanol group; further confirming corner opening.

3.3.3 Synthesis and Characterization of Aminopropyl-hexaIsobutyl-Mercaptopropyl-POSS (AP-hexaIB-MP-POSS).

The synthesis of aminopropyl-hexaisobutyl-mercaptopropyl-POSS (AP-IB-MP-POSS) was carried out through a corner capping reaction, with mercaptopropyltriethoxy silane (MPTES) of previously synthesized AP-hexaIB-POSS. The hydroxyl sites on the cage nucleophilicly attack MPTES leaving behind an ethoxide ion, to afford the final product.

The successful synthesis of AP-hexaIB-MP-POSS was confirmed using ^{1}H, ^{13}C and ^{29}Si NMR, FT-IR and MALDI. The ^{1}H NMR exhibited the peaks corresponding to the isobutyl moiety and the amino propyl group; specifically, the methyne unit appears at 1.70 ppm and the methyl groups at 0.82 ppm. Furthermore, the methylene units adjacent to the cage appear for

both functional groups at 0.54 ppm. The next methylene units on the aminopropyl and mercaptopropyl substituent appear between 1.50 and 1.72 ppm, in order of distance from the cage. The methylene units next to the amino and mercapto groups are observed at 3.32 and 2.52 ppm, respectively. Also, the thiol hydrogen is seen at 1.25 ppm. The ^{13}C NMR shows the methylene units next to the free amine and mercaptopropyl group at 52.93, and 41.8 ppm, respectively. The next methylene unit in the aminopropyl and mercaptopropyl substituents at 30.31 ppm, the methyl units at 25.92 ppm, the methyne substituents at 23.88 ppm, the methylene group at 22.57 ppm and finally the methylene units closer to the cage at 9.58 ppm. ^{29}Si NMR showed four distinct peaks at -67.1 ppm, corresponding to the silicon bonded to aminopropyl group, -66.8 ppm, related to the silicon bearing the mercaptopropyl moiety, -67.5 ppm corresponding to the silicon atoms closer to the silicon bearing the mercaptopropyl group, and -67.9 ppm corresponding to the silicon atoms closer to the silicon bearing the aminopropyl group. In FT-IR the characteristic stretching vibration of the Si-O-Si framework was seen at 1071 cm^{-1} (s, $\nu_{cage\text{-}asym\text{-}Si\text{-}O\text{-}Si}$), further confirming the formation of a siloxane cage (**Figure 24**). Finally, MALDI was employed and a peak at 892.12 m/z was observed.

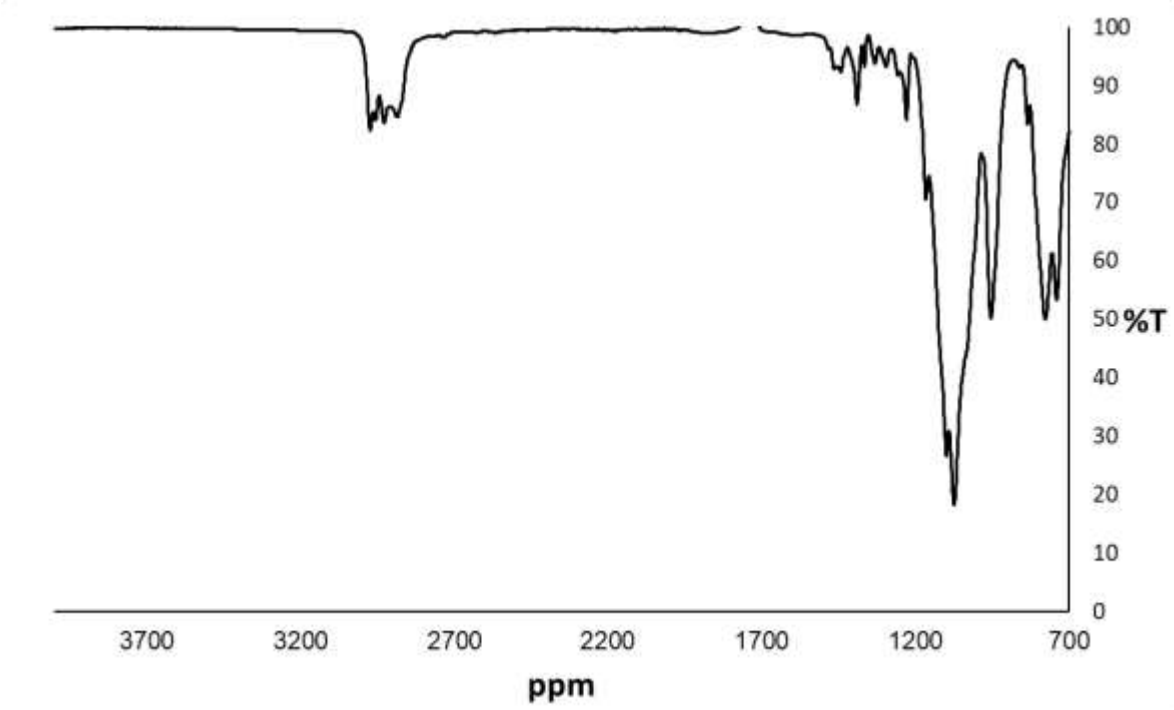

Figure 24. FTIR of AP-hexaIB-MP-POSS. The Si-O-Si stretching vibration is evident at 1071 cm^{-1}, which indicates the formation of a condensed cage. Moreover, the hydroxyl stretch seen for AP-hexaIB-POSS has disappeared, confirming effective capping.

3.4 Photophysical Properties of the synthesized POSS-Porphyrin molecules

3.4.1 Singlet Oxygen Quantum Yield (SOQY) and Fluorescence Quantum Yield (FQY).

Photosensitizers undergo intersystem crossing (ISC) to the excited triplet state encouraging the production of $^1O_2$. Typically, low fluorescence quantum yields indicate that the photons absorbed mainly undergo ISC. Fluorescence quantum yields measurements were determined in DMSO using tetraphenyl-porphyrin (TPP) in benzene as a reference, whereas singlet oxygen production was measured in DMF with TPP as a reference. Along with the POSS-Porphyrin systems synthesized, TPP, Porphyrin-COOH, and solution of physically mixed OA-POSS and Porphyrin-COOH were tested.

Table 1. The excitation wavelength was set to 515 nm, with a starting emission wavelength of 380 nm and a final emission wavelength of 500 nm. The excitation slit width was set at 5 nm, whereas the emission slit width was set to 5 nm with low sensitivity (n=3).

Sample	$\boldsymbol{\phi}_{\Delta}$	$\boldsymbol{\phi}_{F}$
TPP	0.62^{120}	0.11^{120}
Por-COOH	0.64 ± 0.01	0.13 ± 0.003
OA-POSS-Porphyrin	0.70 ± 0.01	0.15 ± 0.01
MOA-POSS-Porphyrin	0.66 ± 0.01	0.10 ± 0.01
OA-POSS + Porphyrin	0.60 ± 0.01	0.06 ± 0.01

The Φ_{Δ} values obtained for the POSS-Porphyrins are shown in **Table 1**. Interestingly, all the Φ_{Δ} values for the POSS-Porphyrin compounds are higher than those corresponding to the parent porphyrin ($p < 0.0001$). In the case of OA-POSS-Porphyrin the Φ_{Δ} value was higher than the compound Por-COOH ($p < 0.001$) with an increase of 9%. To confirm that this increase is indeed associated to the POSS-Porphyrin molecules and not due to the effect of POSS in solution, the Φ_{Δ} values for the physical mixture of compound OA-POSS + Por-COOH are shown in **Table 1**. The Φ_{Δ} values for the mixture is lower that the corresponding POSS-Porphyrin ($p < 0.0001$), which confirms that the enhancing in Φ_{Δ} is intrinsic to the POSS-Porphyrins. The Φ_{Δ} value could dependent on several factors: (i) triplet state properties, including quantum yield, lifetime and energy, (ii) the ability of substituents to quench $^1O_2$ and (iii) the efficiency of energy transfer from the excited triplet state to ground state molecular oxygen. Nevertheless, it is relevant to point out that the increase observed in the Φ_{Δ} values for the POSS-Porphyrins may have an impact on their PDT performance, considering that $^1O_2$ is one of the main components for the phototoxicity of photosensitizers.

3.5 Partition coefficients.

In addition to the photochemical properties of POSS-Porphyrin molecules, other properties may be playing a role to explain the differences in phototoxicities. A key factor when considering the phototherapeutic outcome of photosensitizers deals with its ability to internalize into cells. One approach to evaluate their interaction with cells is by the partition coefficients, which is the ratio of the concentration of a compound in a biphasic organic/aqueous system. Here, determined the *n*-octanol/water partition coefficients (log P_{OW}) for the POSS-Poprhyrins, Porphyrin-COOH and the physical mixture between OA-POSS and Porphyrin-COOH using *n*-butanol/water system were determined (**Table 2**).[118, 121] The negative log P_{OW} values for OA-POSS-Porphyrin and MOA-POSS-Porphyrin indicate that the compounds are slightly hydrophilic. In the case of functionalized porphyrins, previous reports have shown that the log P_{OW} can be associated with their interaction with cells. The cellular uptake increased proportionally with their partition coefficients.[122]

Table 2. The partition coefficients of porphyrins and porphyrin systems were determined using the shake-flask method, measured using UV-vis at 515 nm (n=3).

Compound	LogP_{OW}
Porphyrin-COOH	1.20 $\pm$ 0.02
OA-POSS-Porphyrin	-0.41 $\pm$ 0.003
MOA-POSS-Porphyrin	-0.77 $\pm$ 0.05
OA-POSS + Porphyrin	0.94 $\pm$ 0.04

3.6 Photodynamic Therapy of POSS-Porphyrin molecules

Photodynamic therapy (PDT) is a localized therapeutic approach for potential eradication of cancer tissues. In this work, the cytotoxicity and phototoxicity of the POSS-Porphyrins in MDA-MB-231 cells were evaluated using the MTS assay. As expected, no major cytotoxicity was observed in the range of concentration tested in the absence of light. Surprisingly, MOA-POSS-Porphyrin seems to be toxic under the absence of light (**Figure 25**). We are further studying this effect.

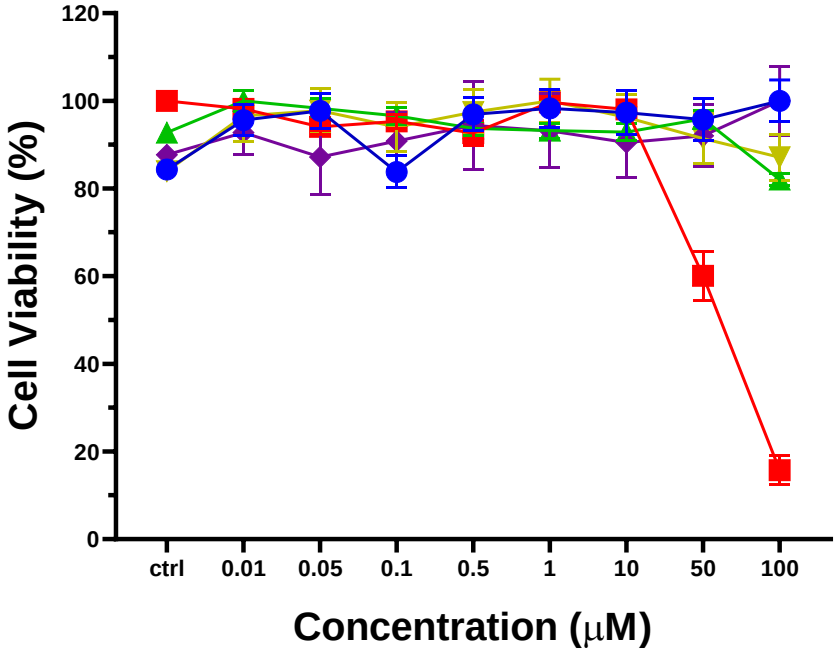

Figure 25. Phototoxicity of compounds tested in the absence of light (blue is for OA-POSS-Porphyrin, red is for MOA-POSS-Porphyrin, green is for OA-POSS, gold is for MOA-POSS, and purple is for Por-COOH).

Photosensitizers are only toxic through the generation of reactive oxygen species after excitation with light and in the presence of molecular oxygen. To compare the PDT performance of all the molecules developed in this work, a non-toxic amount of DMSO was used to carry out these experiments. As shown in **Figure 26**, at the highest

concentration, OA-POSS-Porphyrin (blue) showed a reduction in cell proliferation of 11 ± 2%. Interestingly, this trend in cell phototoxicity follows a similar trend than the Φ_Δ values. This corroborates the importance of the singlet oxygen generation for the PDT effect. MOA-POSS-Porphyrin (red) did not show significant phototoxicity at the highest concentration.

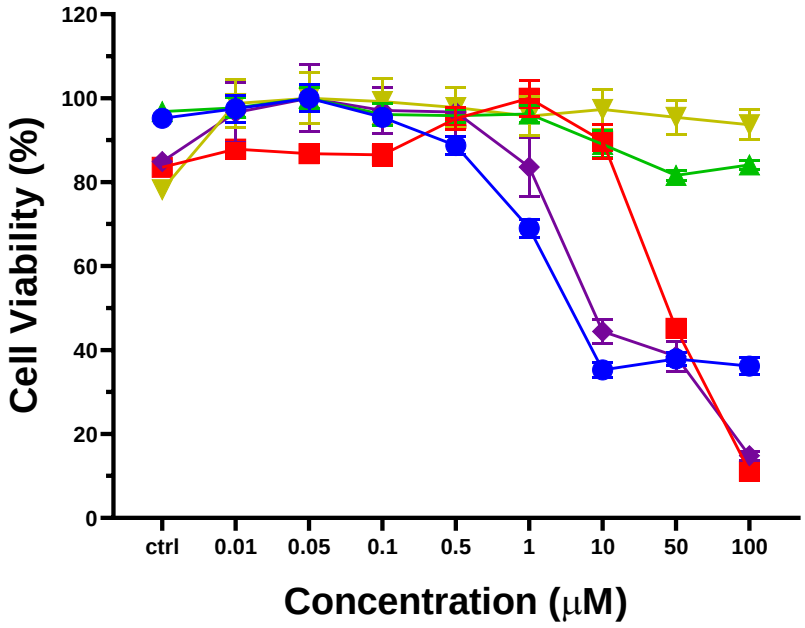

Figure 26. PDT performance of all the molecules developed in this work (blue is for OA-POSS-Porphyrin, red is for MOA-POSS-Porphyrin, green is for OA-POSS, gold is for MOA-POSS, and purple is for Por-COOH).

Overall, OA-POSS-Porphyrin seems to be slightly better at decreasing cell viability compared to the photosensitizer used. This is assumed to be because the experiments were run in DMSO, where the PS is soluble, which does not mimic effective biological conditions. Further experiments will be run testing these molecules in media.

CHAPTER 4: CONCLUSIONS AND FUTURE WORK

Polyhedral oligomeric silsesquioxane (POSS) compounds are a fascinating platform for the development of organic-inorganic hybrid materials with unique and specific properties, which would enable the synthesis of high-performance molecules. POSS's three-dimensional structure makes this compound very valuable for polymeric and nanocomposite materials. POSS compounds have a range of dominant properties such as high chemical and thermal resistance, biocompatibility, and luminescence. Also, its peculiar characteristics, such as excellent biodegradability, biocompatibility, cytocompatibility, non-toxicity, low inflammatory response and ability to be easily incorporated into different polymers makes this class of compounds an interesting compound for the synthesis of hybrid materials employed in biomedical applications.

In this Thesis, OA-POSS was synthesized through a hydrolytic condensation of aminopropyltriethoxy silane (APTES), in the presence of hydrochloric acid. OA-POSS was then characterized using ^{1}H, ^{13}C, ^{29}Si NMR, FTIR and ESI. Particularly, ^{29}Si NMR was important in corroborating the final nanocage structure, as one signal only was observed. Further conjugation with 5-(4-carboxyphenyl)-10,15,20-triphenylporphyrin was afforded through NHS chemistry. The final POSS-Porphyrin compound was characterized using ^{1}H, ^{29}Si NMR, FTIR and ESI. Again, ^{29}Si NMR was important in corroborating the final nanocage structure and three signals were observed corresponding to four different silicon atoms. The free amines on OA-POSS were consecutively alkylated to afford the synthesis of MOA-POSS. MOA-POSS was then characterized using ^{1}H, ^{13}C, ^{29}Si NMR, FTIR and ESI to corroborate the final structure. In this case, ^{1}H NMR was the important piece of data, as the spectrum showed the appearance of the methyl groups, bound to the amine.

MOA-POSS-Porphyrin was synthesized following the same chemistry employed for MOA-POSS. This compound was characterized using ^{1}H, ^{29}Si NMR, FTIR. ESI was not able to obtain due to fragmentation of the compound during the measurement. As with MOA-POSS, the peculiar data used to corroborate the synthesis was the ^{1}H NMR, which showed the appearance of the methyl groups.

One of the advantages that can be foreseen for POSS is the ability to precisely control the functionalization of this material with more than one functional group. The synthesis of aminopropyl-heptaisobutyl-POSS (AP-IB-POSS) was carried out through a corner capping reaction, with aminopropyltrimethoxy silane (APTMS) under catalytic amounts of tetraethylammonium hydroxide (TEAOH). The successful synthesis of AP-IB-POSS was confirmed using ^{1}H, ^{13}C and ^{29}Si NMR, FTIR and MALDI. The final structure was corroborated with FTIR showing the peculiar, sharp vibration of a Si-O-Si stretching in the fingerprint region. The synthesis of aminopropyl-hexaisobutyl-POSS (AP-hexaIB-POSS) was carried out through a corner opening reaction of previously synthesized AP-IB-POSS, using catalytic amounts of TEAOH. The successful synthesis of AP-hexaIB-POSS was confirmed using ^{1}H, ^{13}C and ^{29}Si NMR, FT-IR and MALDI. The final structure was corroborated with FTIR, which shows the cleavage of the siloxane cage as a widened and split stretching vibration. Also, the presence of a hydroxyl stretch indicates the generation of silanols (Si-OH). The synthesis of aminopropyl-hexaisobutyl-mercaptopropyl-POSS (AP-IB-MP-POSS) was carried out through a corner capping reaction, with mercaptopropyltriethoxy silane (MPTES) of previously synthesized AP-hexaIB-POSS. The successful synthesis of AP-hexaIB-MP-POSS was confirmed using ^{1}H, ^{13}C and ^{29}Si NMR, FT-IR and MALDI. The final structure was corroborated with FTIR

showing the peculiar, sharp vibration of a Si-O-Si stretching in the fingerprint region, compared to the spectrum from the open-cornered one.

Photosensitizers undergo intersystem crossing (ISC) to the excited triplet state encouraging the production of $^1O_2$. In this work, it was observed that all the Φ_Δ values for the POSS-Porphyrin compounds are higher than the parent porphyrin ($p < 0.0001$). In the case of OA-POSS-Porphyrin the Φ_Δ value was higher than the compound Por-COOH ($p < 0.001$) with an increase of 9%. The Φ_Δ value could dependent on several factors: (i) triplet state properties, including quantum yield, lifetime and energy, (ii) the ability of substituents to quench $^1O_2$ and (iii) the efficiency of energy transfer from the excited triplet state to ground state molecular oxygen.

In addition to the photochemical properties of POSS-Porphyrin molecules, other properties may be playing a role to explain the differences in phototoxicities. A key factor when considering the phototherapeutic outcome of photosensitizers deals with its ability to internalize into cells. One approach to evaluate their interaction with cells is by the partition coefficients, which is the ratio of the concentration of a compound in a biphasic organic/aqueous system. Here, the negative log P_{OW} values for OA-POSS-Porphyrin and MOA-POSS-Porphyrin indicate that the compounds are slightly hydrophilic.

In this work, the cytotoxicity and phototoxicity of the POSS-Porphyrins in MDA-MB-231 cells were evaluated using the MTS assay. Photosensitizers are only toxic through the generation of reactive oxygen species after excitation with light and in the presence of molecular oxygen. As reported, at the highest concentration, OA-POSS-Porphyrin showed a reduction in cell proliferation of 11 ± 2%. Interestingly, this trend in cell phototoxicity

follows a similar trend than the Φ_Δ values. This corroborates the importance of the singlet oxygen generation for the PDT effect.

The bifunctional POSS synthesized is an interesting platform. As a future direction, for this compound we envision different conjugations for the development of organic-inorganic hybrid materials with unique and specific properties, which would enable the synthesis of high-performance molecules. The two pendant reactive moieties could be used as anchor for the effective conjugations to photosensitizers, or vitamins to names a few. This new class of compounds could be used in several applications where multifunctionality is the key to reaching targets with complex properties.

Furthermore, in the future we plan to test and study POSS-Porphyrins bearing hydrophobic groups around the cage, which have been synthesized, to determine how different substituent around the cage change the physical and chemical properties of PS and hence their PDT efficiency.

The promising results obtained from the PDT experiments have led us to start a collaboration with the Civil and Environmental Engineering Department at UNCC to test different POSS-Porphyrin molecules against different strands of bacteria.

REFERENCES

1. Fundamentals and Applications of Controlled Release Drug Delivery. In *Fundamentals and Applications of Controlled Release Drug Delivery*, Siepmann, J.; Siegel, R. A.; Rathbone, M. J., Eds. 2012; pp 1-592.

2. Tomalia, D. A.; Christensen, J. B.; Boas, U., *Dendrimers, Dendrons, and Dendritic Polymers: Discovery, Applications, and the Future*. 2012; p 1-412.

3. Li, X.; Kim, J.; Yoon, J.; Chen, X., Cancer-Associated, Stimuli-Driven, Turn on Theranostics for Multimodality Imaging and Therapy. *Advanced Materials* **2017,** *29* (23).

4. Ma, J.; Kang, K.; Zhang, Y.; Yi, Q.; Gu, Z., Detachable Polyzwitterion-Coated Ternary Nanoparticles Based on Peptide Dendritic Carbon Dots for Efficient Drug Delivery in Cancer Therapy. *Acs Applied Materials & Interfaces* **2018,** *10* (50), 43923-43935.

5. Peng, S.; Men, Y.; Xie, R.; Tian, Y.; Yang, W., Biodegradable phosphorylcholine-based zwitterionic polymer nanogels with smart charge-conversion ability for efficient inhibition of tumor cells. *J. Colloid Interface Sci.* **2019,** *539*, 19-29.

6. Li, K.; Liu, Y.; Pu, K.-Y.; Feng, S.-S.; Zhan, R.; Liu, B., Polyhedral Oligomeric Silsesquioxanes-Containing Conjugated Polymer Loaded PLGA Nanoparticles with Trastuzumab (Herceptin) Functionalization for HER2-Positive Cancer Cell Detection. *Advanced Functional Materials* **2011,** *21* (2), 287-294.

7. Ghanbari, H.; Cousins, B. G.; Seifalian, A. M., A Nanocage for Nanomedicine: Polyhedral Oligomeric Silsesquioxane (POSS). *Macromolecular Rapid Communications* **2011,** *32* (14), 1032-1046.

8. Li, Y. M.; Xu, B.; Bai, T.; Liu, W. G., Co-delivery of doxorubicin and tumor-suppressing p53 gene using a PUSS-based star-shaped polymer for cancer therapy. *Biomaterials* **2015,** *55*, 12-23.

9. Feher, F. J.; Wyndham, K. D.; Scialdone, M. A.; Hamuro, Y., Octafunctionalized polyhedral oligosilsesquioxanes as scaffolds: synthesis of peptidyl silsesquioxanes. *Chemical Communications* **1998,** (14), 1469-1470.

10. Zhu, Y. X.; Jia, H. R.; Chen, Z.; Wu, F. G., Photosensitizer (PS)/polyhedral oligomeric silsesquioxane (POSS)-crosslinked nanohybrids for enhanced imaging-guided photodynamic cancer therapy. *Nanoscale* **2017,** *9* (35), 12874-12884.

11. Atar, N.; Grossman, E.; Gouzman, I.; Bolker, A.; Murray, V. J.; Marshall, B. C.; Qian, M.; Minton, T. K.; Hanein, Y., Atomic-Oxygen-Durable and Electrically-Conductive CNT-POSS-Polyimide Flexible Films for Space Applications. *Acs Applied Materials & Interfaces* **2015,** *7* (22), 12047-12056.

12. John, L.; Malik, M.; Janeta, M.; Szafert, S., First step towards a model system of the drug delivery network based on amide-POSS nanocarriers. *Rsc Advances* **2017,** *7* (14), 8394-8401.

13. Sun, J. S.; Chen, Y. L.; Zhao, L. Y.; Chen, Y. T.; Qi, D. D.; Choi, K. M.; Shin, D. S.; Jiang, J. Z., Porphyrin-POSS Molecular Hybrids. *Chemistry-a European Journal* **2013,** *19* (38), 12613-12618.

14. Cordes, D. B.; Lickiss, P. D.; Rataboul, F., Recent Developments in the Chemistry of Cubic Polyhedral Oligosilsesquioxanes. *Chemical Reviews* **2010,** *110* (4), 2081-2173.

15. Feng, X.; Zhu, S.; Yue, K.; Su, H.; Guo, K.; Wesdemiotis, C.; Zhang, W.-B.; Cheng, S. Z. D.; Li, Y., T-10 Polyhedral Oligomeric Silsesquioxane-Based Shape

Amphiphiles with Diverse Head Functionalities via "Click" Chemistry. *Acs Macro Letters* **2014,** *3* (9), 900-905.

16. Handke, M.; Jastrzebski, W., Vibrational spectroscopy of the double 4-, 6-membered rings in silicates and siloxanes. *Journal of Molecular Structure* **2005,** *744*, 671-675.

17. Janeta, M.; John, L.; Ejfler, J.; Szafert, S., Novel organic-inorganic hybrids based on T-8 and T-10 silsesquioxanes: synthesis, cage-rearrangement and properties. *Rsc Advances* **2015,** *5* (88), 72340-72351.

18. Applications of Polyhedral Oligomeric Silsesquioxanes. In *Applications of Polyhedral Oligomeric Silsesquioxanes*, HartmannThompson, C., Ed. Springer: Dordrecht, 2011; Vol. 3, pp 1-420.

19. Kaneko, Y.; Shoiriki, M.; Mizumo, T., Preparation of cage-like octa(3-aminopropyl)silsesquioxane trifluoromethanesulfonate in higher yield with a shorter reaction time. *Journal of Materials Chemistry* **2012,** *22* (29), 14475-14478.

20. Feher, F. J.; Wyndham, K. D.; Soulivong, D.; Nguyen, F., Syntheses of highly functionalized cube-octameric polyhedral oligosilsesquioxanes (R8Si8O12). *Journal of the Chemical Society-Dalton Transactions* **1999,** (9), 1491-1497.

21. Feher, F. J.; Wyndham, K. D., Amine and ester-substituted silsesquioxanes: synthesis, characterization and use as a core for starburst dendrimers. *Chemical Communications* **1998,** (3), 323-324.

22. Zhang, Z. P.; Liang, G. Z.; Lu, T. L., Synthesis and characterization of cage octa(aminopropylsilsesquioxane). *Journal of Applied Polymer Science* **2007,** *103* (4), 2608-2614.

23. Manickam, S.; Cardiano, P.; Mineo, P. G.; Lo Schiavo, S., Star-Shaped Quaternary Alkylammonium Polyhedral Oligomeric Silsesquioxane Ionic Liquids. *European Journal of Inorganic Chemistry* **2014,** (16), 2704-2710.

24. Neyertz, S.; Brown, D.; Pilz, M.; Rival, N.; Arstad, B.; Mannle, F.; Simon, C., The Stability of Amino-Functionalized Polyhedral Oligomeric Silsesquioxanes in Water. *Journal of Physical Chemistry B* **2015,** *119* (21), 6433-6447.

25. Olivero, F.; Reno, F.; Carniato, F.; Rizzi, M.; Cannas, M.; Marchese, L., A novel luminescent bifunctional POSS as a molecular platform for biomedical applications. *Dalton Transactions* **2012,** *41* (25), 7467-7473.

26. Carniato, F.; Boccaleri, E.; Marchese, L., A versatile route to bifunctionalized silsesquioxane (POSS): synthesis and characterisation of Ti-containing aminopropylisobutyl-POSS. *Dalton Transactions* **2008,** (1), 36-39.

27. Froehlich, J. D.; Young, R.; Nakamura, T.; Ohmori, Y.; Li, S.; Mochizuki, A.; Lauters, M.; Jabbour, G. E., Synthesis of multi-functional POSS emitters for OLED applications. *Chemistry of Materials* **2007,** *19* (20), 4991-4997.

28. Lorenz, V.; Fischer, A.; Giessmann, S.; Gilje, J. W.; Gun'ko, Y.; Jacob, K.; Edelmann, F. T., Disiloxanediolates and polyhedral metallasilsesquioxanes of the early transition metals and f-elements. *Coordination Chemistry Reviews* **2000,** *206*, 321-368.

29. Feher, F. J.; Terroba, R.; Ziller, J. W., Base-catalyzed cleavage and homologation of polyhedral oligosilsesquioxanes. *Chemical Communications* **1999,** (21), 2153-2154.

30. Zhang, L.; Abbenhuis, H. C. L.; Gerritsen, G.; Ni Bhriain, N.; Magusin, P. C. M. M.; Mezari, B.; Han, W.; van Santen, R. A.; Yang, Q.; Li, C., An efficient hybrid,

nanostructured, epoxidation catalyst: Titanium silsesquioxane-polystyrene copolymer supported on SBA-15. *Chemistry-a European Journal* **2007,** *13* (4), 1210-1221.

31. Skowronska-Ptasinska, M. D.; Vorstenbosch, M. L. W.; van Santen, R. A.; Abbenhuis, H. C. L., Titanium silsesquioxanes grafted on three-dimensionally netted polysiloxanes: Catalytic ensembles for epoxidation of alkenes with aqueous hydrogen peroxide. *Angewandte Chemie-International Edition* **2002,** *41* (4), 637-+.

32. Tanaka, K.; Inafuku, K.; Nakab, K.; Chujo, Y., Enhancement of entrapping ability of dendrimers by a cubic silsesquioxane core. *Organic & Biomolecular Chemistry* **2008,** *6* (21), 3899-3901.

33. Zou, Q.-C.; Yan, Q.-J.; Song, G.-W.; Zhang, S.-L.; Wu, L.-M., Detection of DNA using cationic polyhedral oligomeric silsesquioxane nanoparticles as the probe by resonance light scattering technique. *Biosensors & Bioelectronics* **2007,** *22* (7), 1461-1465.

34. Maegawa, T.; Irie, Y.; Fueno, H.; Tanaka, K.; Naka, K., Synthesis and Polymerization of a para-Disubstituted T8-caged Hexaisobutyl-POSS Monomer. *Chemistry Letters* **2014,** *43* (10), 1532-1534.

35. Feher, F. J.; Budzichowski, T. A., NEW POLYHEDRAL OLIGOSILSESQUIOXANES VIA THE CATALYTIC-HYDROGENATION OF ARYL-CONTAINING SILSESQUIOXANES. *Journal of Organometallic Chemistry* **1989,** *373* (2), 153-163.

36. Feher, F. J.; Newman, D. A.; Walzer, J. F., SILSESQUIOXANES AS MODELS FOR SILICA SURFACES. *Journal of the American Chemical Society* **1989,** *111* (5), 1741-1748.

37. Sulaiman, S.; Bhaskar, A.; Zhang, J.; Guda, R.; Goodson, T., III; Laine, R. M., Molecules with perfect cubic symmetry as nanobuilding blocks for 3-D assemblies. Elaboration of octavinylsilsesquioxane. Unusual luminescence shifts may indicate extended conjugation involving the silsesquioxane core. *Chemistry of Materials* **2008,** *20* (17), 5563-5573.

38. Itami, Y.; Marciniec, B.; Kubicki, M., Functionalization of octavinylsilsesquioxane by ruthenium-catalyzed silylative coupling versus cross-metathesis. *Chemistry-a European Journal* **2004,** *10* (5), 1239-1248.

39. Anderson, S. E.; Bodzin, D. J.; Haddad, T. S.; Boatz, J. A.; Mabry, J. M.; Mitchell, C.; Bowers, M. T., Structural investigation of encapsulated fluoride in polyhedral oligomeric silsesquioxane cages using ion mobility mass spectrometry and molecular mechanics. *Chemistry of Materials* **2008,** *20* (13), 4299-4309.

40. Soh, M. S.; Yap, A. U. J.; Sellinger, A., Methacrylate and epoxy functionalized nanocomposites based on silsesquioxane cores for use in dental applications. *European Polymer Journal* **2007,** *43* (2), 315-327.

41. Takamura, N.; Viculis, L.; Zhang, C.; Laine, R. M., Completely discontinuous organic/inorganic hybrid nanocomposites by self-curing of nanobuilding blocks constructed from reactions of HMe2SiOSiO1.5 (8) with vinylcyclohexene. *Polymer International* **2007,** *56* (11), 1378-1391.

42. Chomel, A. D.; Dempsey, P.; Latournerie, J.; Hourlier-Bahloul, D.; Jayasooriya, U. A., Gel to glass transformation of methyltriethoxysilane: A silicon oxycarbide glass precursor investigated using vibrational spectroscopy. *Chemistry of Materials* **2005,** *17* (17), 4468-4473.

43. Baney, R. H.; Itoh, M.; Sakakibara, A.; Suzuki, T., SILSESQUIOXANES. *Chemical Reviews* **1995,** *95* (5), 1409-1430.

44. Wang, W. J.; Hai, X.; Mao, Q. X.; Chen, M. L.; Wang, J. H., Polyhedral Oligomeric Silsesquioxane Functionalized Carbon Dots for Cell Imaging. *Acs Applied Materials & Interfaces* **2015,** *7* (30), 16609-16616.

45. Liu, Y. H.; Zheng, S. X.; Nie, K. M., Epoxy nanocomposites with octa(propylglycidyl ether) polyhedral oligomeric silsesquioxane. *Polymer* **2005,** *46* (25), 12016-12025.

46. Lickiss, P. D.; Rataboul, F., Fully condensed polyhedral oligosilsesquioxanes(POSS): From synthesis to application. In *Advances in Organometallic Chemistry, Vol 57*, Hill, A. F.; Fink, M. J., Eds. 2008; Vol. 57, pp 1-116.

47. Chojnowski, J.; Fortuniak, W.; Rosciszewski, P.; Werel, W.; Lukasiak, J.; Kamysz, W.; Halasa, R., Polysilsesquioxanes and oligosilsesquioxanes substituted by alkylammonium salts as antibacterial biocides. *Journal of Inorganic and Organometallic Polymers and Materials* **2006,** *16* (3), 219-230.

48. Gao, Y.; Eguchi, A.; Kakehi, K.; Lee, Y. C., Efficient preparation of glycoclusters from silsesquioxanes. *Organic Letters* **2004,** *6* (20), 3457-3460.

49. Cheng, G.; Peng, X. Z.; Hao, G. L.; Kennedy, V. O.; Ivanov, I. N.; Knappenberger, K.; Hill, T. J.; Rodgers, M. A. J.; Kenney, M. E., Synthesis, photochemistry, and electrochemistry of a series of phthalocyanines with graded steric hindrance. *Journal of Physical Chemistry A* **2003,** *107* (18), 3503-3514.

50. Ceyhan, T.; Yueksek, M.; Yaghoglu, H. G.; Salih, B.; Erbil, M. K.; Elmali, A.; Bekaroglu, O., Synthesis, characterization and nonlinear absorption of novel octakis-POSS

substituted metallophthalocyanines and strong optical limiting property of CuPc. *Dalton Transactions* **2008,** (18), 2407-2413.

51. Kaftory, M.; Kapon, M.; Botoshansky, M., The structural chemistry of organosilicon compounds. *Chemistry of Organic Silicon Compounds, Vol 2, Pts 1-3* **1998,** *2*, 181-265.

52. Clark, J. C.; Saengkerdsub, S.; Eldridge, G. T.; Campana, C.; Barnes, C. E., Synthesis and structure of functional spherosilicate building block molecules for materials synthesis. *Journal of Organometallic Chemistry* **2006,** *691* (15), 3213-3222.

53. Jiao, J.; Lee, M.-Y.; Barnes, C. E.; Hagaman, E. W., Sn-119 NMR chemical shift tensors in anhydrous and hydrated Si8O20(SnMe3)(8) crystals. *Magnetic Resonance in Chemistry* **2008,** *46* (7), 690-692.

54. Bassindale, A. R.; Chen, H. P.; Liu, Z. H.; MacKinnon, L. A.; Parker, D. J.; Taylor, P. G.; Yang, Y. X.; Light, M. E.; Horton, P. N.; Hursthouse, M. B., A higher yielding route to octasilsesquioxane cages using tetrabutylammonium fluoride, Part 2: further synthetic advances, mechanistic investigations and X-ray crystal structure studies into the factors that determine cage geometry in the solid state. *Journal of Organometallic Chemistry* **2004,** *689* (21), 3287-3300.

55. Lucky, S. S.; Soo, K. C.; Zhang, Y., Nanoparticles in Photodynamic Therapy. *Chemical Reviews* **2015,** *115* (4), 1990-2042.

56. Yuan, A.; Tang, X.; Qiu, X.; Jiang, K.; Wu, J.; Hu, Y., Activatable photodynamic destruction of cancer cells by NIR dye/photosensitizer loaded liposomes. *Chemical Communications* **2015,** *51* (16), 3340-3342.

57. Shemesh, C. S.; Hardy, C. W.; Yu, D. S.; Fernandez, B.; Zhang, H., Indocyanine green loaded liposome nanocarriers for photodynamic therapy using human triple negative breast cancer cells. *Photodiagnosis and Photodynamic Therapy* **2014,** *11* (2), 193-203.

58. Di Corato, R.; Bealle, G.; Kolosnjaj-Tabi, J.; Espinosa, A.; Clement, O.; Silva, A. K. A.; Menager, C.; Wilhelm, C., Combining Magnetic Hyperthermia and Photodynamic Therapy for Tumor Ablation with Photoresponsive Magnetic Liposomes. *Acs Nano* **2015,** *9* (3), 2904-2916.

59. Feng, L.; Cheng, L.; Dong, Z.; Tao, D.; Barnhart, T. E.; Cai, W.; Chen, M.; Liu, Z., Theranostic Liposomes with HypoxiaActivated Prodrug to Effectively Destruct Hypoxic Tumors Post-Photodynamic Therapy. *Acs Nano* **2017,** *11* (1), 927-937.

60. Lin, J.; Wang, S.; Huang, P.; Wang, Z.; Chen, S.; Niu, G.; Li, W.; He, J.; Cui, D.; Lu, G.; Chen, X.; Nie, Z., Photosensitizer-Loaded Gold Vesicles with Strong Plasmonic Coupling Effect for Imaging-Guided Photothermal/Photodynamic Therapy. *Acs Nano* **2013,** *7* (6), 5320-5329.

61. Cheng, L.; Kamkaew, A.; Sun, H.; Jiang, D.; Valdovinos, H. F.; Gong, H.; England, C. G.; Goel, S.; Barnhart, T. E.; Cai, W., Dual-Modality Positron Emission Tomography/Optical Image-Guided Photodynamic Cancer Therapy with Chlorin e6-Containing Nanomicelles. *Acs Nano* **2016,** *10* (8), 7721-7730.

62. Guo, M.; Mao, H.; Li, Y.; Zhu, A.; He, H.; Yang, H.; Wang, Y.; Tian, X.; Ge, C.; Peng, Q.; Wang, X.; Yang, X.; Chen, X.; Liu, G.; Chen, H., Dual imaging-guided photothermal/photodynamic therapy using micelles. *Biomaterials* **2014,** *35* (16), 4656-4666.

63. Nair, L. V.; Nazeer, S. S.; Jayasree, R. S.; Ajayaghosh, A., Fluorescence Imaging Assisted Photo dynamic Therapy Using Photosensitizer-Linked Gold Quantum Clusters. *Acs Nano* **2015,** *9* (6), 5825-5832.

64. Jang, B.; Park, J.-Y.; Tung, C.-H.; Kim, I.-H.; Choi, Y., Gold Nanorod-Photosensitizer Complex for Near-Infrared Fluorescence Imaging and Photodynamic/Photothermal Therapy In Vivo. *Acs Nano* **2011,** *5* (2), 1086-1094.

65. Simon, T.; Potara, M.; Gabudean, A.-M.; Licarete, E.; Banciu, M.; Astilean, S., Designing Theranostic Agents Based on Pluronic Stabilized Gold Nanoaggregates Loaded with Methylene Blue for Multimodal Cell Imaging and Enhanced Photodynamic Therapy. *Acs Applied Materials & Interfaces* **2015,** *7* (30), 16191-16201.

66. Wang, S.; Huang, P.; Nie, L.; Xing, R.; Liu, D.; Wang, Z.; Lin, J.; Chen, S.; Niu, G.; Lu, G.; Chen, X., Single Continuous Wave Laser Induced Photodynamic/Plasmonic Photothermal Therapy Using Photosensitizer-Functionalized Gold Nanostars. *Advanced Materials* **2013,** *25* (22), 3055-3061.

67. Lee, S. J.; Koo, H.; Jeong, H.; Huh, M. S.; Choi, Y.; Jeong, S. Y.; Byun, Y.; Choi, K.; Kim, K.; Kwon, I. C., Comparative study of photosensitizer loaded and conjugated glycol chitosan nanoparticles for cancer therapy. *Journal of Controlled Release* **2011,** *152* (1), 21-29.

68. Lee, S. J.; Koo, H.; Lee, D.-E.; Min, S.; Lee, S.; Chen, X.; Choi, Y.; Leary, J. F.; Park, K.; Jeong, S. Y.; Kwon, I. C.; Kim, K.; Choi, K., Tumor-homing photosensitizer-conjugated glycol chitosan nanoparticles for synchronous photodynamic imaging and therapy based on cellular on/off system. *Biomaterials* **2011,** *32* (16), 4021-4029.

69. Chen, Q.; Wang, X.; Wang, C.; Feng, L.; Li, Y.; Liu, Z., Drug-Induced Self-Assembly of Modified Albumins as Nano-theranostics for Tumor-Targeted Combination Therapy. *Acs Nano* **2015,** *9* (5), 5223-5233.

70. Song, X.; Liang, C.; Gong, H.; Chen, Q.; Wang, C.; Liu, Z., Photosensitizer-Conjugated Albumin-Polypyrrole Nanoparticles for Imaging-Guided In Vivo Photodynamic/Photothermal Therapy. *Small* **2015,** *11* (32), 3932-3941.

71. Li, Y.; Wen, T.; Zhao, R.; Liu, X.; Ji, T.; Wang, H.; Shi, X.; Shi, J.; Wei, J.; Zhao, Y.; Wu, X.; Nie, G., Localized Electric Field of Plasmonic Nanoplatform Enhanced Photodynamic Tumor Therapy. *Acs Nano* **2014,** *8* (11), 11529-11542.

72. Ma, X.; Qu, Q.; Zhao, Y., Targeted Delivery of 5-Aminolevulinic Acid by Multifunctional Hollow Mesoporous Silica Nanoparticles for Photodynamic Skin Cancer Therapy. *Acs Applied Materials & Interfaces* **2015,** *7* (20), 10671-10676.

73. Tian, B.; Wang, C.; Zhang, S.; Feng, L.; Liu, Z., Photothermally Enhanced Photodynamic Therapy Delivered by Nano-Graphene Oxide. *Acs Nano* **2011,** *5* (9), 7000-7009.

74. Luo, S.; Yang, Z.; Tan, X.; Wang, Y.; Zeng, Y.; Wang, Y.; Li, C.; Li, R.; Shi, C., Multifunctional Photosensitizer Grafted on Polyethylene Glycol and Polyethylenimine Dual-Functionalized Nanographene Oxide for Cancer-Targeted Near-Infrared Imaging and Synergistic Phototherapy. *Acs Applied Materials & Interfaces* **2016,** *8* (27), 17176-17186.

75. Beack, S.; Kong, W. H.; Jung, H. S.; Do, I. H.; Han, S.; Kim, H.; Kim, K. S.; Yun, S. H.; Hahn, S. K., Photodynamic therapy of melanoma skin cancer using carbon dot - chlorin e6-hyaluronate conjugate. *Acta Biomaterialia* **2015,** *26*, 295-305.

76. Huang, P.; Lin, J.; Wang, X.; Wang, Z.; Zhang, C.; He, M.; Wang, K.; Chen, F.; Li, Z.; Shen, G.; Cui, D.; Chen, X., Light-Triggered Theranostics Based on Photosensitizer-Conjugated Carbon Dots for Simultaneous Enhanced-Fluorescence Imaging and Photodynamic Therapy. *Advanced Materials* **2012,** *24* (37), 5104-5110.

77. Au-Yeung, H. L.; Tam, A. Y. Y.; Leung, S. Y. L.; Yam, V. W. W., Supramolecular assembly of platinum-containing polyhedral oligomeric silsesquioxanes: an interplay of intermolecular interactions and a correlation between structural modifications and morphological transformations. *Chemical Science* **2017,** *8* (3), 2267-2276.

78. Chatterjee, S.; Ooya, T., Hydrophobic Nature of Methacrylate-POSS in Combination with 2-(Methacryloyloxy)ethyl Phosphorylcholine for Enhanced Solubility and Controlled Release of Paclitaxel. *Langmuir* **2019,** *35* (5), 1404-1412.

79. Ni, C. H.; Ni, G. F.; Zhang, S. W.; Liu, X. Y.; Chen, M. Q.; Liu, L. H., The preparation of inorganic/organic hybrid nanomaterials containing silsesquioxane and its reinforcement for an epoxy resin network. *Colloid and Polymer Science* **2010,** *288* (4), 469-477.

80. Castriciano, M. A.; Leone, N.; Cardiano, P.; Manickam, S.; Scolaro, L. M.; Lo Schiavo, S., A new supramolecular polyhedral oligomeric silsesquioxanes (POSS)-porphyrin nanohybrid: synthesis and spectroscopic characterization. *Journal of Materials Chemistry C* **2013,** *1* (31), 4746-4753.

81. McCusker, C.; Carroll, J. B.; Rotello, V. M., Cationic polyhedral oligomeric silsesquioxane (POSS) units as carriers for drug delivery processes. *Chemical Communications* **2005,** (8), 996-998.

82. Laine, R. M., Nanobuilding blocks based on the OSiO1.5 (x) (x=6, 8, 10) octasilsesquioxanes. *Journal of Materials Chemistry* **2005,** *15* (35-36), 3725-3744.

83. Fan, L. F.; Wang, X.; Cao, Q. C.; Yang, Y. Y.; Wu, D. C., POSS-based supramolecular amphiphilic zwitterionic complexes for drug delivery. *Biomaterials Science* **2019,** *7* (5), 1984-1994.

84. Janeta, M.; John, L.; Ejfler, J.; Lis, T.; Szafert, S., Multifunctional imine-POSS as uncommon 3D nanobuilding blocks for supramolecular hybrid materials: synthesis, structural characterization, and properties. *Dalton Transactions* **2016,** *45* (31), 12312-12321.

85. Maschmeyer, T.; Klunduk, M. C.; Martin, C. M.; Shephard, D. S.; Thomas, J. M.; Johnson, B. F. G., Modelling the active sites of heterogeneous titanium-centred epoxidation catalysts with soluble silsesquioxane analogues. *Chemical Communications* **1997,** (19), 1847-1848.

86. Jin, J. G.; Zhu, Y. C.; Zhang, Z. H.; Zhang, W. A., Enhancing the Efficacy of Photodynamic Therapy through a Porphyrin/POSS Alternating Copolymer. *Angewandte Chemie-International Edition* **2018,** *57* (50), 16354-16358.

87. Chen, J.; Xu, Y.; Gao, Y.; Yang, D.; Wang, F.; Zhang, L.; Bao, B.; Wang, L., Nanoscale Organic-Inorganic Hybrid Photosensitizers for Highly Effective Photodynamic Cancer Therapy. *Acs Applied Materials & Interfaces* **2018,** *10* (1), 248-255.

88. Gotlib-Vainstein, K.; Gouzman, I.; Girshevitz, O.; Bolker, A.; Atar, N.; Grossman, E.; Sukenik, C. N., Liquid Phase Deposition of a Space-Durable, Antistatic SnO2 Coating on Kapton. *Acs Applied Materials & Interfaces* **2015,** *7* (6), 3539-3546.

89. Atar, N.; Grossman, E.; Gouzman, I.; Bolker, A.; Hanein, Y., Reinforced Carbon Nanotubes as Electrically Conducting and Flexible Films for Space Applications. *Acs Applied Materials & Interfaces* **2014,** *6* (22), 20400-20407.

90. Minton, T. K.; Wright, M. E.; Tomczak, S. J.; Marquez, S. A.; Shen, L.; Brunsvold, A. L.; Cooper, R.; Zhang, J.; Vij, V.; Guenthner, A. J.; Petteys, B. J., Atomic Oxygen Effects on POSS Polyimides in Low Earth Orbit. *Acs Applied Materials & Interfaces* **2012,** *4* (2), 492-502.

91. Minton, T. K.; Wu, B.; Zhang, J.; Lindholm, N. F.; Abdulagatov, A. I.; O'Patchen, J.; George, S. M.; Groner, M. D., Protecting Polymers in Space with Atomic Layer Deposition Coatings. *Acs Applied Materials & Interfaces* **2010,** *2* (9), 2515-2520.

92. Janaszewska, A.; Gradzinska, K.; Marcinkowska, M.; Klajnert-Maculewicz, B.; Stanczyk, W. A., In Vitro Studies of Polyhedral Oligo Silsesquioxanes: Evidence for Their Low Cytotoxicity. *Materials* **2015,** *8* (9), 6062-6070.

93. Ihara, N.; Kurisawa, M.; Chung, J. E.; Uyama, H.; Kobayashi, S., Enzymatic synthesis of a catechin conjugate of polyhedral oligomeric silsesquioxane and evaluation of its antioxidant activity. *Applied Microbiology and Biotechnology* **2005,** *66* (4), 430-433.

94. Chen, J.; Shan, J. Y.; Xu, Y.; Su, P.; Tong, L.; Yuwen, L. H.; Weng, L. X.; Bao, B. Q.; Wang, L. H., Polyhedral Oligomeric Silsesquioxane (POSS)-Based Cationic Conjugated Oligoelectrolyte/Porphyrin for Efficient Energy Transfer and Multiamplified Antimicrobial Activity. *Acs Applied Materials & Interfaces* **2018,** *10* (40), 34455-34463.

95. Pu, K.-Y.; Li, K.; Zhang, X.; Liu, B., Conjugated Oligoelectrolyte Harnessed Polyhedral Oligomeric Silsesquioxane as Light-Up Hybrid Nanodot for Two-Photon Fluorescence Imaging of Cellular Nucleus. *Advanced Materials* **2010,** *22* (37), 4186-+.

96. Tan, M.; Ye, Z.; Jeong, E.-K.; Wu, X.; Parker, D. L.; Lu, Z.-R., Synthesis and Evaluation of Nanoglobular Macrocyclic Mn(II) Chelate Conjugates as Non-Gadolinium(III) MRI Contrast Agents. *Bioconjugate Chemistry* **2011,** *22* (5), 931-937.

97. Pu, K.-Y.; Li, K.; Liu, B., Cationic Oligofluorene-Substituted Polyhedral Oligomeric Silsesquioxane as Light-Harvesting Unimolecular Nanoparticle for Fluorescence Amplification in Cellular Imaging. *Advanced Materials* **2010,** *22* (5), 643-+.

98. Xie, M.; Ge, J.; Lei, B.; Zhang, Q.; Chen, X.; Ma, P. X., Star-Shaped, Biodegradable, and Elastomeric PLLA-PEG-POSS Hybrid Membrane With Biomineralization Activity for Guiding Bone Tissue Regeneration. *Macromolecular Bioscience* **2015,** *15* (12), 1656-1662.

99. Zhao, X.; Du, J.; Wu, Y.; Liu, H.; Hao, X., Synthesis of highly luminescent POSS-coated CdTe quantum dots and their application in trace Cu2+ detection. *Journal of Materials Chemistry A* **2013,** *1* (38), 11748-11753.

100. He, Y.; Wang, H.-F.; Yan, X.-P., Self-Assembly of Mn-Doped ZnS Quantum Dots/Octa(3-aminopropyl)octasilsequioxane Octahydrochloride Nanohybrids for Optosensing DNA. *Chemistry-a European Journal* **2009,** *15* (22), 5436-5440.

101. Wu, M.; Ma, B.; Pan, T.; Chen, S.; Sun, J., Silver-Nanoparticle-Colored Cotton Fabrics with Tunable Colors and Durable Antibacterial and Self-Healing Superhydrophobic Properties. *Advanced Functional Materials* **2016,** *26* (4), 569-576.

102. Aflori, M.; Simionescu, B.; Bordianu, I.-E.; Sacarescu, L.; Varganici, C.-D.; Doroftei, F.; Nicolescu, A.; Olaru, M., Silsesquioxane-based hybrid nanocomposites with methacrylate units containing titania and/or silver nanoparticles as antibacterial/antifungal

coatings for monumental stones. *Materials Science and Engineering B-Advanced Functional Solid-State Materials* **2013,** *178* (19), 1339-1346.

103. Bordianu, I.-E.; David, G.; Simionescu, B.; Aflori, M.; Ursu, C.; Coroaba, A.; Hitruc, G.; Cotofana, C.; Olaru, M., Functional silsesquioxane-based hierarchical assemblies for antibacterial/antifungal coatings. *Journal of Materials Chemistry B* **2015,** *3* (5), 723-727.

104. Baptista, M. S.; Wainwright, M., Photodynamic antimicrobial chemotherapy (PACT) for the treatment of malaria, leishmaniasis and trypanosomiasis. *Brazilian Journal of Medical and Biological Research* **2011,** *44* (1), 1-10.

105. Giroldo, L. M.; Felipe, M. P.; de Oliveira, M. A.; Munin, E.; Alves, L. P.; Costa, M. S., Photodynamic antimicrobial chemotherapy (PACT) with methylene blue increases membrane permeability in Candida albicans. *Lasers in Medical Science* **2009,** *24* (1), 109-112.

106. dos Reis, J. A., Jr.; dos Santos, J. N.; Barreto, B. S.; de Assis, P. N.; Almeida, P. F.; Barbosa Pinheiro, A. L., Photodynamic Antimicrobial Chemotherapy (PACT) in osteomyelitis induced by Staphylococcus aureus: Microbiological and histological study. *Journal of Photochemistry and Photobiology B-Biology* **2015,** *149,* 235-242.

107. De Sordi, L.; Butt, M. A.; Pye, H.; Kohoutova, D.; Mosse, C. A.; Yahioglu, G.; Stamati, I.; Deonarain, M.; Battah, S.; Ready, D.; Allan, E.; Mullany, P.; Lovat, L. B., Development of Photodynamic Antimicrobial Chemotherapy (PACT) for Clostridium difficile. *Plos One* **2015,** *10* (8).

108. Lee, W.; Seo, J. H.; Woo, H. Y., Conjugated polyelectrolytes: A new class of semiconducting material for organic electronic devices. *Polymer* **2013,** *54* (19), 5104-5121.

109. Zhao, Q.; Li, J.; Zhang, X.; Li, Z.; Tang, Y., Cationic Oligo(thiophene ethynylene) with Broad-Spectrum and High Antibacterial Efficiency under White Light and Specific Biocidal Activity against S. aureus in Dark. *Acs Applied Materials & Interfaces* **2016,** *8* (1), 1019-1024.

110. Parthasarathy, A.; Goswami, S.; Corbitt, T. S.; Ji, E.; Dascier, D.; Whitten, D. G.; Schanze, K. S., Photophysics and Light-Activated Biocidal Activity of Visible-Light-Absorbing Conjugated Oligomers. *Acs Applied Materials & Interfaces* **2013,** *5* (11), 4516-4520.

111. Garner, L. E.; Park, J.; Dyar, S. M.; Chworos, A.; Sumner, J. J.; Bazan, G. C., Modification of the Optoelectronic Properties of Membranes via Insertion of Amphiphilic Phenylenevinylene Oligoelectrolytes. *Journal of the American Chemical Society* **2010,** *132* (29), 10042-10052.

112. Qiao, Y.; Yang, C.; Coady, D. J.; Ong, Z. Y.; Hedrick, J. L.; Yang, Y.-Y., Highly dynamic biodegradable micelles capable of lysing Gram-positive and Gram-negative bacterial membrane. *Biomaterials* **2012,** *33* (4), 1146-1153.

113. Janeta, M.; John, L.; Ejfler, J.; Szafert, S., High-Yield Synthesis of Amido-Functionalized Polyoctahedral Oligomeric Silsesquioxanes by Using Acyl Chlorides. *Chemistry-a European Journal* **2014,** *20* (48), 15966-15974.

114. Vicente, M. D. H.; Smith, K. M., Syntheses and Functionalizations of Porphyrin Macrocycles. *Curr. Org. Synth.* **2014,** *11* (1), 3-28.

115. Matsumoto, J.; Matsumoto, T.; Senda, Y.; Shiragami, T.; Yasuda, M., Preparation and characterization of porphyrin chromophores immobilized on micro-silica gel beads. *Journal of Photochemistry and Photobiology a-Chemistry* **2008,** *197* (1), 101-109.

116. Angell, N. G.; Lagorio, M. G.; San Roman, E. A.; Dicelio, L. E., Meso-substituted cationic porphyrins of biological interest. Photophysical and physicochemical properties in solution and bound to liposomes. *Photochemistry and Photobiology* **2000,** *72* (1), 49-56.

117. Marin, D. M.; Payerpaj, S.; Collier, G. S.; Ortiz, A. L.; Singh, G.; Jones, M.; Walter, M. G., Efficient intersystem crossing using singly halogenated carbomethoxyphenyl porphyrins measured using delayed fluorescence, chemical quenching, and singlet oxygen emission. *Physical Chemistry Chemical Physics* **2015,** *17* (43), 29090-29096.

118. Ran, Y. Q.; He, Y.; Yang, G.; Johnson, J. L. H.; Yalkowsky, S. H., Estimation of aqueous solubility of organic compounds by using the general solubility equation. *Chemosphere* **2002,** *48* (5), 487-509.

119. Zhang, Z.; Liang, G.; Lu, T., Synthesis and characterization of cage octa(aminopropylsilsesquioxane). *Journal of Applied Polymer Science* **2007,** *103* (4), 2608-2614.

120. Caminos, D. A.; Spesia, M. B.; Durantini, E. N., Photodynamic inactivation of Escherichia coli by novel meso-substituted porphyrins by 4-(3-N,N,N-trimethylammoniumpropoxy)phenyl and 4-(trifluoromethyl)phenyl groups. *Photochemical & Photobiological Sciences* **2006,** *5* (1), 56-65.

121. Engelmann, F. M.; Rocha, S. V.; Toma, H. E.; Araki, K.; Baptista, M. S., Determination of n-octanol/water partition and membrane binding of cationic porphyrins. *Int J Pharm* **2007,** *329* (1-2), 12-8.

122. Engelmann, F. M.; Mayer, I.; Gabrielli, D. S.; Toma, H. E.; Kowaltowski, A. J.; Araki, K.; Baptista, M. S., Interaction of cationic meso-porphyrins with liposomes, mitochondria and erythrocytes. *J Bioenerg Biomembr* **2007,** *39* (2), 175-85.

APPENDIX

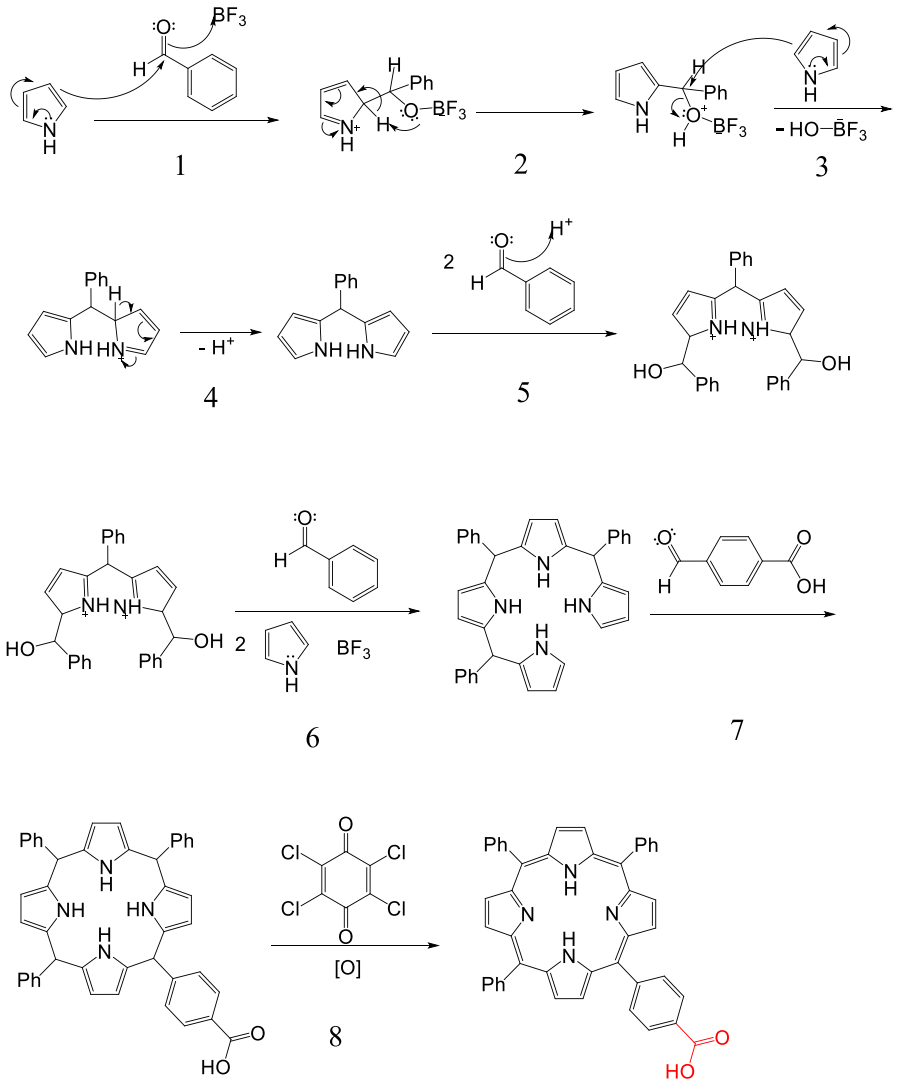

Figure A1. Mechanism of cyclization of pyrrole to afford Porphyrin-COOH. The final product is obtained through a series of electron transfers involving pyrrole and a catalyst, $BF_3{\cdot}Et_2O$.

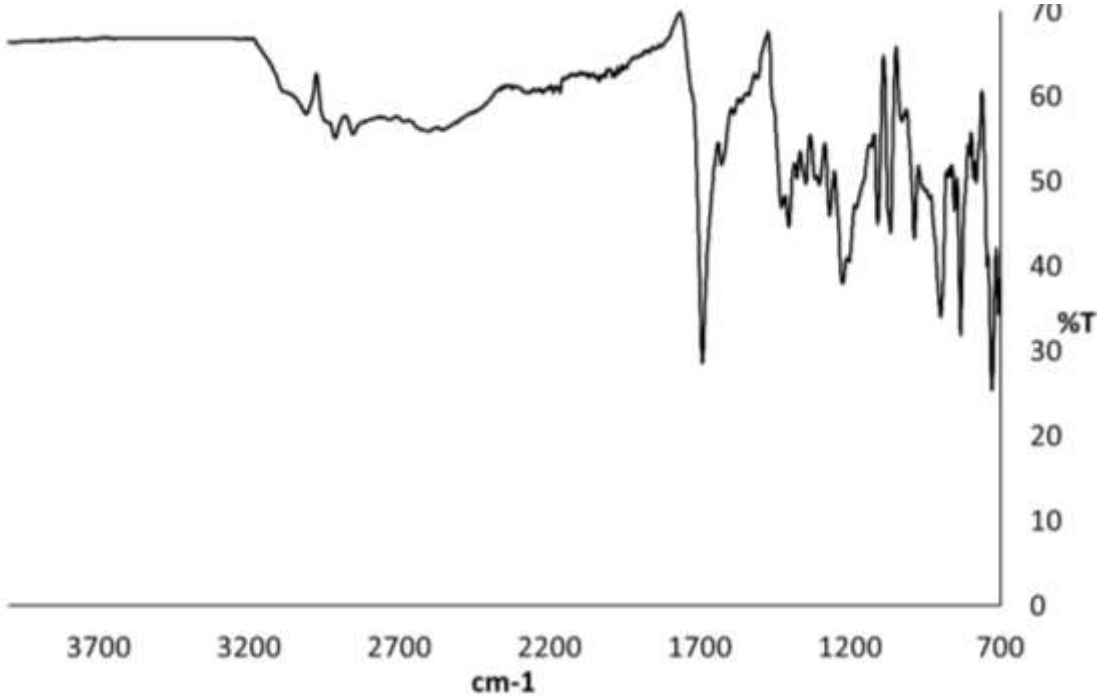

Figure A2. IR spectrum of Porphyrin-COOH. FTIR (KBr pellets, cm^{-1}) = 3700-2400 (b, ν_{COOH}), 1692.4 ($s, \nu_{C=O}$), 1600 (s, $\nu_{C=C}$).

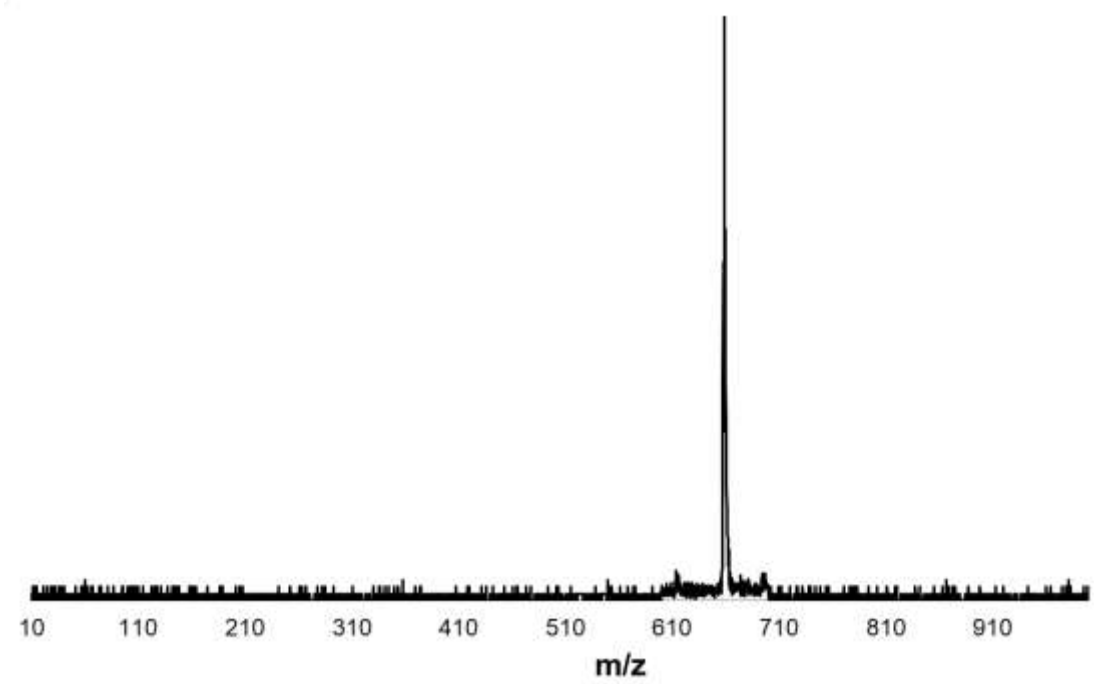

Figure A3. MALDI of Porphyrin-COOH. MALDI: m/z 659.02 $[M-H]^+$ observed; 658.88 calculated.

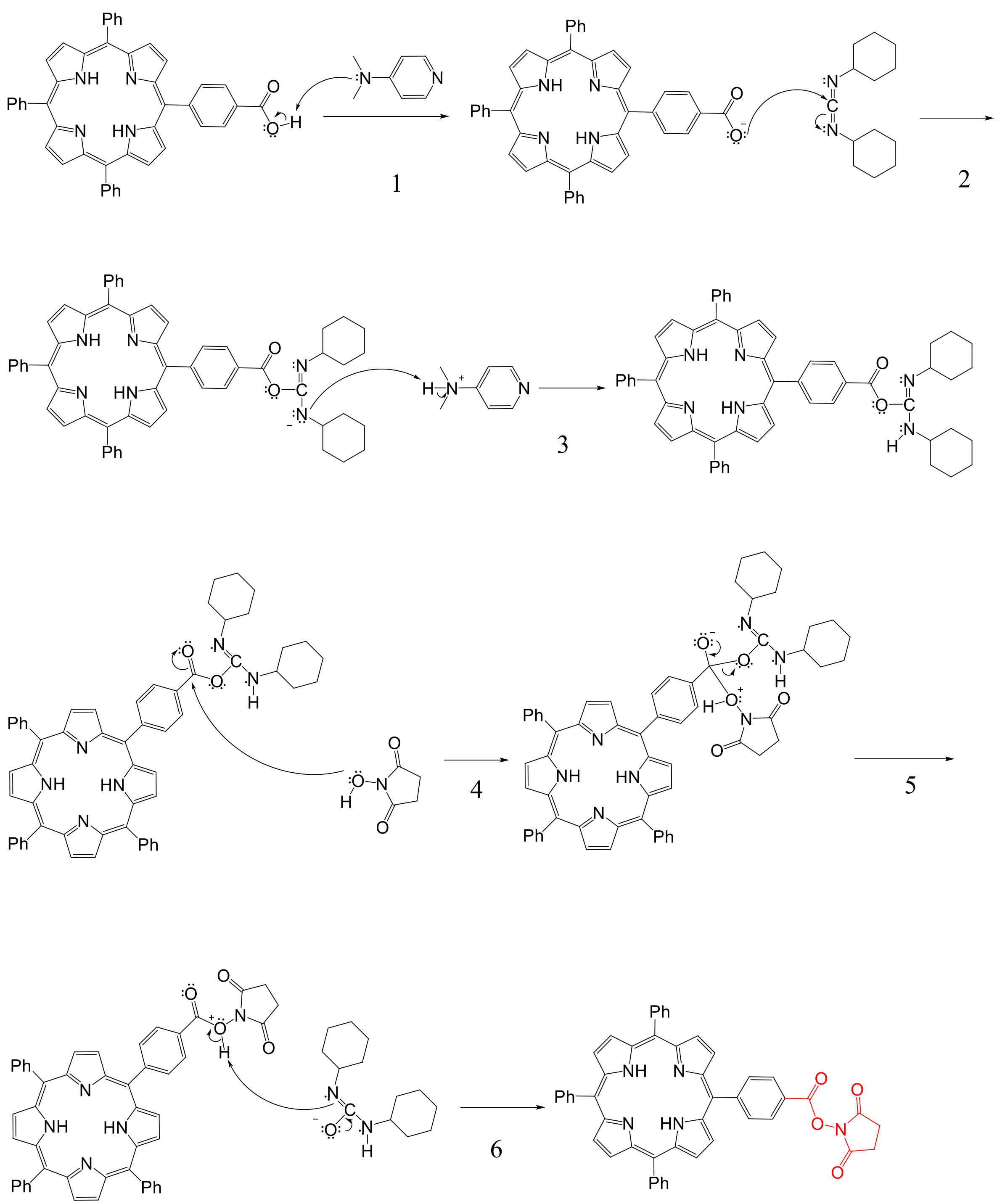

Figure A4. Mechanism of esterification of Porphyrin-COOH to afford Porphyrin-NHS. The final compound is obtained through NHS chemistry with catalytic amounts of DMAP and DCC.

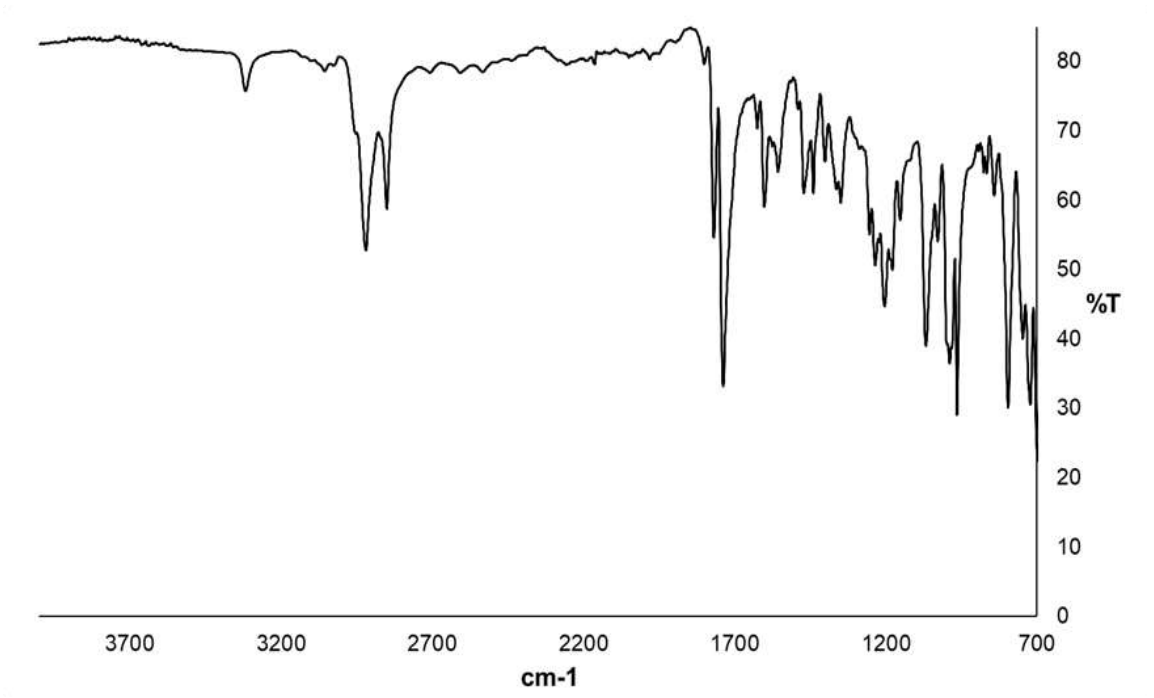

Figure A5. IR of Por-NHS. FTIR (KBr pellets, cm^{-1}) = 3319 (s, $\nu_{N\text{-}H}$), 2916 (m, $\nu_{C\text{-}H}$), 2848 (m, $\nu_{C\text{-}H}$), 1738 ($s, \nu_{C=O}$), 1603 (s, $\nu_{C=C}$).

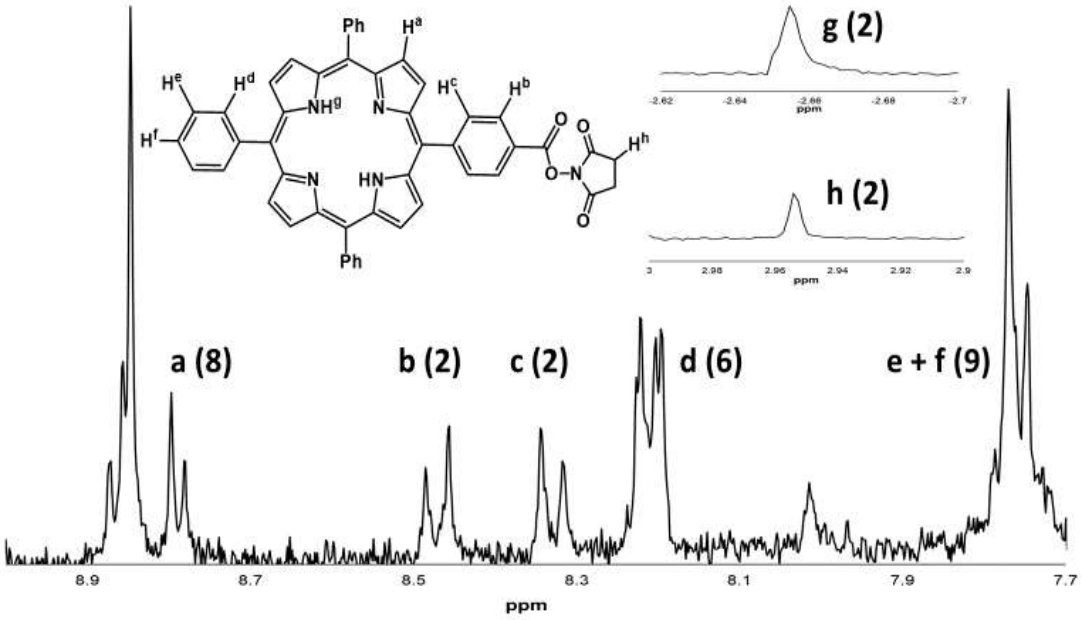

Figure A6. ^{1}H NMR of Por-NHS. MALDI: m/z 755.29 $[M\text{-}H]^{+}$ observed; 755.23 calculated.

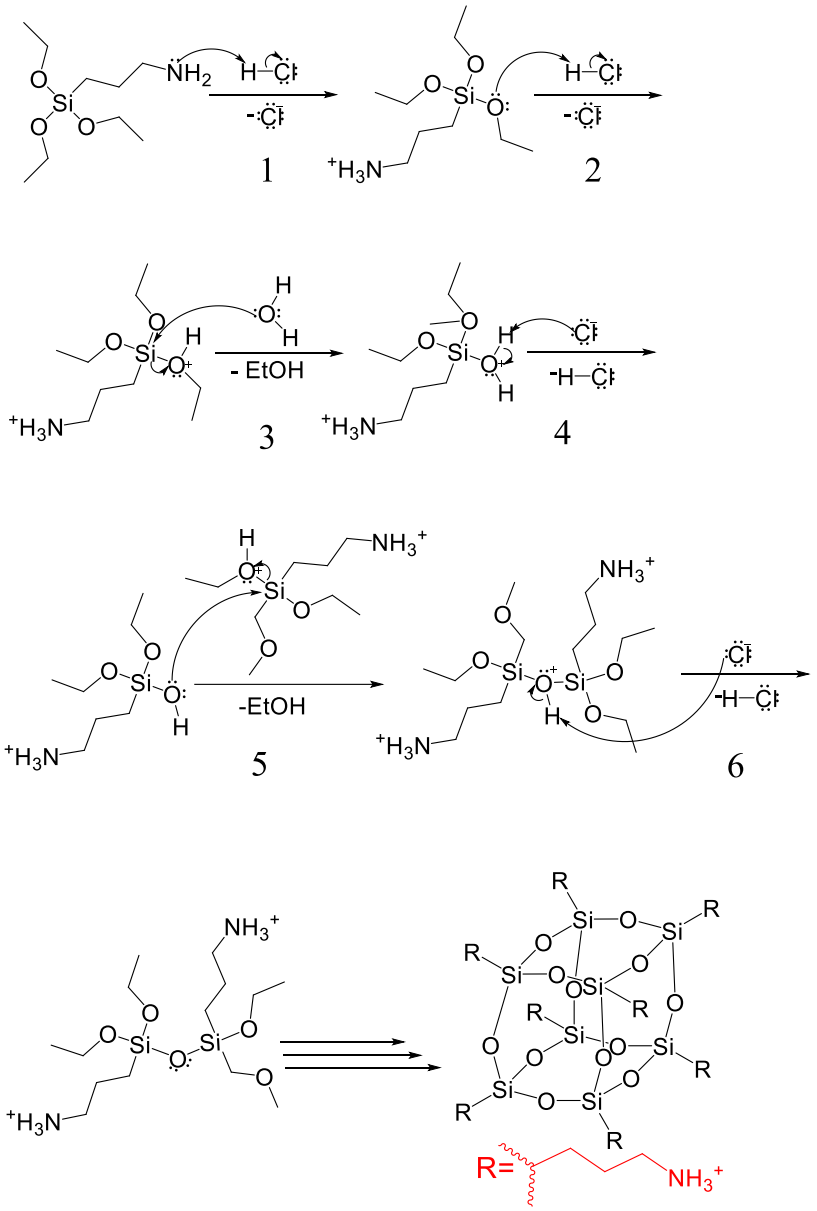

Figure A7. Mechanism of hydrolytic condensation of octaaminopropyl-POSS, under catalytic amount of HCl.

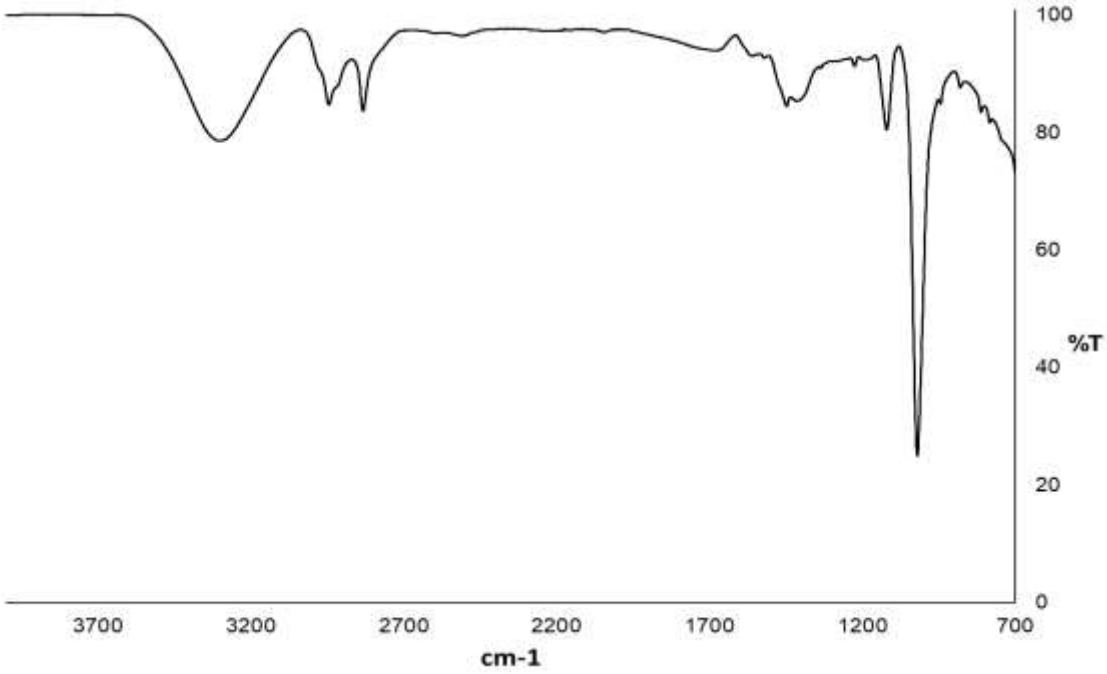

Figure A8. IR of OA-POSS. FTIR (KBr pellets, cm^{-1}): = 3134 (s, ν_{N-H}), 2944 (s, ν_{C-H}), 2876 (s, ν_{C-H}), 1489 (m, ν_{C-N}), 1098 (s, $\nu_{cage-Si-O-Si}$).

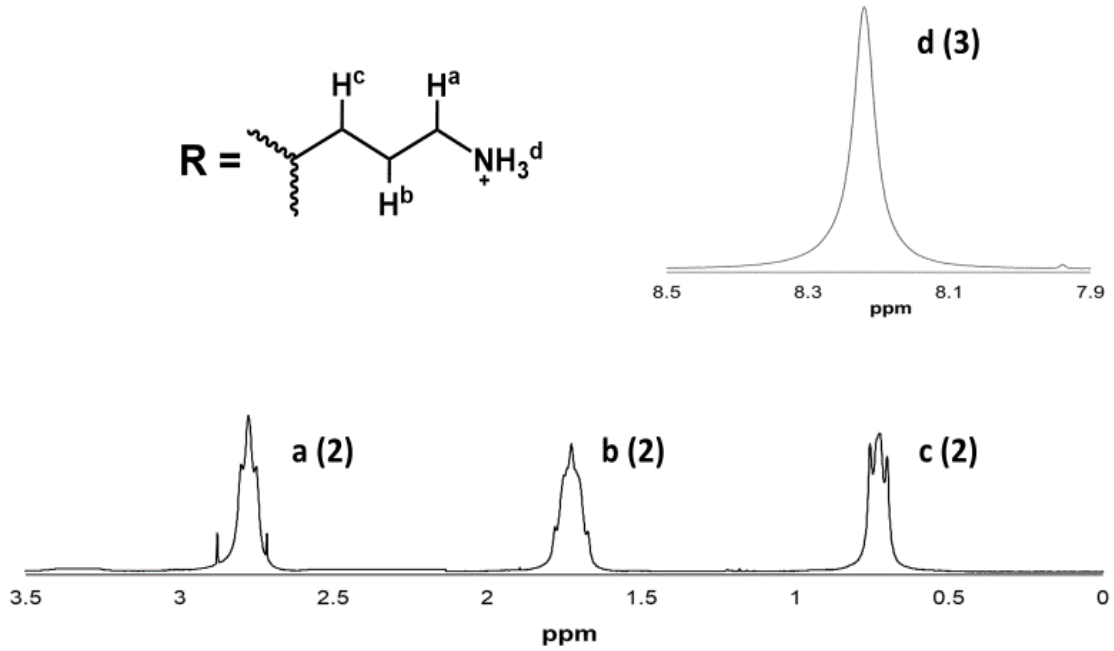

Figure A9. ^{1}H NMR of OA-POSS. ^{1}H NMR (300 MHz, DMSO-D_6, ppm) δ: 8.2 (s, 3H; -NH_3^+), 2.79 (t, 2H; -C$H_2$$NH_3^+$), 1.74 (m, 2H; -$CH_2CH_2CH_2NH_3^+$), 0.74 (t, 2H; Si-C$H_2$).

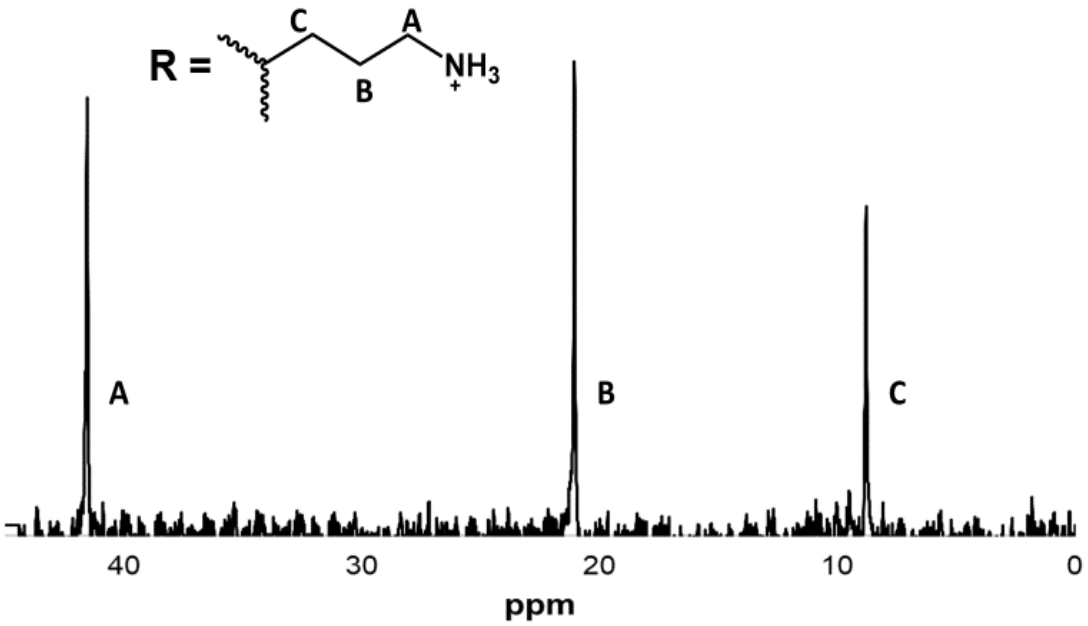

Figure A10. ^{13}C NMR of OA-POSS. ^{13}C NMR (300 MHz, DMSO, ppm) δ: 40.7 (-*C*$H_2NH_3^+$), 21.3 (-CH_2*C*$H_2NH_3^+$), 9.2 (Si-*C*H_2).

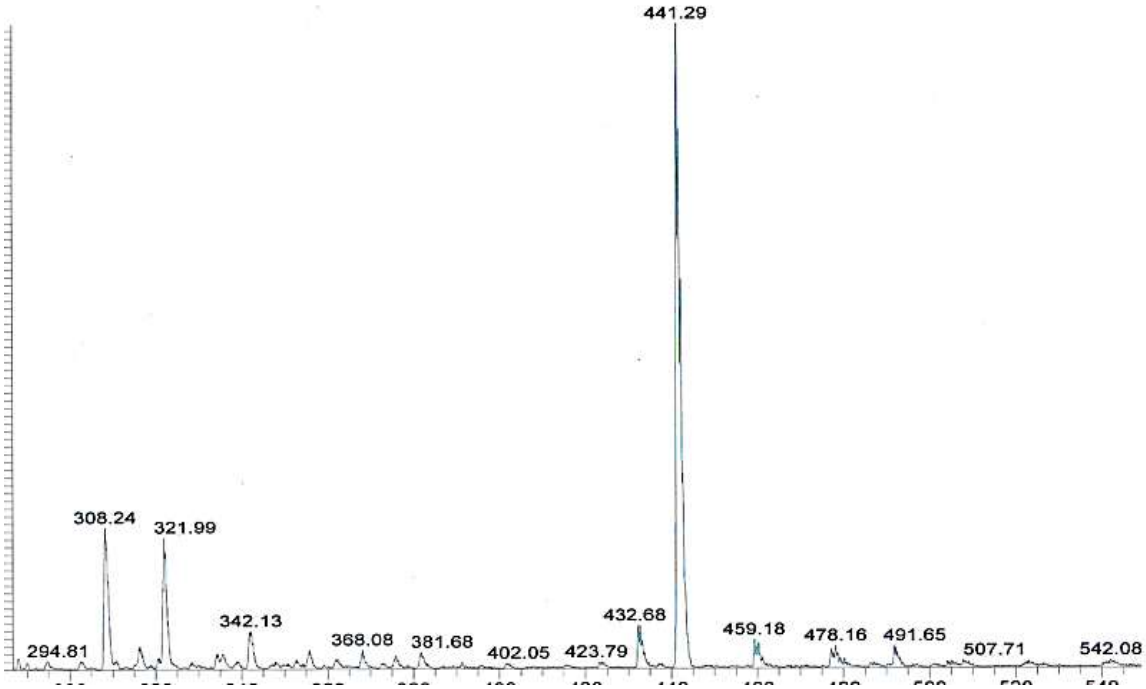

Figure A11. ESI of OA-POSS. MS (ESI): m/z (%): 441.19 $[M-2H]^{2+}$ observed; 440.75 calculated.

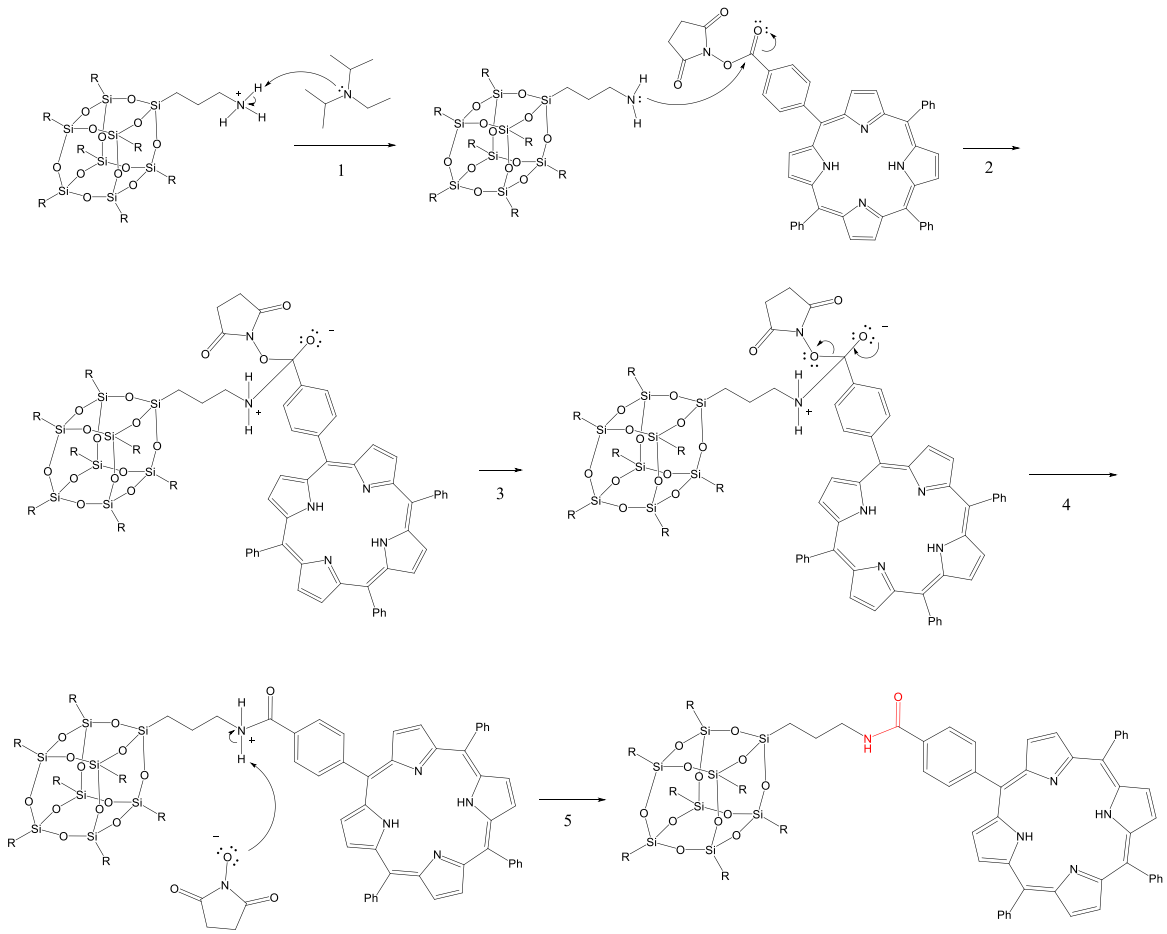

Figure A12. Mechanism of amidation to generate OA-POSS-Porphyrin. This is carried out under catalytic amounts of DIPEA in DMSO.

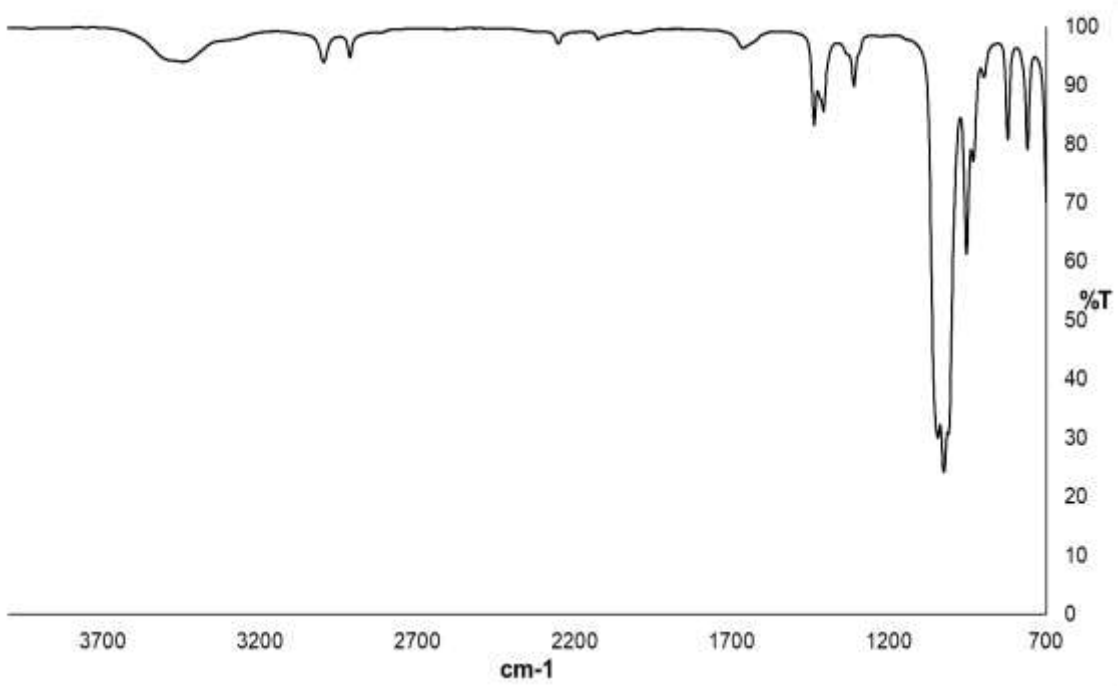

Figure A13. IR of OA-POSS-Porphyrin. FTIR (KBr pellets, cm^{-1}): = 3385 (s, ν_{N-H}), 2992.8 (m, ν_{C-H}), 1658.6 (m, $\nu_{C=O}$), 1425 (m, ν_{C-N}), 1279 (m, ν_{Si-C}), 1113 (s, $\nu_{cage-asym-Si-O-Si}$), 899 (m, $\nu_{cage-sym-Si-O-Si}$), 708 (s, ν_{Si-C}).

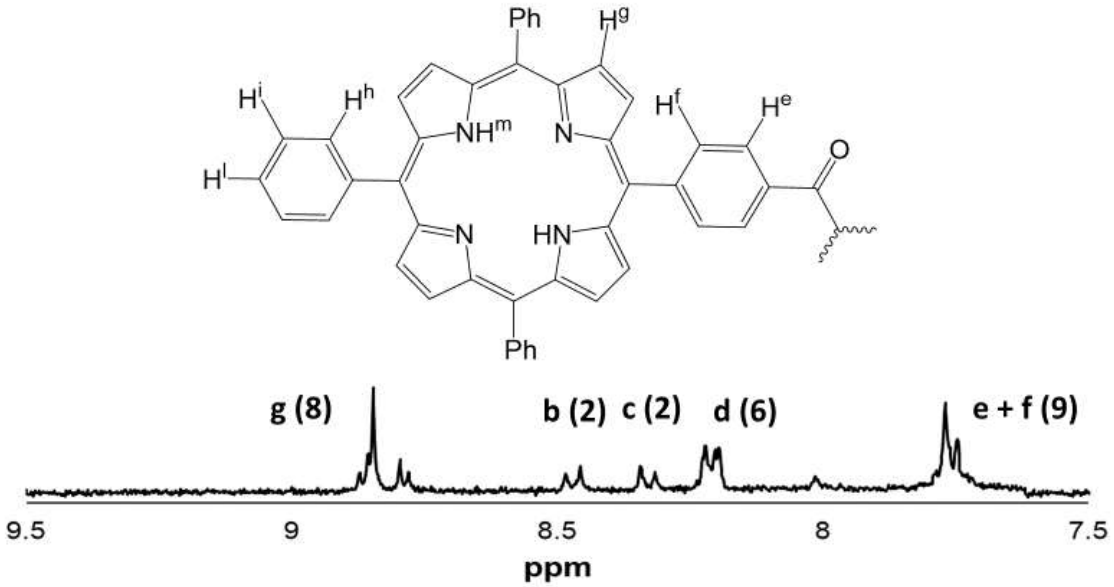

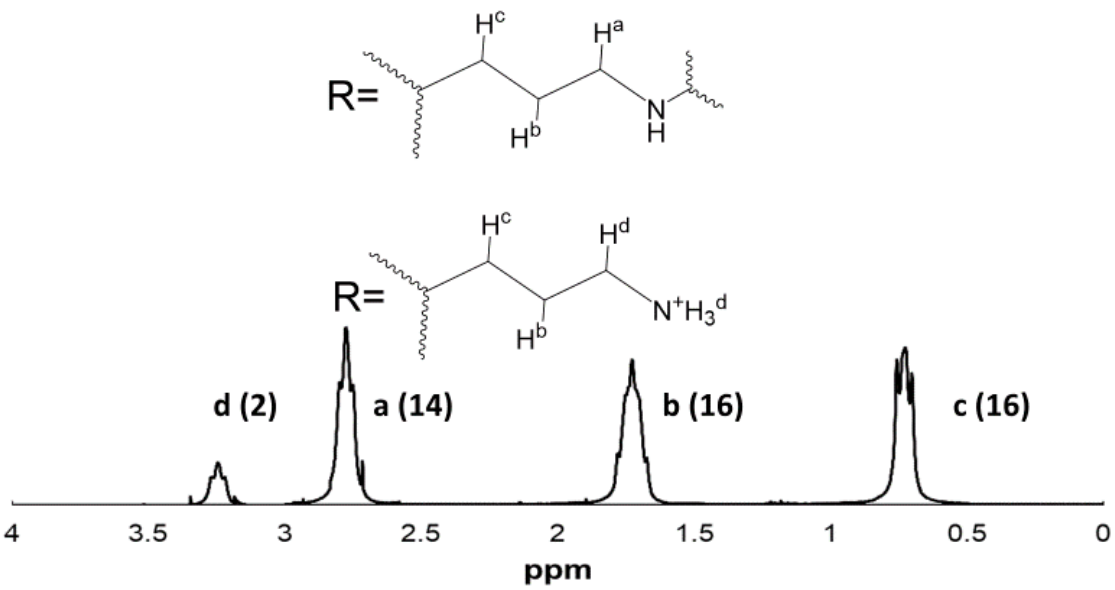

Figure A14. ^{1}H NMR of OA-POSS-Porphyrin. ^{1}H NMR (500 MHZ, DMSO-D_6, ppm) δ = 8.77 (m, 8H), 8.22 (m, 10H), 7.76 (m, 9H), 3.24 (t, 2H), 2.75 (t, 14H), 1.65 (m,16H), 0.65 (t, 16H), −3.0 (s, 2H).

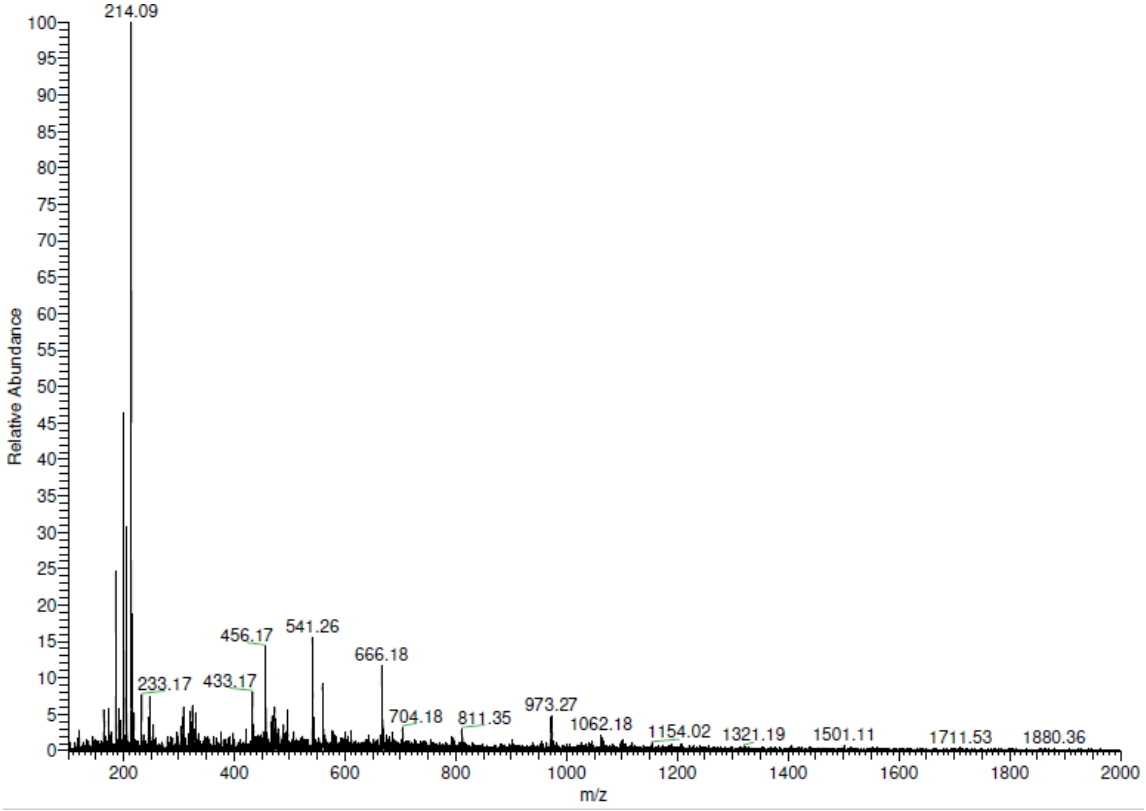

Figure A15. ESI of OA-POSS-Porphyrin. MS (ESI): m/z (%): 217.21 $[M-8H]^{8+}$ observed; 217.14 calculated.

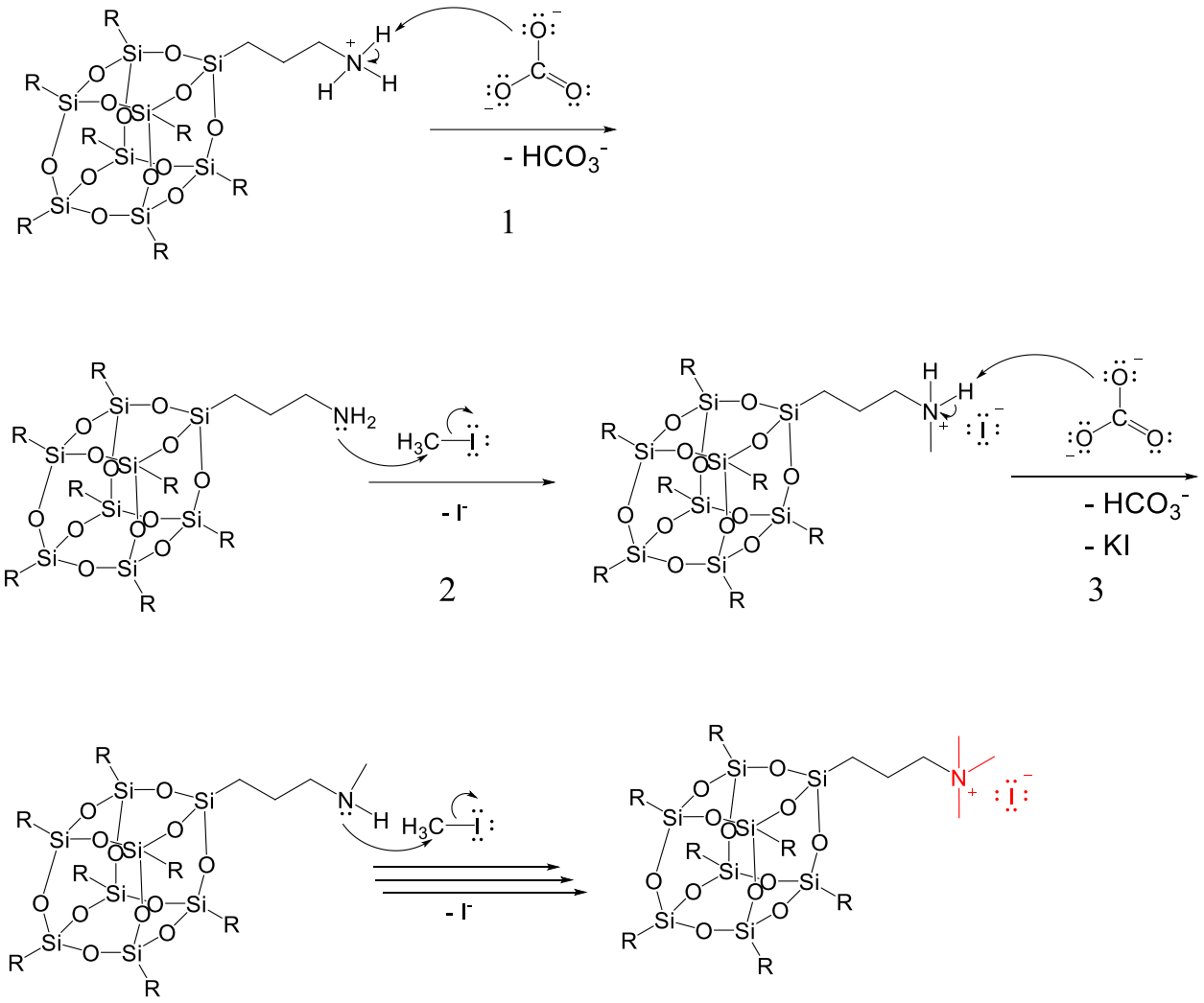

Figure A16. Mechanism of formation of MOA-POSS. Potassium bicarbonate is used as a base to deprotonate the ammonium sites on the cage and generate the free amine, which reacts with methyl iodide.

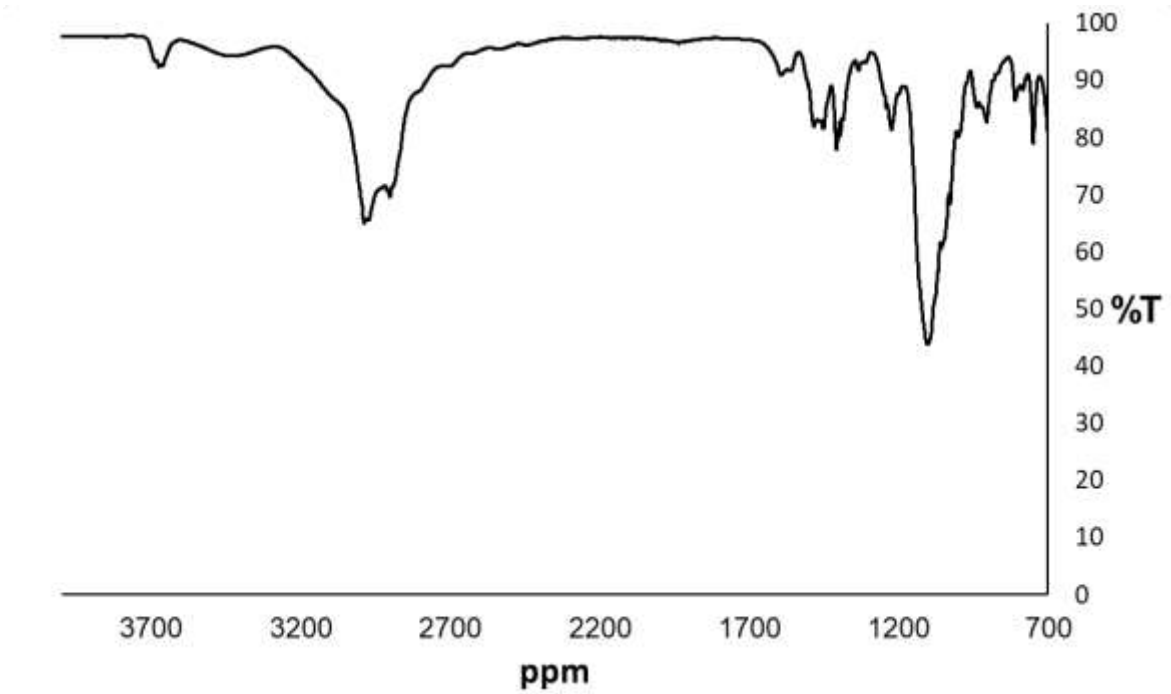

Figure A17. IR of MOA-POSS. FTIR (KBr pellets, cm^{-1}): = 3532 (s, $\nu_{N\text{-}H}$), 2926 (m, $\nu_{C\text{-}H}$), 1445 (m, $\nu_{C\text{-}N}$), 1379 (m, $\nu_{Si\text{-}C}$), 1032 (s, $\nu_{cage\text{-}asym\text{-}Si\text{-}O\text{-}Si}$), 919 (m, $\nu_{cage\text{-}sym\text{-}Si\text{-}O\text{-}Si}$).

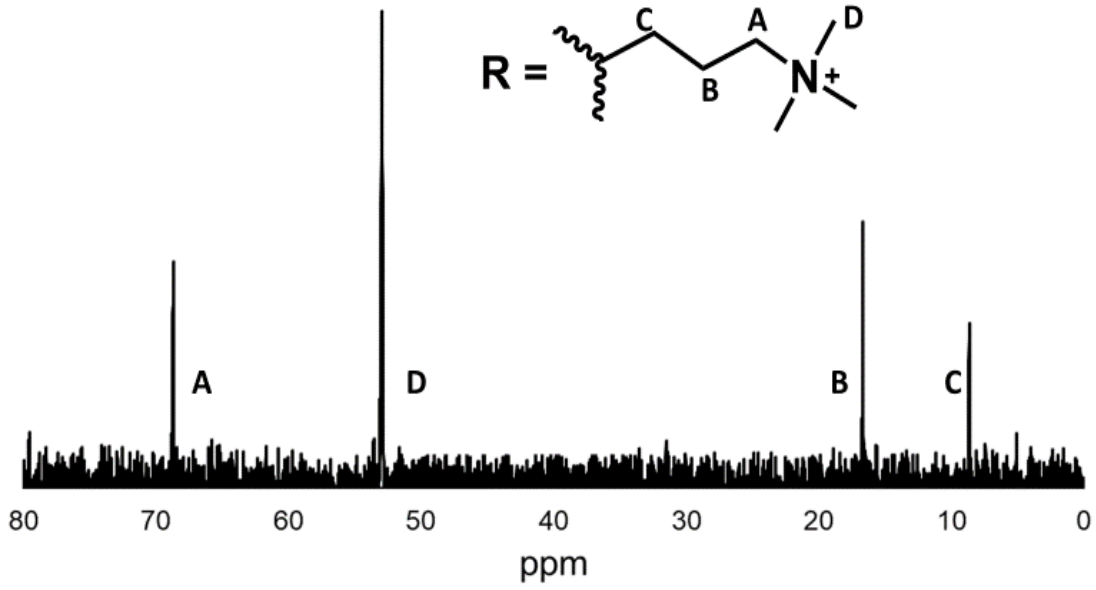

Figure A18. ^{13}C NMR of MOA-POSS. ^{13}C NMR (300 MHz, DMSO, ppm) δ: 68.89 (s, -$CH_2N^+(CH_3)_3$), 52.97 (s, -$CH_2N^+(CH_3)_3$), 16.71 (s, -$CH_2CH_2N^+(CH_3)_3$), 8.61 (s, Si-CH_2).

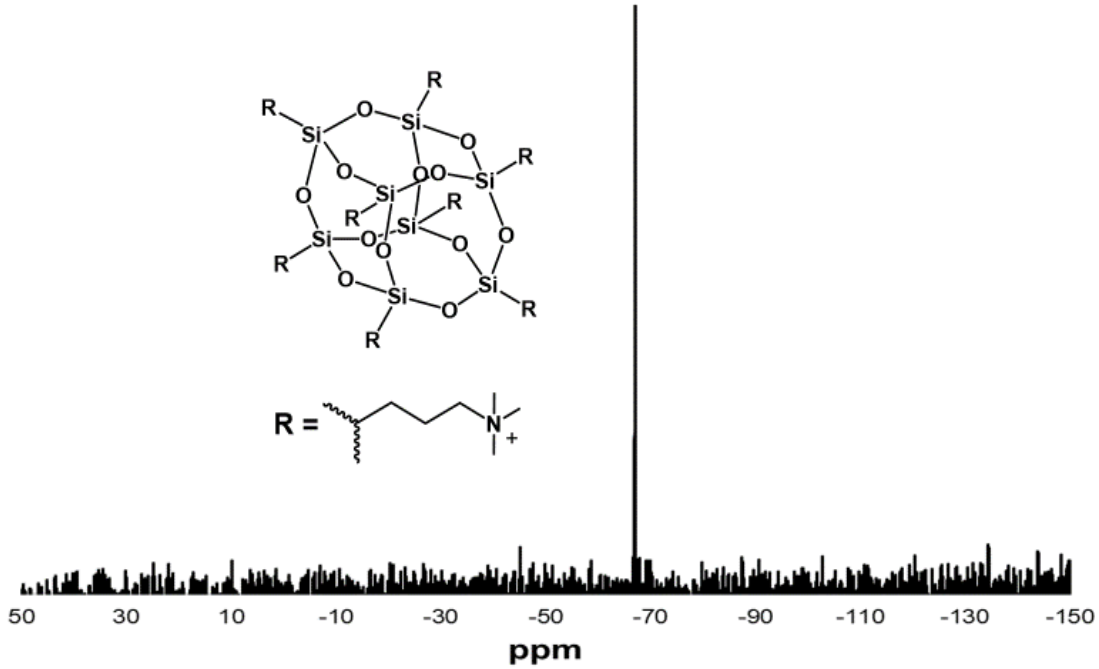

Figure A19. ^{29}Si NMR of MOA-POSS. ^{29}Si NMR (500 MHz, D_2O, ppm) δ: -67.2 (s, T^3).

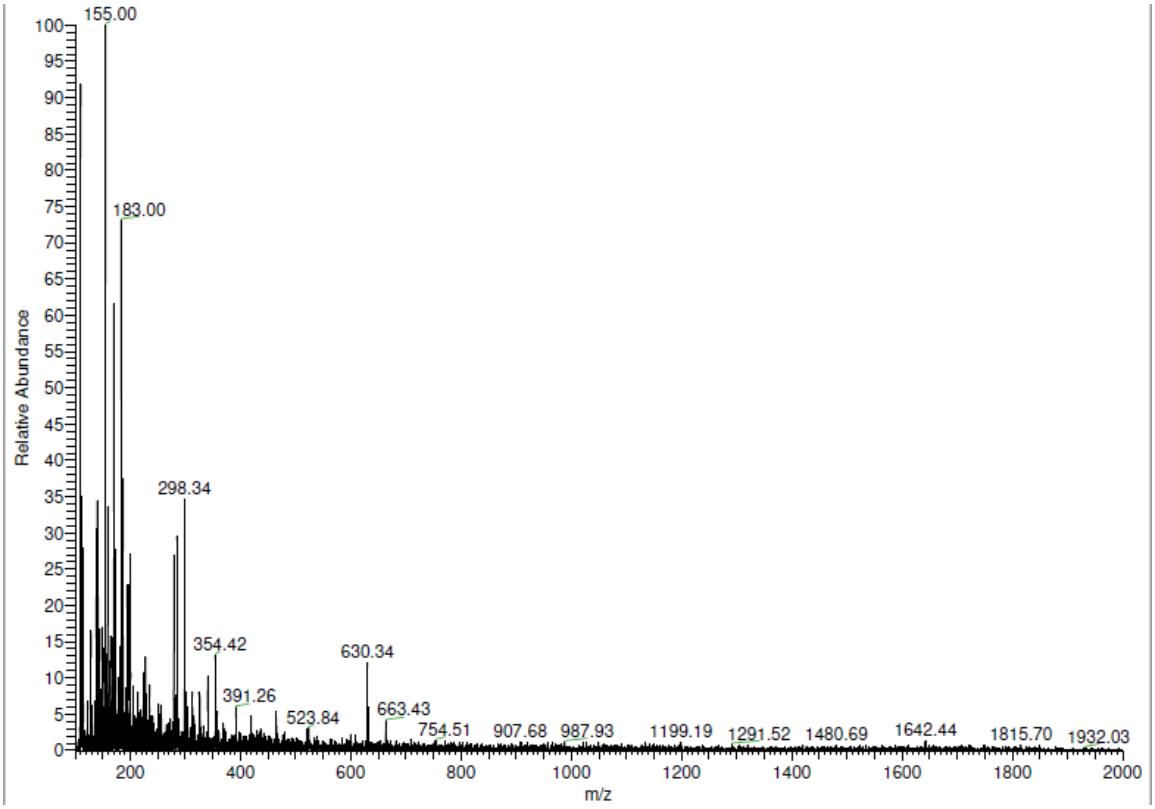

Figure A20. ESI of MOA-POSS. MS (ESI): m/z (%): 153.89 $[M-2H]^{2+}$ observed; 155.1 calculated.

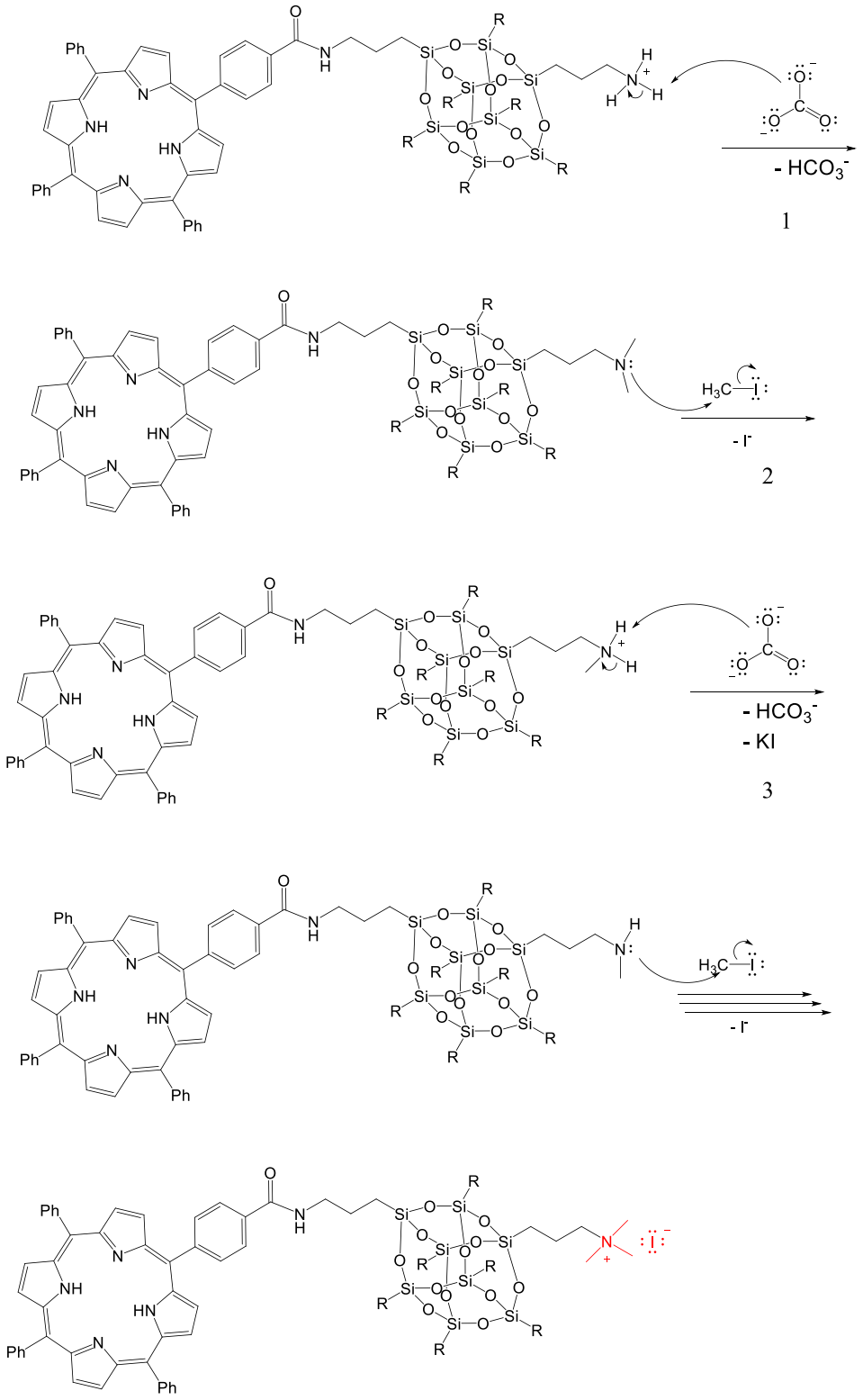

Figure A21. Mechanism of formation of MOA-POSS-Porphyrin. Potassium bicarbonate is used as a base to deprotonate the ammonium sites on the cage and generate the free amine, which reacts with methyl iodide. This allows for the formation of a permanent positive charge on the system.

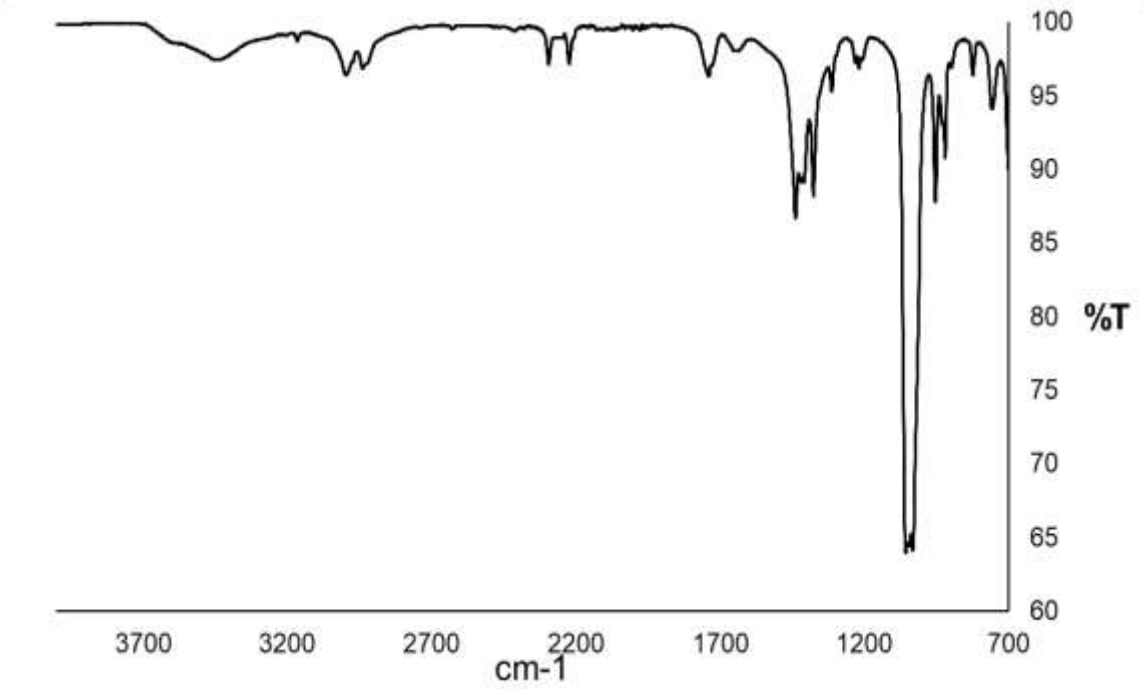

Figure A22. IR of MOA-POSS-Porphyrin. FTIR (KBr pellets): = 3323 (s, $\nu_{N\text{-}H}$); 2872 (m, $\nu_{C\text{-}H}$); 1660 (s, $\nu_{C\text{-}O}$); 1428 (m, $\nu_{C\text{-}N}$); 1372 (m, $\nu_{Si\text{-}C}$); 1017 (s, $\nu_{cage\text{-}asym\text{-}Si\text{-}O\text{-}Si}$); 931 (m, $\nu_{cage\text{-}sym\text{-}Si\text{-}O\text{-}Si}$).

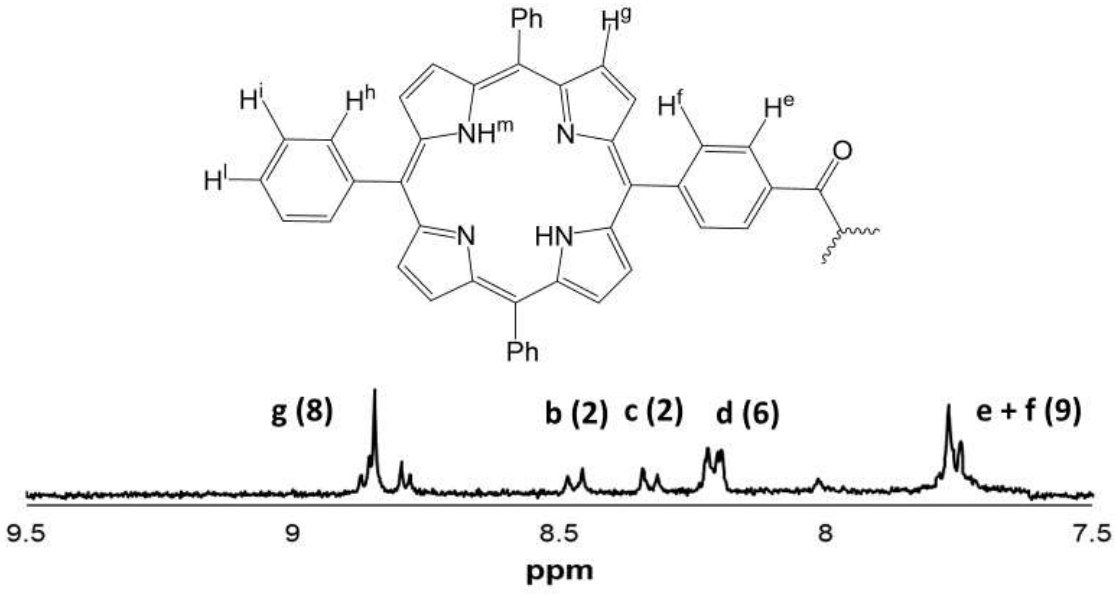

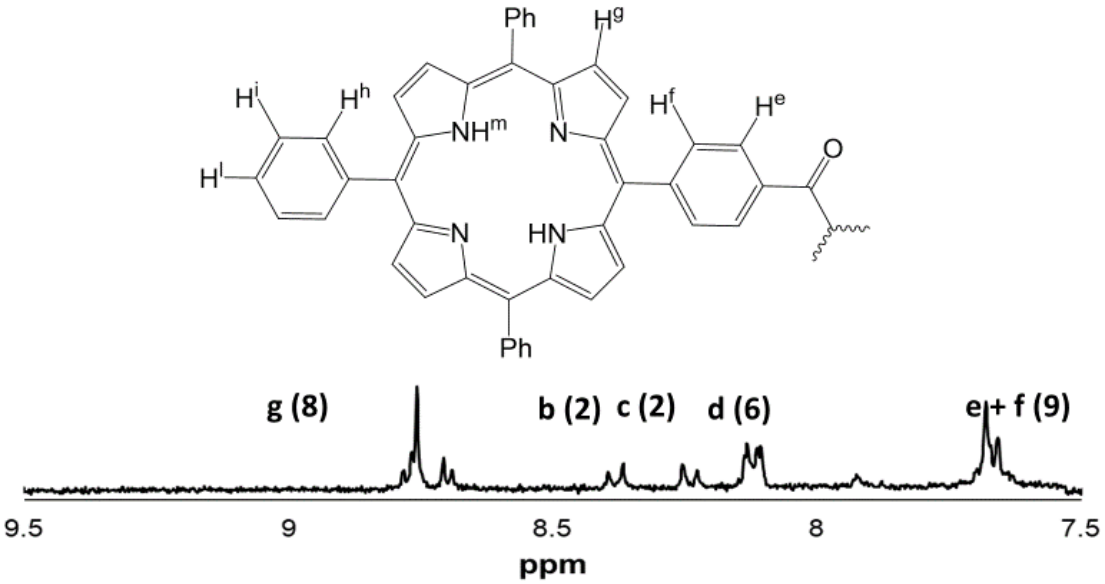

Figure A23. ^{1}H NMR of MOA-POSS-Porphyrin. ^{1}H NMR (500 MHZ, DMSO-D_6, ppm) δ = 8.67 (m, 8H), 8.48 (d, 2H), 8.32 (d, 2H), 8.25 (m, 6H), 7.65 (m, 9H), 3.35 (m, 16H), 3.24 (t, 2H), 2.94 (s, 63H), 1.93 (m, 16H), 0.39 (t, 16H).

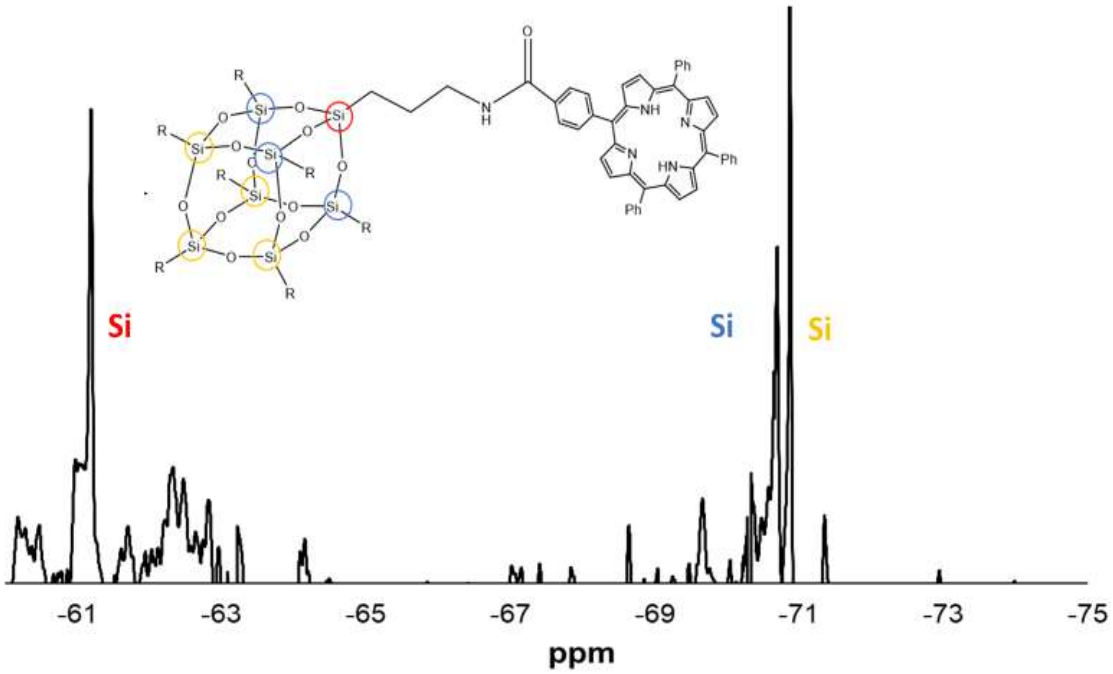

Figure A24. ^{29}Si NMR of MOA-POSS-Porphyrin. ^{29}Si NMR (500 MHz, DMSO-D_6, with 0.1% TMS, ppm) δ = -61.2 (one Si-$CH_2CH_2CH_2NH_2$), -69.6 (three Si close to Si-$CH_2CH_2CH_2NH_2$), -70.9 (remaining four Si on the cage).

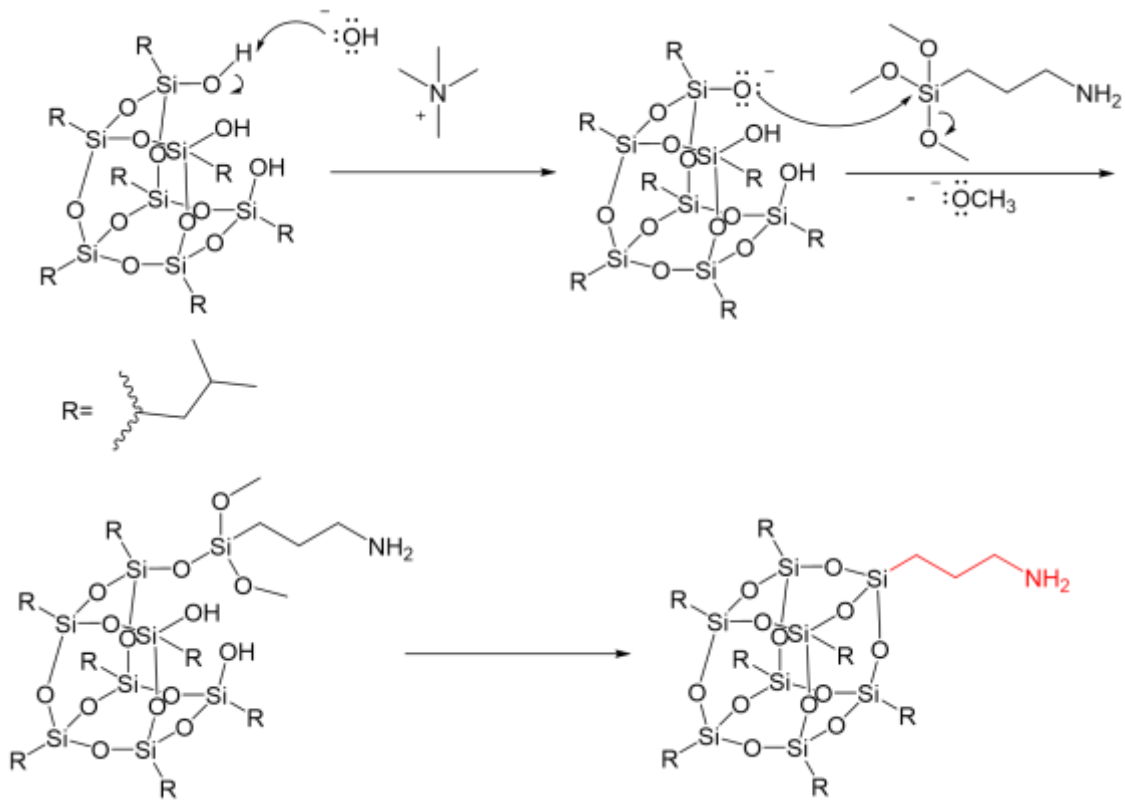

Figure A25. Mechanism of corner capping reaction of a partially condensed trisilanol POSS under catalytic amounts of TEAOH. The reactive group targeted is an aminopropyl moiety.

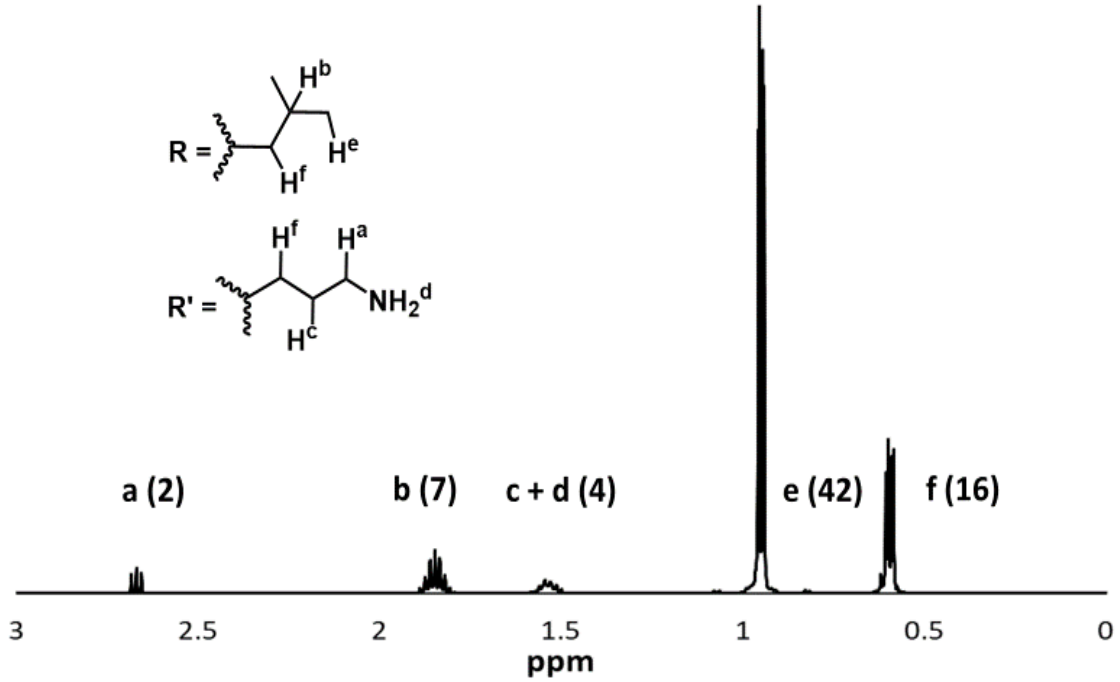

Figure A26. ^{1}H NMR of APIB-POSS.^{1}H NMR (300 MHz, CD_3Cl, ppm) δ: 0.85 (m, 16H; C*H*$_2$-Si), 0.99 (d, 42H; -C*H*$_3$), 1.53 (m, 4H; -$CH_2CH_2CH_2NH_2$), 1.85 (m, 7H; -$CH_2CH(CH_3)_2$), 2.69 (t, 2H, -C*H*$_2$$NH_2$).

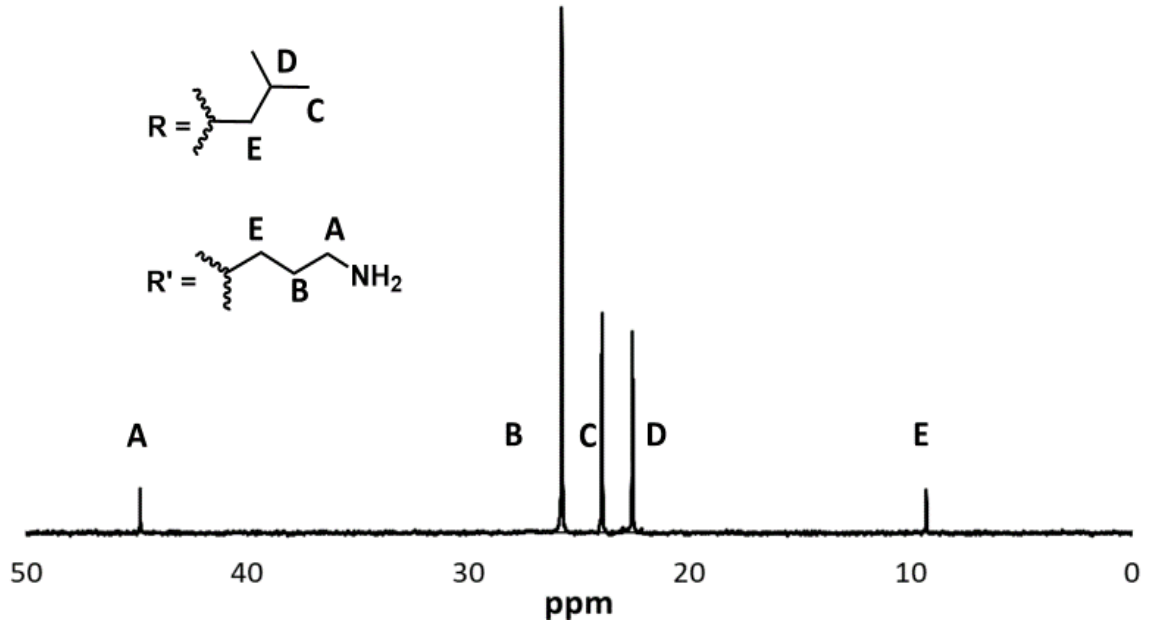

Figure A27. ^{13}C NMR of APIB-POSS. ^{13}C NMR (300 MHz, CD_3Cl, ppm) δ: 44.82 (s, -CH_2NH_2), 25.84 (s, -CH_3), 23.95 (s, -$CH_2CH_2CH_2NH_2$), 22.57 (s, -$CH_2CH(CH_3)_2$) 9.30 (s, -CH_2-Si).

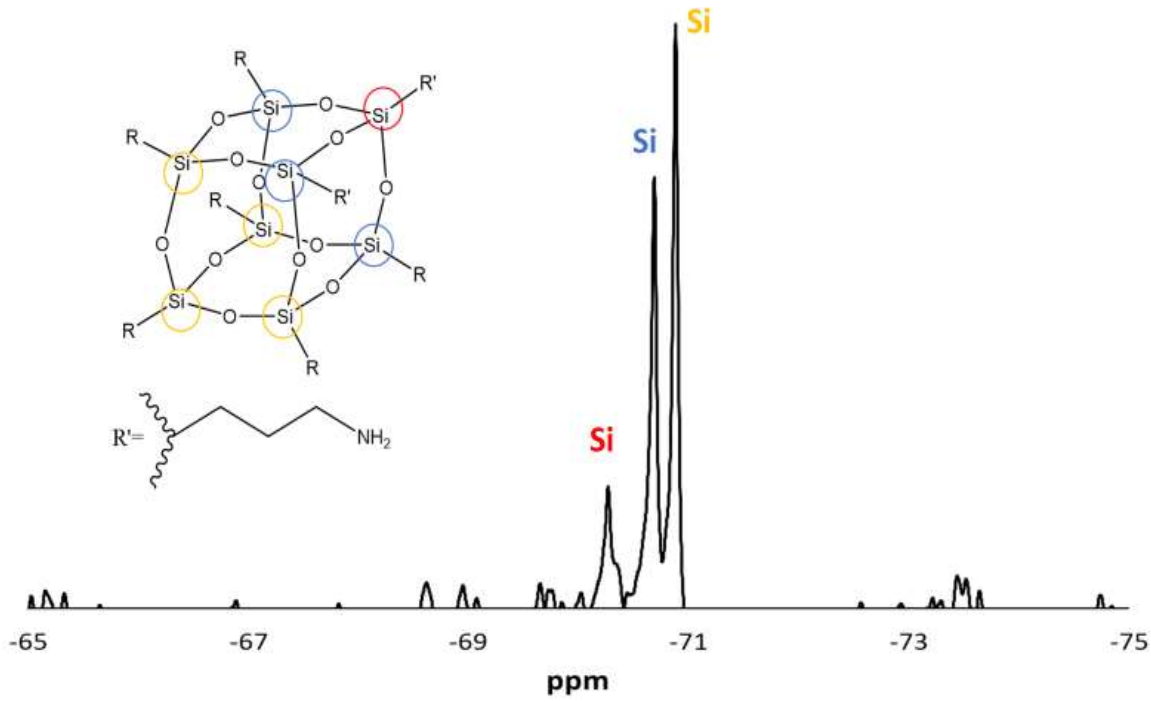

Figure A28. ^{29}Si NMR of APIB-POSS. ^{29}Si NMR (500 MHz, CD_3Cl with 0.1% TMS, ppm) δ: -66.7 (one Si-$CH_2CH_2CH_2NH_2$), -67.5 (three Si close to Si-$CH_2CH_2CH_2NH_2$) and -67.3 (remaining four Si on the cage).

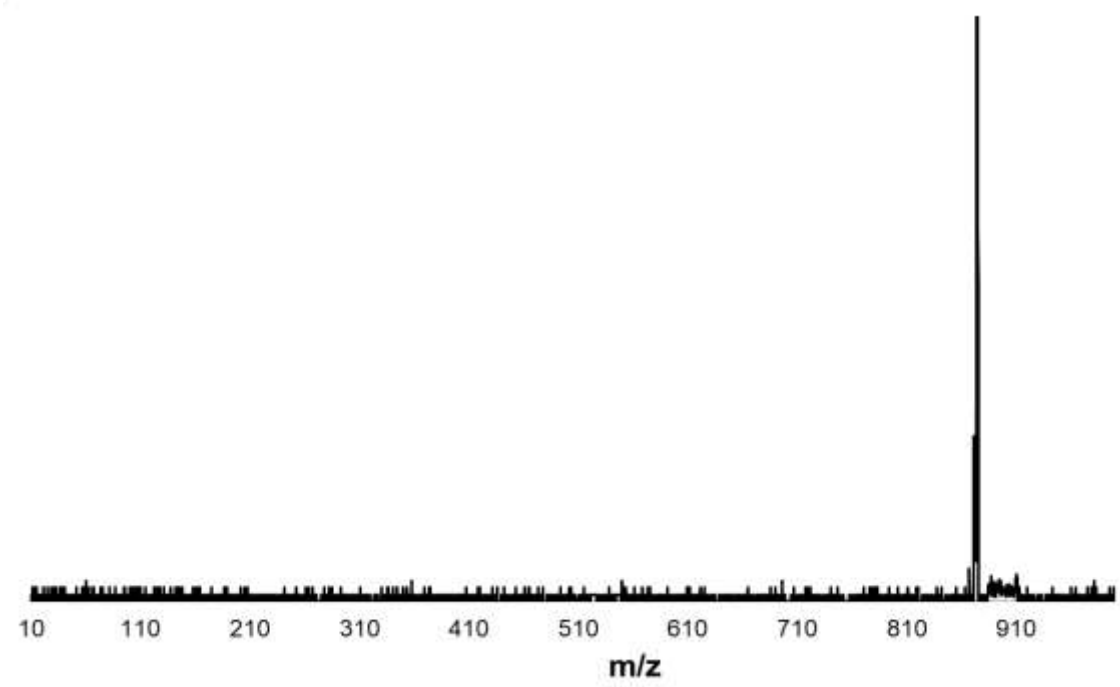

Figure A29. MALDI of APIB-POSS. MALDI (m/z): 874.58 [calculated for $[M-H]^+$] 875.12.

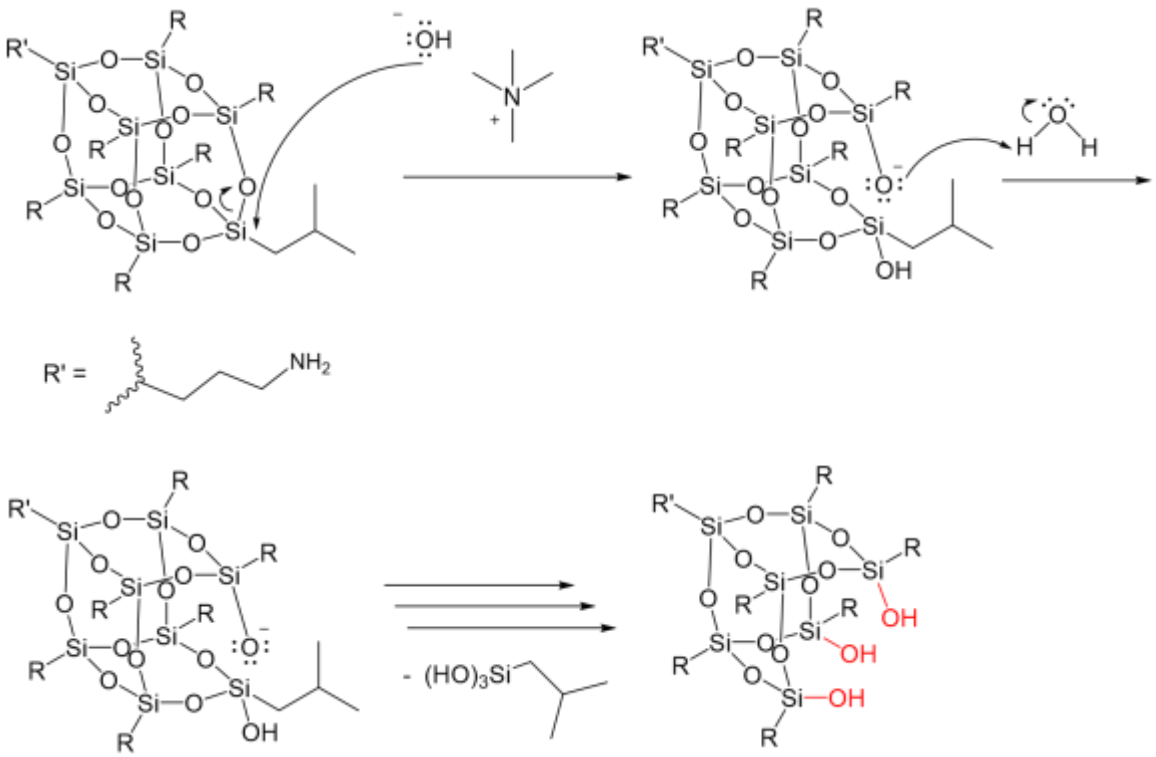

Figure A30. Mechanism of corner opening reaction of AP-IB-POSS under reflux at 80 ℃ to afford a partially condensed POSS. The corner opened is the one opposite to the corner bearing the most reactive group, which in this case is the aminopropyl moiety.

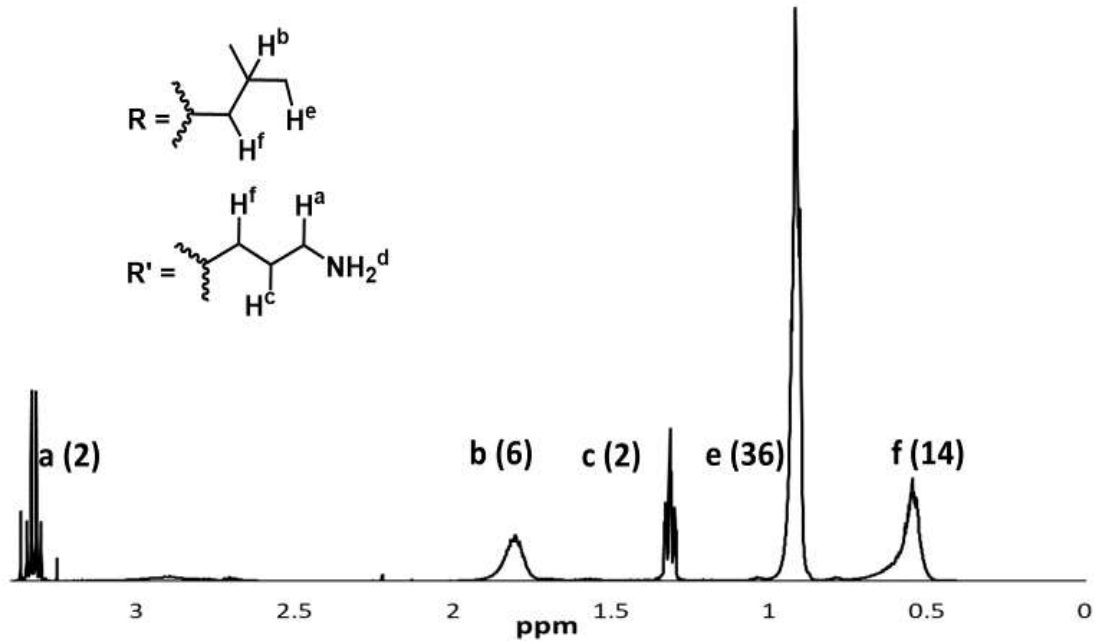

Figure A31. ^{1}H NMR of AP-hexaIB-POSS. ^{1}H NMR (500 MHz, CD_3Cl, ppm) δ: 0.54 (m, 14H; C*H*$_2$-Si), 0.90 (d, 36H; -C*H*$_3$), 1.30 (m, 4H; -$CH_2CH_2CH_2NH_2$), 1.80 (m, 6H; -$CH_2CH(CH_3)_2$), 3.32 (t, 2H, -C*H*$_2$$NH_2$).

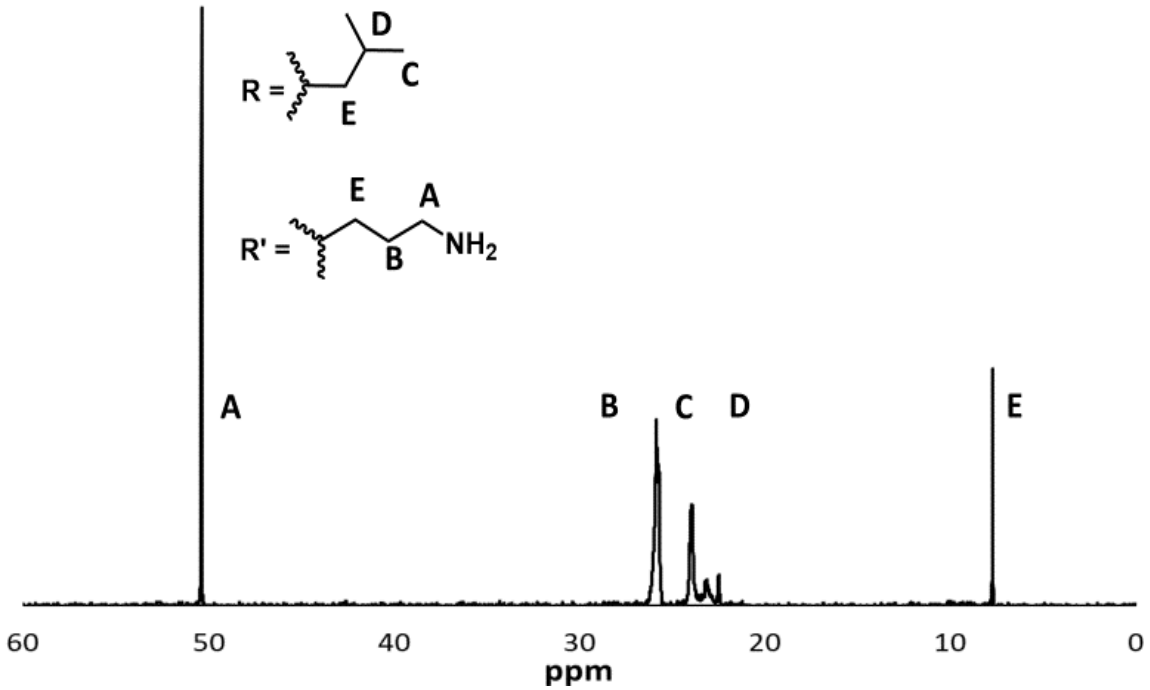

Figure A32. ^{13}C NMR of AP-hexaIB-POSS. ^{13}C NMR (300 MHz, CD_3Cl, ppm) δ: 52.93 (s, -*C*H_2NH_2), 30.40 (s, -CH_2*C*$H_2CH_2NH_2$), 25.86 (s, -*C*H_3), 23.89 (s, -CH_2*C*H$(CH_3)_2$), 22.48 (s, -*C*H_2CH$(CH_3)_2$) 7.58 (s, *C*H_2-Si).

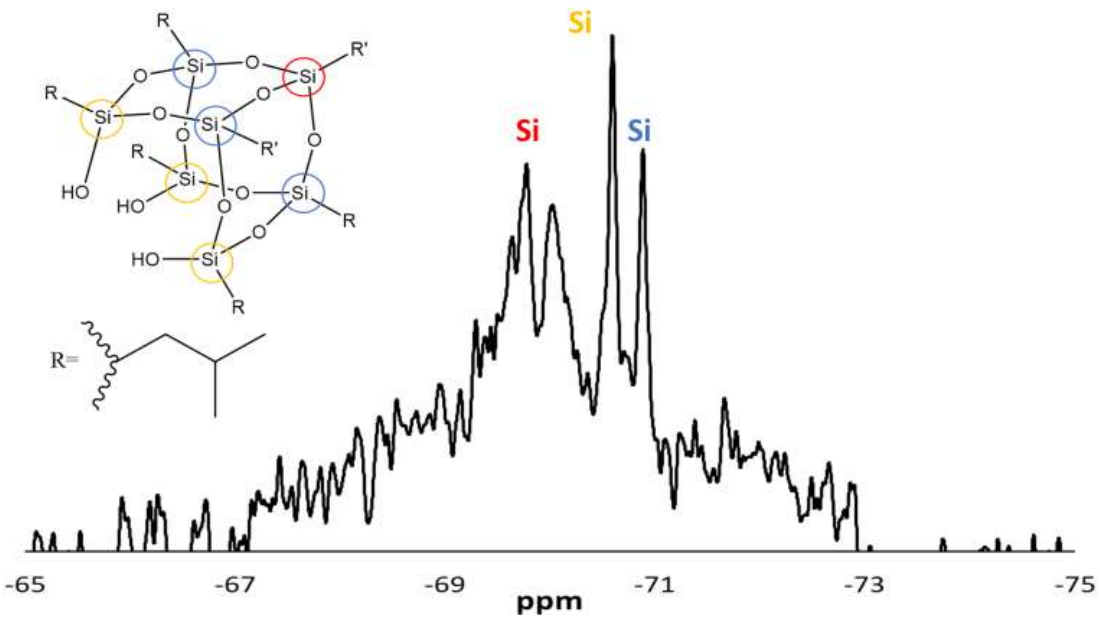

Figure A33. ^{29}Si NMR of AP-hexaIB-POSS. ^{29}Si NMR (500 MHz, CD_3Cl with 0.1% TMS, ppm) δ: -58.9 (three Si-OH), -67.5 (one Si-$CH_2CH_2CH_2NH_2$) and -68.3 (remaining three Si on the cage).

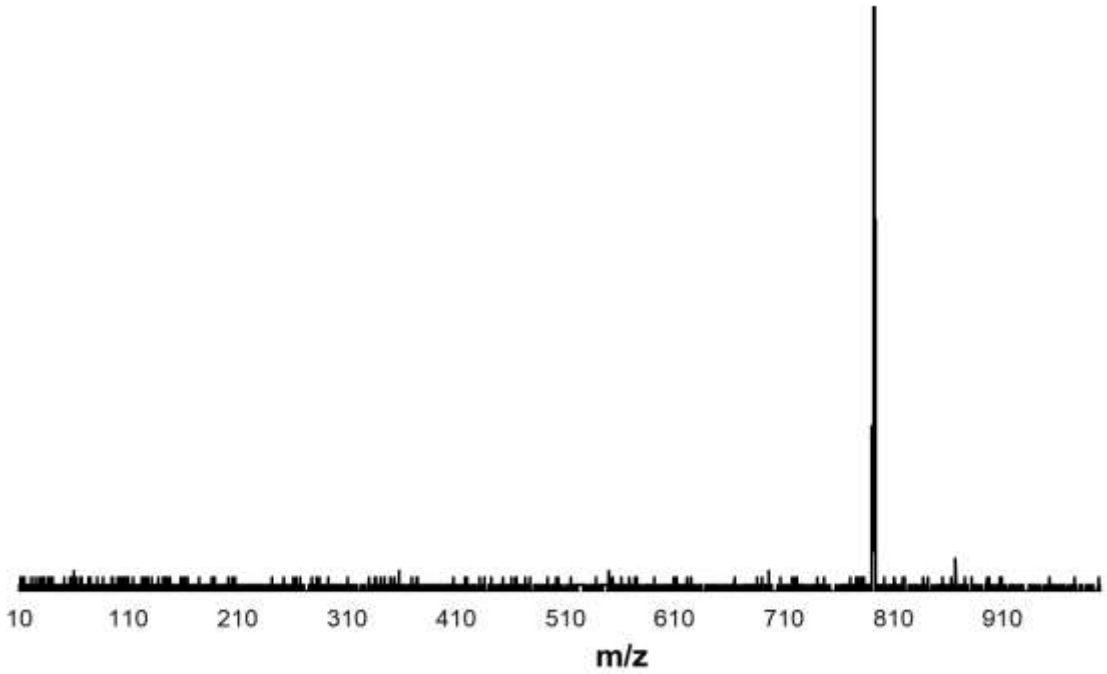

Figure A34. MALDI of AP-hexaIB-POSS. MALDI (m/z): 792.29 [calculated for $[M-H]^+$] 792.43.

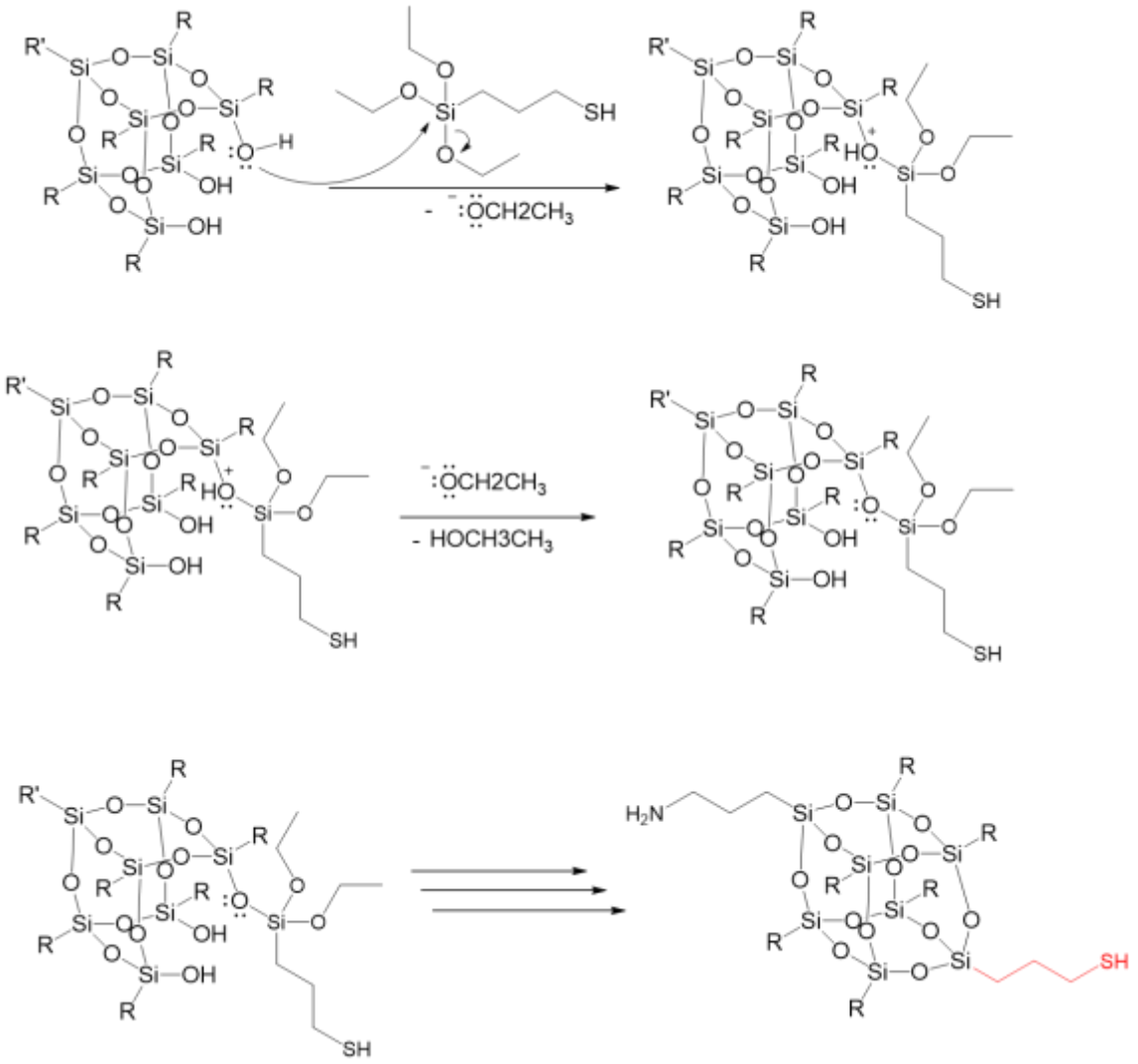

Figure A35. Mechanism of corner capping reaction of a partially condensed AP-hexaIB-POSS under catalytic amounts of TEAOH. The reactive group targeted is an mercapto moiety to generate a multifunctional group.

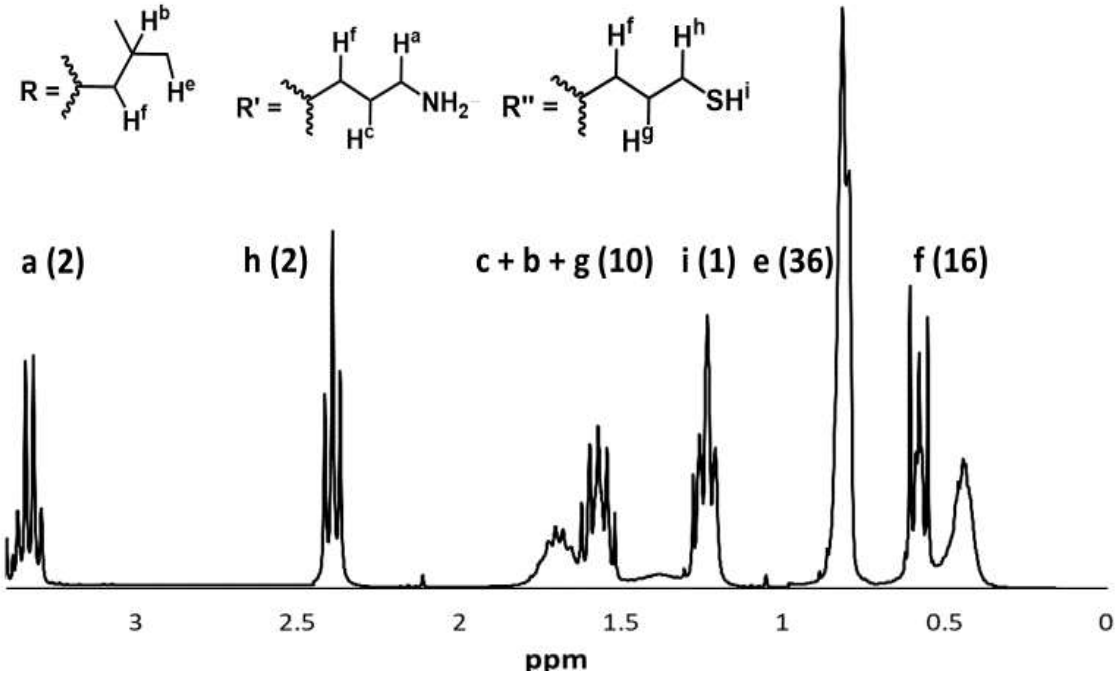

Figure A36. ^{1}H NMR of AP-IB-MP-POSS. ^{1}H NMR (500 MHz, CD_3Cl, ppm) δ: 0.54 (m, 16H; C*H*$_2$-Si), 0.82 (d, 36H; -CH_3), 1.25 (m, 3H; -SH,-NH_2), 1.50-1.72 (m, 10H; -$CH_2CH(CH_3)_2$, -$CH_2CH_2CH_2SH$, $CH_2CH_2CH_2NH_2$), 2.52 (t, $CH_2CH_2CH_2SH$), 3.32 (t, 2H, -CH_2NH_2).

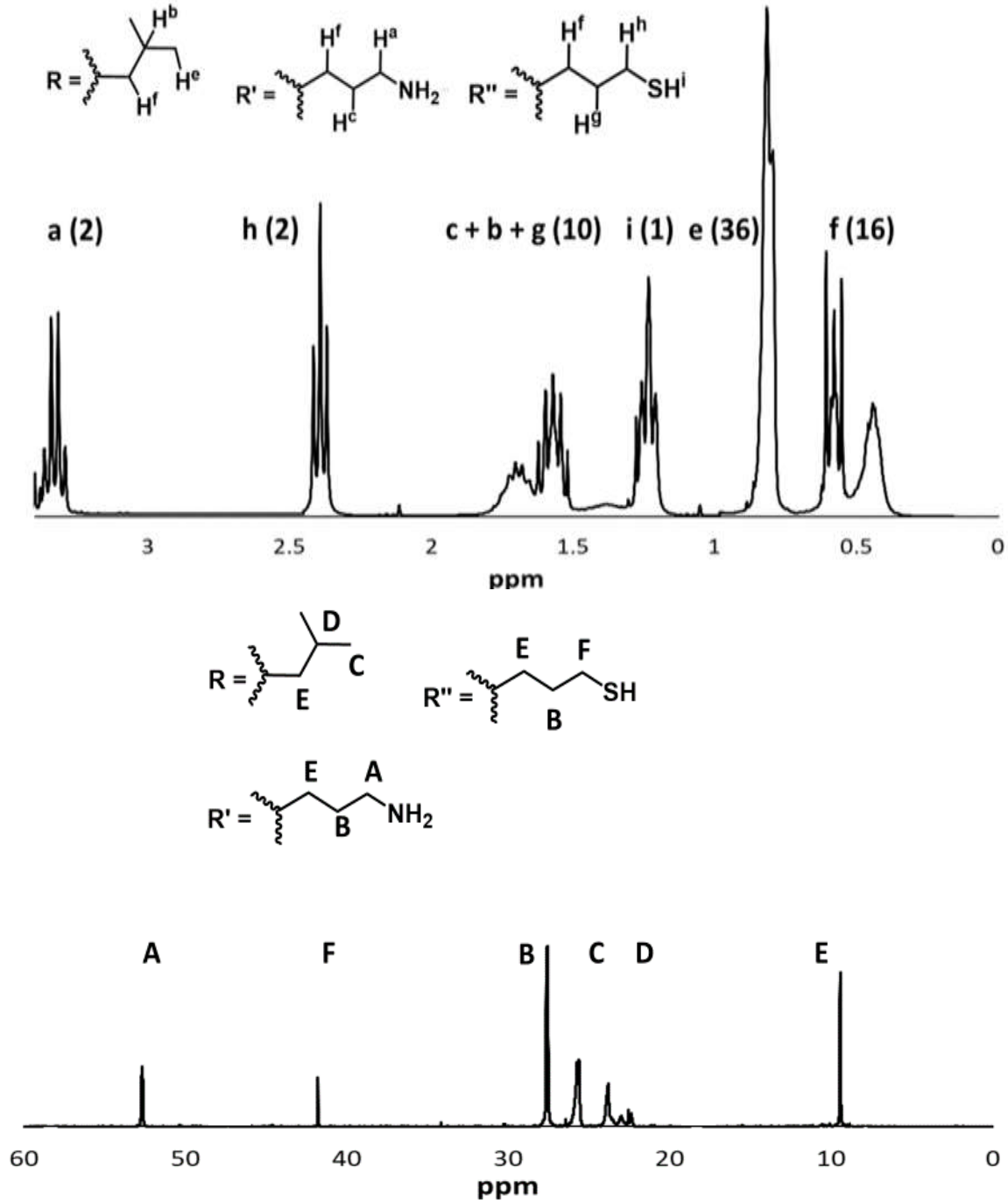

Figure A37. ^{13}C NMR of AP-IB-MP-POSS. ^{13}C NMR (300 MHz, CD_3Cl, ppm) δ: 52.93 (s, -*C*H_2NH_2), 30.31 (s, -CH_2CH_2*C*H_2SH, -CH_2CH_2*C*H_2NH_2), 25.92 (s, -*C*H_3), 23.88 (s, -CH_2*C*$H(CH_3)_2$), 22.48 (s, -CH_2*C*H_2CH_2SH) 9.58 (s, *C*H_2-Si).

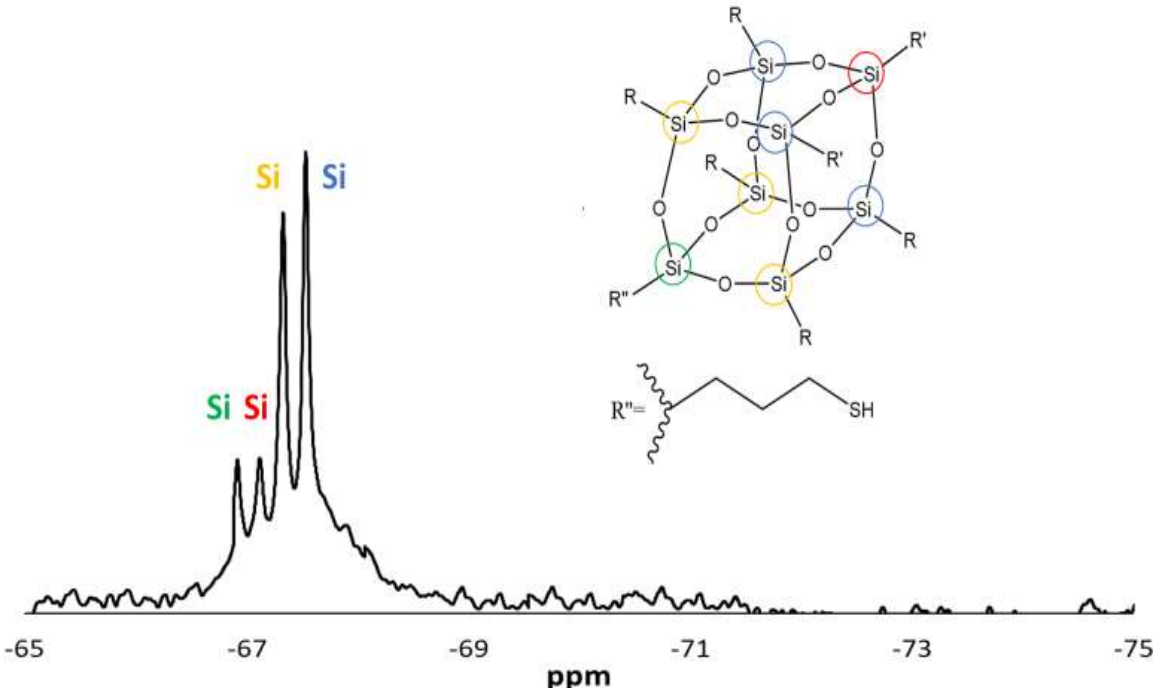

Figure A38. ^{29}Si NMR of AP-IB-MP-POSS. ^{29}Si NMR (500 MHz, CD_3Cl with 0.1% TMS, ppm) δ: -66.8 (one Si-$CH_2CH_2CH_2SH$), -67.1 (one Si-$CH_2CH_2CH_2NH_2$), -67.5 (three Si on the cage closer to the Si bearing the mercaptopropyl group), 67.9 (three Si on the cage closer to the Si bearing the aminopropyl group).

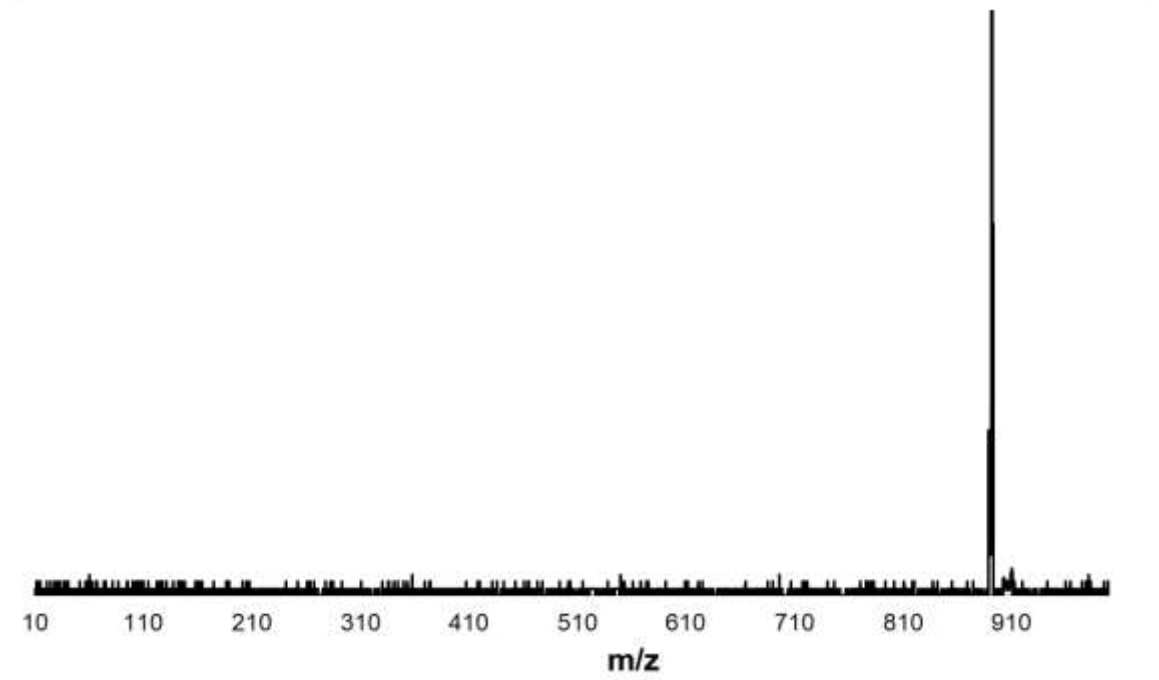

Figure A39. MALDI of AP-IB-MP-POSS. MALDI (m/z): 892.03 [calculated for $[M-H]^+$] 892.12.

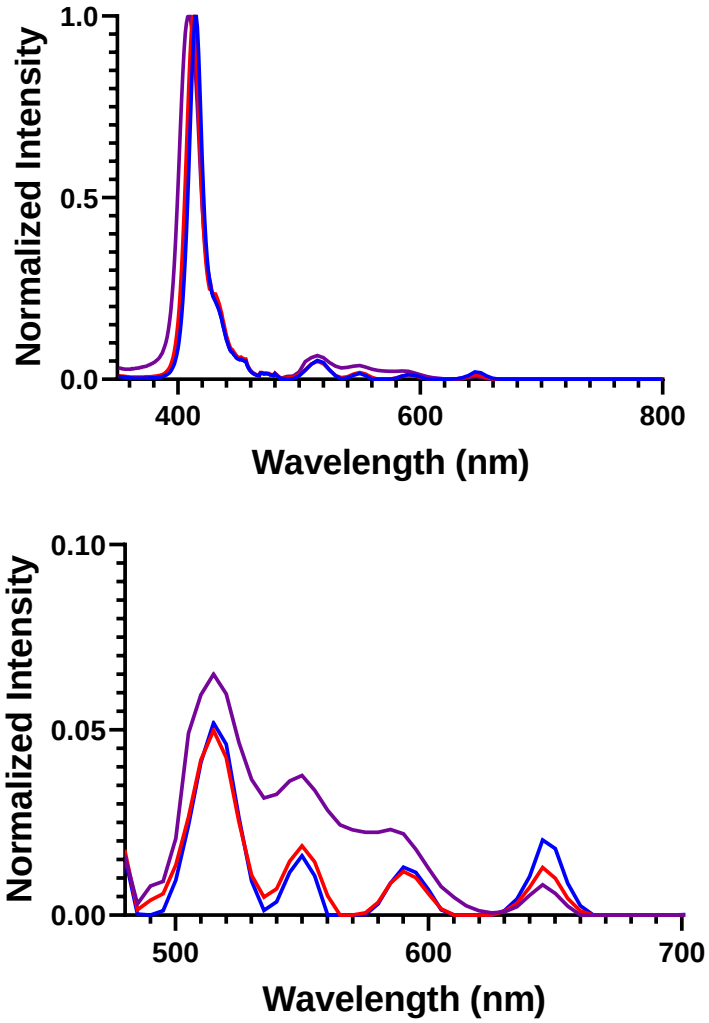

Figure A40. UV-vis spectra of OA-POSS-Porphyrin, MOA-POSS-Porphyrin and Por-COOH (purple is for Por-COOH, blue is for OA-POSS-Porphyrin, red is for MOA-POSS-Porphyrin).

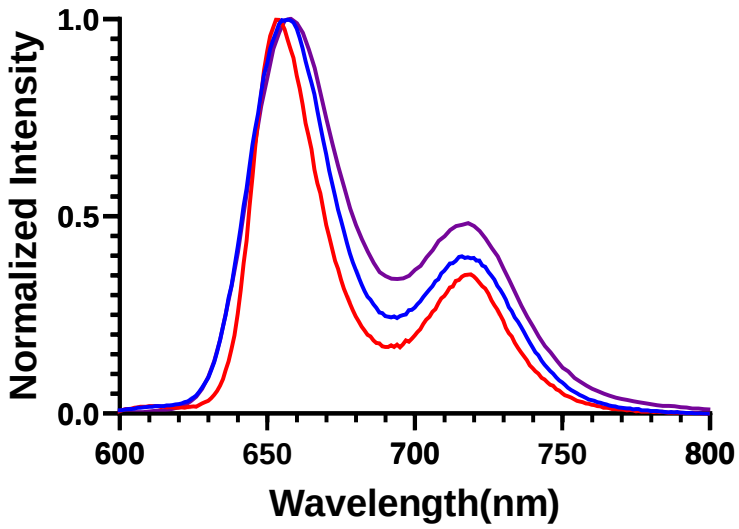

Figure A41. Fluorescence spectra of OA-POSS-Porphyrin, MOA-POSS-Porphyrin and Por-COOH (purple is for Por-COOH, blue is for OA-POSS-Porphyrin, red is for MOA-POSS-Porphyrin).

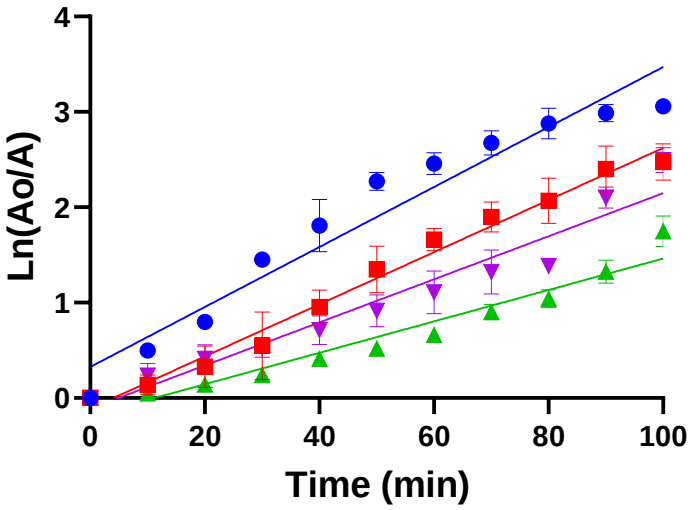

Figure A42. DMA time dependent plots of OA-POSS-Porphyrin, MOA-POSS-Porphyrin and Por-COOH (purple is for Por-COOH, blue is for OA-POSS-Porphyrin, red is for MOA-POSS-Porphyrin, green is for OA-POSS + Porphyrin).